Not Restricted to the Ends: Yeast Telomere Proteins Rif1 and Cdc13 Function in Double-Strand Break Repair Pathways with Implications for Genome Stability

By

Udochukwu Chinyere Obodo

Dissertation
Submitted to the Faculty of the
Graduate School of Vanderbilt University
in partial fulfillment of the requirements
for the degree of

DOCTOR OF PHILOSOPHY
in

Biological Sciences
August, 2016
Nashville, Tennessee

Approved:
Katherine L. Friedman, Ph.D.
Todd R. Graham, Ph.D.
Kathleen L. Gould, Ph.D.
P. Anthony Weil, Ph.D.
Donna J. Webb, Ph.D.

DEDICATION

I dedicate this work to the memories of my beloved uncles, Ferdinand Obodo and Felix Obodo. They were unwavering champions for education of both the men and women alike of our family. I know they are resting in eternal peace with the Lord Almighty and that they would be incredibly proud, not just of my accomplishment, but of how much we have achieved as a family.

ACKNOWLEDGEMENTS

Never in my wildest dream could I have imagined the journey that would bring me here, to this point in my life. I left my home in Nigeria as a teenager, excited for the opportunities that awaited me. It has been exhilarating to say the least. I have met so many amazing people along the way who have welcomed me with open arms into their homes and their lives and given me the wonderful gift of a home away from home. To Laureen and Dan Evans especially, I would like to say thank you for showing me true kindness. You may not know it, but I think of you always.

I want to thank the Vanderbilt International Scholar Program (VISP) for providing me with support in my first few years of graduate school. My gratitude also goes to Vanderbilt Department of Biological Sciences and the Gisela Mosig Fund for providing me with all forms of support (stipend, travel, and more) that have helped shaped my growth as a scientist.

On that note, I would like to thank my thesis advisor, Dr. Katherine Friedman, for her support through the years. She is a truly gifted scientist and I am emerging from her lab confident that I have a great foundation to build on for my own scientific career. Thank you to my committee members for all of your advice and support through the years. It was great to get your different perspectives on my projects and it has taught me the value of always keeping an open mind when it comes to scientific work.

To my family, it feels like I have been in school forever, and I thank you for sticking with me through it all. To Daddy and Mummy, thank you for all your love. You two are the most resilient people I know and I trust that I can always find strength in you if I need it. Daddy, thank you for teaching all of us, your kids, the value of faith and trust in God. You have always been a champion for everyone, especially the women, in your life. Thank you for teaching me the value of using one's success to bring

others up. Everything I have done and will continue to do is in the hopes that I can have the privilege of doing just that. Mummy, you are a force of nature. I always marvel at the way you juggled so many responsibilities while raising us. Thank you for teaching us the value of hard work and to always keep going even when things get rough. If I can be even half as resilient as you are, I know I will be a great mother too. And to my dear brothers Moses, Onos, and my gorgeous sister Nneoma, thank you for all the good times and the laughs. Our bond will be forever, no matter what.

To the rest of my big extended family, I could not possibly mention everyone here. But, I would like to thank you all for all of your love and support. We have worked so hard as a whole to get to where we are today. I sincerely hope that we continue to pass on, to our young ones and to successive generations, the values of hard work, a passion for education, and compassion for others, so that we can continue to progress as a family and make lasting positive impacts in this world.

Thank you to the true friends that I have made over the years. Thank you for taking the time to understand me in all my complicated glory. No matter where we are or will be, I will always appreciate your friendship. Last, but not least, I thank my heavenly father to whom I owe everything that I am and everything that I have accomplished, and whose blessings and unconditional love have guided me to where I am today.

TABLE OF CONTENTS

Page

LIST OF TABLES

LIST OF FIGURES

Figure Page

LIST OF ABBREVIATIONS

5-FOA - 5-Fluoroorotic acid

α-aa - alpha-aminoadipate

ALT - Alternative Lengthening of Telomeres

AP - Abasic (Apurinic or apyrimidinic)

APC - Anaphase-promoting complex

ARP - Autonomously replicating piece

ARS - Autonomously replicating sequence

BIR - Break-induced replication

BER - Base excision repair

BrdU - 5-bromo-2′-deoxyuridine

BS - Bloom syndrome

ChIP - Chromatin immunoprecipitation

C-NHEJ - Classical NHEJ

CO - Crossover

DBD - DNA-binding domain

dHJ - Double Holliday junction

DKC - Dyskeratosis congenita

D-loop - Displacement loop

DSB - Double-strand break

dsDNA - Double-stranded DNA

EMS - Ethyl methanesulfonate

EST - Ever shorter telomere

G_1 - Gap phase 1

G_2 - Gap phase 2

GC - Gene conversion

GCR - Gross chromosomal rearrangement

H1 - Histone 1

H2A - Histone 2A

H2B - Histone 2B

H3 - Histone 3

H4 - Histone 4

H5 - Histone 5

HO endonuclease - HOmothallic switching endonuclease

HR - Homologous recombination

IPF - Idiopathic pulmonary fibrosis

IR - Ionizing radiation

IRIF - Ionizing radiation-induced foci

M - Mitosis phase

MMEJ - Microhomology-mediated end joining

MMR - Mismatch repair

MMS - Methyl methanesulphonate

NCO - Non-crossover

NER - Nucleotide excision repair

NHEJ - Non-homologous end joining

ORC - Origin recognition complex

PARPi - poly(ADP-ribose) polymerase inhibitor

PP1 - Protein phosphatase-1

RAP - Repeat addition processivity

RT-PCR - Reverse transcription-polymerase chain reaction

S phase - Synthesis phase

SDSA - Synthesis-dependent strand annealing

SSA - Single-strand annealing

SSB - Single-strand break

TEN domain - Telomerase essential N-terminus domain

T loop - Telomere loop

ssDNA - Single-stranded DNA

TPE - Telomere position effect

WS - Werner Syndrome

CHAPTER I

INTRODUCTION: DNA DAMAGE AND REPAIR

Overview

Linear eukaryotic chromosomes consist of chromatin, nucleoprotein structures containing DNA and its associated proteins. The basic unit, and the best understood scale, of chromatin structure is the nucleosome, a compact, ~10-nm thick structure containing 160-200 base pairs of DNA wrapped approximately 1.7 times around a core histone octamer comprised of two copies each of the core histone proteins, H2A, H2B, H3, and H4 (reviewed in refs. (1-3)). Linker DNA sequences, each about 30-60 base pairs in length and bound by a single molecule of linker histone (H1 or H5), connect nucleosomes and aid in further compaction of the DNA molecule (reviewed in (2)). Beyond the nucleosomal scale, eukaryotic DNA undergoes orders of magnitude more folding to form the highly condensed chromosomes that are typical of metaphase chromosomes, although this larger scale folding of chromatin is less understood (reviewed in (2, 3)).

DNA is constantly subjected to various insults from both endogenous and exogenous sources. To ensure genome integrity and cell survival, any DNA damage must be repaired within the context of tightly packed chromatin. Eukaryotic cells possess an arsenal of non-histone proteins that recognize and repair DNA damage, and histones themselves, which constitute the bulk of proteins in chromatin, also play important roles in DNA repair. Though important, the role of histones in DNA double-strand break (DSB) repair is not extensively discussed in this thesis, but has been reviewed elsewhere (4).

In this introductory chapter, I present an extensive review of DNA damage and repair in eukaryotic cells, with a particular focus on the recognition and repair of DNA lesions in the model eukaryotic organism *Saccharomyces cerevisiae*. I discuss various sources and types of DNA damage,

followed by a review of the processes that recognize and repair DNA damage. The two main pathways of DSB repair in eukaryotes, homologous recombination (HR) and non-homologous end joining (NHEJ), are extensively discussed. I also discuss DSB resection as a key factor that determines whether DSBs are repaired by HR or NHEJ, before delving into the role of Rif1 in the regulation of HR and NHEJ.

1.1 Sources and Types of DNA Damage

DNA damage arises from endogenous and exogenous sources. One source of endogenous DNA damage is spontaneous hydrolysis of the *N*-glycosidic bond between a base and a sugar. This process creates an abasic (apurinic or apyrimidic) or AP site. Other endogenous sources of DNA damage include free radical species and spontaneous deamination. Free radical species, often generated as metabolic by-products, cause oxidative DNA lesions. Amine-containing bases can undergo spontaneous deamination: examples include the deamination of adenine to hypoxanthine or of cytosine to uracil. Oxidized or deaminated bases may be excised by enzymatic hydrolysis of the *N*-glycosidic bonds, also resulting in AP site formation. DNA replication errors, resulting in mismatched base pairs, represent another source of endogenous DNA damage.

Exogenous sources of DNA damage include ultraviolet radiation, ionizing radiation (IR), and chemical compounds. Ultraviolet radiation induces the formation of pyrimidine dimers by covalently linking neighboring pyrimidines. IR represents another source of oxidative free radical species. Chemical compounds covalently modify DNA to form DNA adducts: DNA alkylating agents, such as methyl methanesulphonate (MMS), attach alkyl groups to bases, while larger chemical compounds covalently attach to DNA, resulting in the formation of so-called “bulky adducts.” The sources and types of DNA damage discussed above are reviewed in (5).

Two other types of DNA damage that can arise both from endogenous and exogenous sources are single-strand breaks (SSBs) and DSBs. SSBs arise directly by free radical species-induced disintegration of deoxyribose, or indirectly, as intermediates during the repair of modified bases (6) (see below). SSBs can also result from topoisomerase I activity. Topoisomerase I (Top1), as part of its DNA unwinding activity, creates and reseals a nick in one strand of the double helix. However, in certain situations, such as when the transcription machinery runs into Top1, the SSB can be uncoupled from Top1 (7), presumably because the transcription bubble displaces the free 5′ end and prevents DNA religation (8). In these cases, the stalled Top1 remains covalently attached to the 3′ end, forming a Top1-SSB.

DSBs can also be induced directly by IR (so-called Prompt DSBs) (9), as well as by the attempted repair of other kinds of DNA lesions. IR produces isolated, as well as clustered DNA lesions (lesions spaced 1-10 bp apart) (reviewed in (9)). Because SSBs form as intermediates during repair of damaged bases (below), simultaneous repair, on both DNA strands, of damaged bases within clustered DNA lesions can result in DSBs (9). Another source of DSBs is programmed DSBs that are induced during a number of physiological and developmental processes, the most prevalent example of which is meiotic recombination. DSBs are also created and repaired in developing lymphocytes (B and T cells) during a process known as V(D)J recombination that generates the diverse repertoire of antigen-recognizing cell surface receptors on those cells (reviewed in (10)). Another immunological process that involves the formation and repair of DSBs is immunoglobulin/antibody class switching, a process by which mature B cells switch antibody production from one class to another (reviewed in (10)). Finally, DSBs are induced and repaired during mating-type switching in *S. cerevisiae*. The two *S. cerevisiae* haploid mating types (**a** and α) are regulated by proteins encoded by the *MAT***a** and *MAT*α genes, respectively. Each haploid cell contains one MAT gene, as well as two silent copies of the

mating-type sequences (*HML*α and *HMR***a**). *HML*α and *HMR***a** serve as donors for switching to the opposite mating-type when they are used as template for repair of a DSB induced at the MAT locus (reviewed in (11)).

1.2 Repair of DNA Damage

1.2.1 Repair of non-DSB Lesions

With the exception of DSBs, the other DNA lesions discussed previously are repaired by three main pathways: base excision repair, nucleotide excision repair, and mismatch repair. These pathways are described here in general terms, as they are not the primary focus of this thesis. Base excision repair (BER) typically repairs single-base modifications. The modified base is recognized and excised by a DNA glycosylase, generating an AP site. Processing of the sugar-phosphate backbone by a series of endonuclease, and in some cases exonuclease, activities (reviewed in (12)) generates a single-nucleotide gap (SSB), which is filled by a DNA polymerase and then ligated (Figure 1A).

Nucleotide excision repair (NER) removes bulky DNA adducts, as well as the DNA lesions induced by ultraviolet radiation. During NER, the damage-containing strand is cleaved by endonucleases on both sides of the damage, resulting in excision of a short segment of single-stranded DNA (ssDNA) (~ 25 nucleotides) containing the lesion. Like in BER, the resulting single-stranded gap is filled in by a DNA polymerase, then ligated (Figure 1B) (reviewed in (12)).

Mismatch repair (MMR) removes mismatched bases erroneously incorporated during DNA replication. As in NER, a short segment of ssDNA is excised. However, in contrast to NER, this excision is achieved by way of exonucleolytic degradation initiated from a nick introduced a short

distance away on either the 5′ or 3′ side of the lesion (Figure 1C). Finally, the resulting gap is filled in by a polymerase and ligated (reviewed in (12)).

As demonstrated above, single-strand nicks or gaps that arise as intermediates during excision repair and mismatch repair are simply repaired as those pathways progress. Top1-SSBs, however, must first be processed by Tdp1 (tyrosyl-DNA phosphodiesterase). Tdp1 removes Top1 from the 3′ terminus, allowing repair to proceed (7).

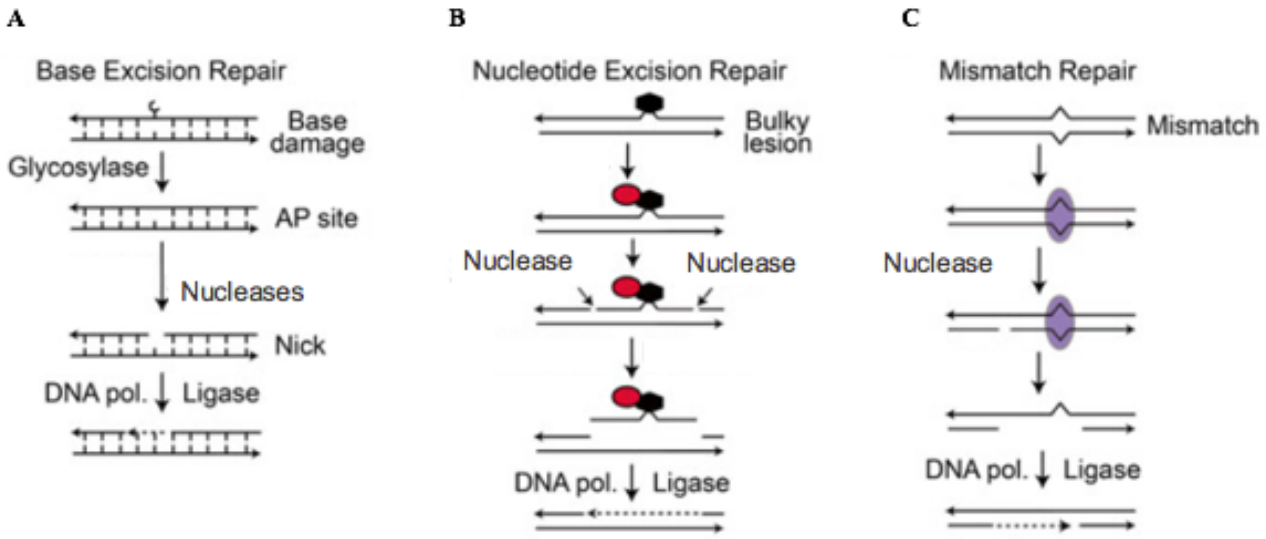

Figure 1. DNA repair by BER, NER, and MMR. (A) The BER pathway repairs single-base modifications. The modified base is removed by a glycosylase. Nucleases remove the deoxyribosephosphate, creating a single-nucleotide gap/nick. The gap is filled in and ligated. (B) The NER pathway handles "bulky" lesions. A lesion recognition protein (red oval) binds the lesion first. Endonucleases recruited to the lesion excise a short (~25-nucleotide) segment containing the lesion. The resulting gap is filled in and ligated. (C) The MMR pathway repairs mismatched bases. A lesion recognition protein complex (purple oval) binds to the lesion and creates a nick a short distance away from it. An exonuclease recruited by the recognition complex removes a short segment of DNA starting from the nick and ending just past the lesion. The resulting gap is filled in and ligated. Figure modified from (13).

1.2.2 Cellular Response to DSBs: The DNA Damage Checkpoint

DSBs are the most dangerous type of DNA lesions, as even one unrepaired DSB can have lethal consequences. In eukaryotes, DSBs that are not immediately repaired trigger the activation of a DNA damage checkpoint, an evolutionarily conserved, highly coordinated and complex signal transduction cascade. The process of checkpoint activation can be viewed as consisting of four general steps: the "sensing" or recognition of the DSB, recruitment and activation of the apical checkpoint kinases (Mec1 and Tel1), recruitment and activation of effector kinases (Rad53 and Chk1), and finally, modulation of downstream targets by Rad53 and Chk1. Downstream targets include, among others, proteins involved in cell cycle control and in DNA repair.

In *S. cerevisiae*, the first proteins to arrive at a DSB are the Ku70-Ku80 heterodimer and the Mre11-Rad50-Xrs2 (MRX) complex (14, 15), although MRX is the major DSB sensor (16) (Figure 2B). The MRX complex plays a critical role in the initiation of the DNA damage checkpoint by facilitating recruitment of the apical kinases Mec1 and Tel1. In contrast to a *tel1*Δ mutant, a *mec1*Δ mutant displays significant sensitivity to DSB-inducing agents (17), indicating that Mec1 is the primary apical kinase of the DNA damage checkpoint. Tel1 is, however, not completely dispensable for checkpoint activation since deletion of *TEL1* in a *mec1*Δ background causes enhanced sensitivity to DNA damaging agents (17).

While Tel1 is recruited to the DSB via a direct interaction with the C-terminus of Xrs2 (18), Mec1 localization to the break is contingent on MRX-mediated resection of the break. The details of DSB resection are discussed in Section 1.3.1 in the context of the role of resection in DSB repair. As resection proceeds, the ensuing ssDNA is bound by replication protein A (RPA) (Figure 2D). This RPA-coated ssDNA is then bound by three distinct complexes: "a checkpoint clamp loader" Rad24-Rfc2-5, a "checkpoint clamp" Rad17-Ddc1-Mec3, and the kinase complex Mec1-Ddc2 (Figure 2E).

As its name implies, the checkpoint clamp loader facilitates loading of the checkpoint clamp to the DNA end. The Mec1-Ddc2 complex, on the other hand, is recruited to RPA-coated ssDNA independently of either of the other two complexes (19, 20), although Ddc1 does stimulate Mec1 kinase activity (21).

The ability of Mec1 to phosphorylate and thereby activate the effector kinases Rad53 and Chk1 is promoted by mediator (or adaptor) proteins such as Rad9. There are three modes of recruitment for the *S. cerevisiae* checkpoint adaptor protein Rad9 to DSBs. Two of these modes involve histone modifications by the Mec1 and Tel1 kinases, and the histone methyltransferase Dot1. Mec1 and Tel1 both phosphorylate H2A on serine 129 (γ-H2A) (22), while Dot1 methylates H3 on lysine 79 (23). Rad9 interacts with these modified sites (Figure 2E) via its tandem BRCT domain (24) and Tudor domain (25), respectively. The third mode of Rad9 localization to DSBs is Mec1-dependent and involves the replication protein Dpb11. This function of Dpb11 requires two pairs of BRCT domains in the protein, one in its N-terminal region and one in its C-terminal region. Mec1 phosphorylates the checkpoint clamp protein Ddc1 (26, 27), and consequently, Dpb11 interacts with phosphorylated Ddc1 via its C-terminal tandem BRCT domain (28). Rad9 is normally phosphorylated by Cdk1 (29) and therefore exists in a partially phosphorylated state even in the absence of DNA damage. Cdk1-dependent phosphorylation of Rad9 at multiple serine and threonine residues in its C terminus (29) facilitates the interaction between Dpb11 and Rad9 (Figure 2E), bringing Rad9 into the vicinity of the break for its hyperphosphorylation by Mec1 and Tel1.

Hyperphosphorylated Rad9 serves as an adaptor or scaffold for activation of the effector kinase Rad53 (Figure 2F). The adaptor function of hyperphosphorylated Rad9 in Rad53 activation is two-fold: i) it brings Rad53, which interacts with hyperphosphorylated Rad9 via its FHA domains (30, 31),

into the vicinity of Mec1 for phosphorylation, and ii) it facilitates *in trans* autophosphorylation of Rad53 by bringing Rad53 molecules into close proximity with each other (32) (Figure 2F).

Activation of the second effector kinase Chk1, while also dependent on Rad9, proceeds by a slightly different mechanism than that of Rad53. In contrast to Rad53, which interacts only with Mec1-phosphorylated Rad9, Chk1 forms a constitutive DNA damage-independent complex with Rad9 (33). Phosphorylation of Rad9 at threonine 143 promotes this damage-independent interaction between Rad9 and Chk1 (33). Following DNA damage, the Rad9-Chk1 complex is recruited to the damage site, where Chk1 is then activated both by Mec1 phosphorylation and by autophosphorylation (34).

Once activated, the effector kinases are released from damage sites to mediate their effector functions. In response to a DSB, *S. cerevisiae* cells activate the G2/M checkpoint. The G2/M checkpoint prevents entry into mitosis in mammalian cells. In contrast, in *S. cerevisiae*, the G2/M checkpoint prevents the metaphase-to-anaphase transition (35). The Rad53 and Chk1 effector kinases inhibit the degradation of the securin Pds1 by the anaphase-promoting complex (36), thereby inhibiting sister chromatid separation. Cell cycle arrest provides time for DSB repair, after which the checkpoint is "turned off", allowing cells to re-enter the cell cycle.

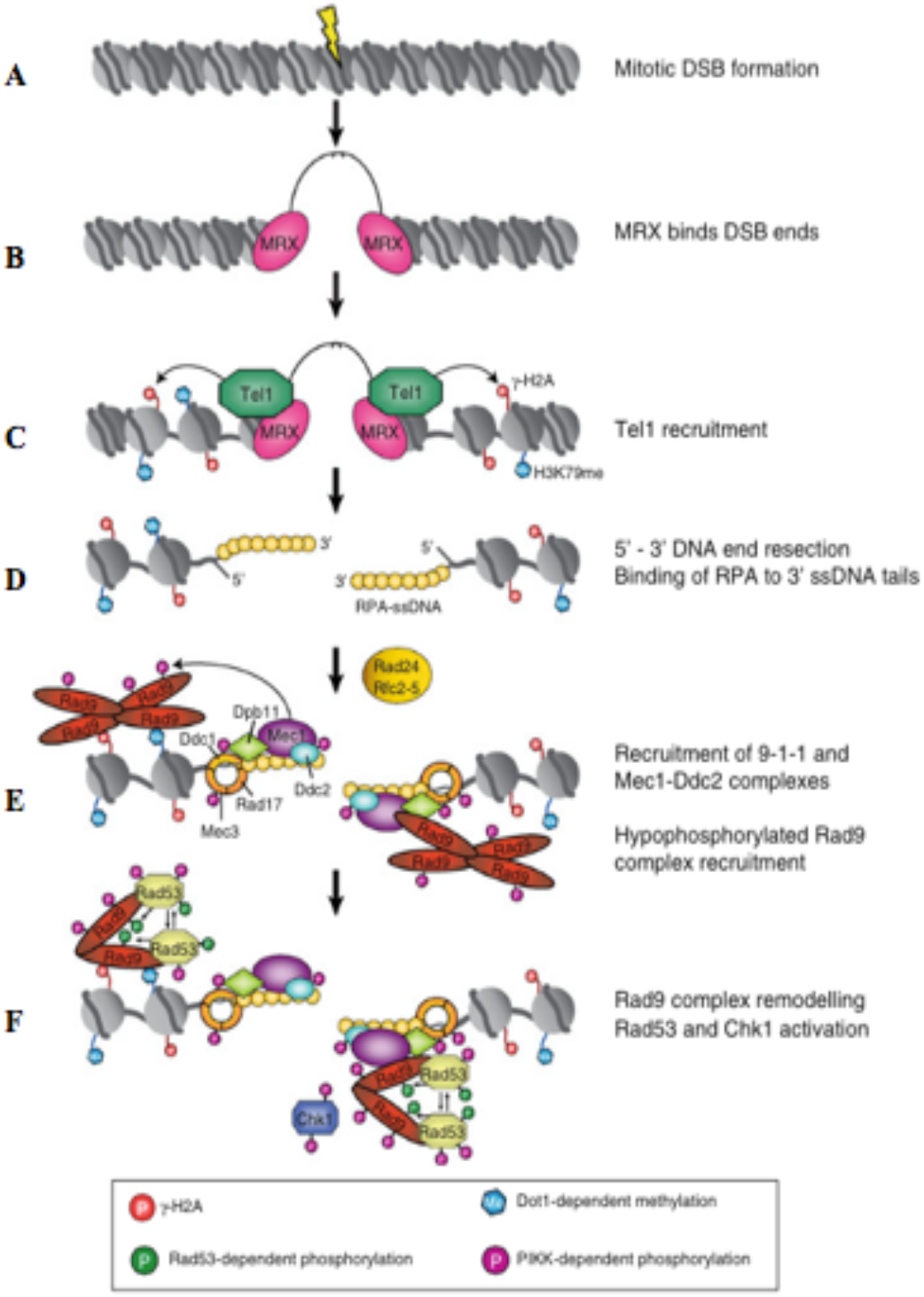

Figure 2. DNA damage checkpoint activation in *S. cerevisiae*. Following a DSB (A), DNA damage sensors Ku (not shown) and MRX arrive at the DSB (B). MRX directly recruits the checkpoint kinase Tel1 (C) and initiates DSB resection (D). Mec1, the primary checkpoint kinase in *S. cerevisiae*, binds to the RPA-coated ssDNA generated by resection (E). The adaptor protein Rad9, recruited to the DSB by both Tel1- and Mec1-dependent mechanisms, is phosphorylated by Mec1

(E). Mec1-dependent phosphorylation of Rad9 promotes its interaction with the primary effector kinase in *S. cerevisiae* Rad53 (F). The second effector kinase Chk1 is recruited to DSBs (F) via an interaction (not depicted here) with Rad9. The effector kinases are activated by Mec1 and by autophosphorylation (F) and activated effector kinases are released from the damage sites to mediate their effector functions. See text for detailed description of DNA damage checkpoint activation. Figure modified from (37).

1.2.3 DSB Repair

DSBs are repaired by two major pathways in *S. cerevisiae*: homologous recombination (HR) and non-homologous end joining (NHEJ). The HR pathway utilizes homologous sequences, preferably a sister chromatid in *S. cerevisiae*, as template for DSB repair. NHEJ, in contrast, repairs DSBs in the absence of any extensive homologous sequence, although short microhomologies flanking the DSB ends may be utilized. DSB repair by HR may proceed by one of four subpathways: double Holliday junction, synthesis-dependent strand annealing, break-induced replication, and single-strand annealing. Likewise, NHEJ consists of two subpathways: classical NHEJ (C-NHEJ) and microhomology-mediated end joining (MMEJ). These pathways have been studied and characterized using mainly two types of assays: plasmid end-joining assays (Figure 3A), and chromosomal DSB repair assays in which endonucleases are employed to create DSBs at specific sites in the genome (Figure 3B). In the following sections, I present a review of the DSB repair pathways in *S. cerevisiae*, including the factors involved in each pathway, and additionally discuss how some of these factors regulate the choice between HR and NHEJ in *S. cerevisiae.*

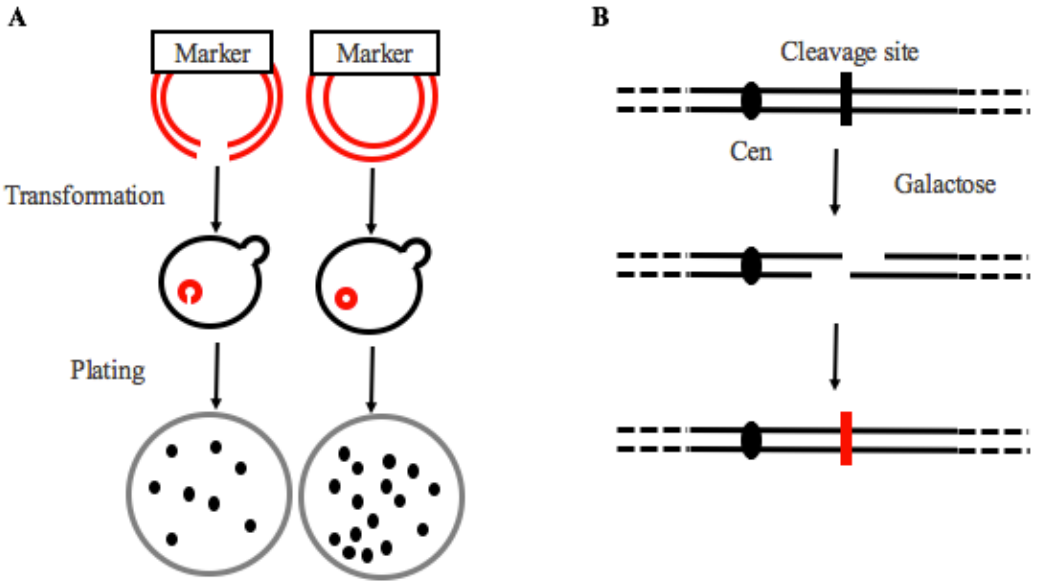

Figure 3. Commonly used DSB repair assays in *S. cerevisiae*. (A) Plasmid recircularization assay for analysis of NHEJ. A single-copy plasmid, containing an autonomously replicating sequence (ARS) (not shown) and a nutritional marker, is linearized with a restriction enzyme and transformed into yeast cells. In parallel, circular (uncut) plasmid is also transformed into yeast cells. Transformed cells are plated on media lacking the desired amino acid, and on which only cells expressing the marker gene can survive, to select for plasmid retention. Of the cells transformed with cut plasmid, only those that rejoin the plasmid by NHEJ survive on selective media. The frequency of NHEJ is expressed as the proportion of transformants recovered with cut plasmid relative to uncut plasmid. (B) Chromosomal DSB repair assay. Typically haploid strains utilized for this assay contain a gene for an endonuclease placed under the control of a galactose-inducible promoter (not shown). Plating to medium containing galactose induces expression of the endonuclease, which subsequently introduces a DSB at a unique recognition sequence (black rectangle). Constitutive expression of the endonuclease imposes the restriction that only cells that mutate or lose the recognition sequence survive the DSB. An NHEJ repair outcome involving mutations (red rectangle) in the cleavage site is shown here, although this assay has other iterations, for assaying homologous recombination, that usually involve the addition of regions of homology to mediate repair.

HR

Single-strand Annealing

All forms of homologous recombination repair are initiated by, and require, extensive resection of the 5′ strands of the DSB to generate long 3′ ssDNA tails and expose the homologous sequences needed for repair (reviewed in (38)). In cases where the homologous sequences utilized for repair are located on the same chromatid as the break, flanking the DSB ends, repair proceeds by the single-strand

annealing (SSA) pathway. During SSA, the homologous sequences anneal, followed by nucleolytic removal of the intervening non-homologous sequences. Finally, any gaps are filled in by DNA polymerase(s) and then sealed by ligase(s) (Figure 4A) (reviewed in (38)).

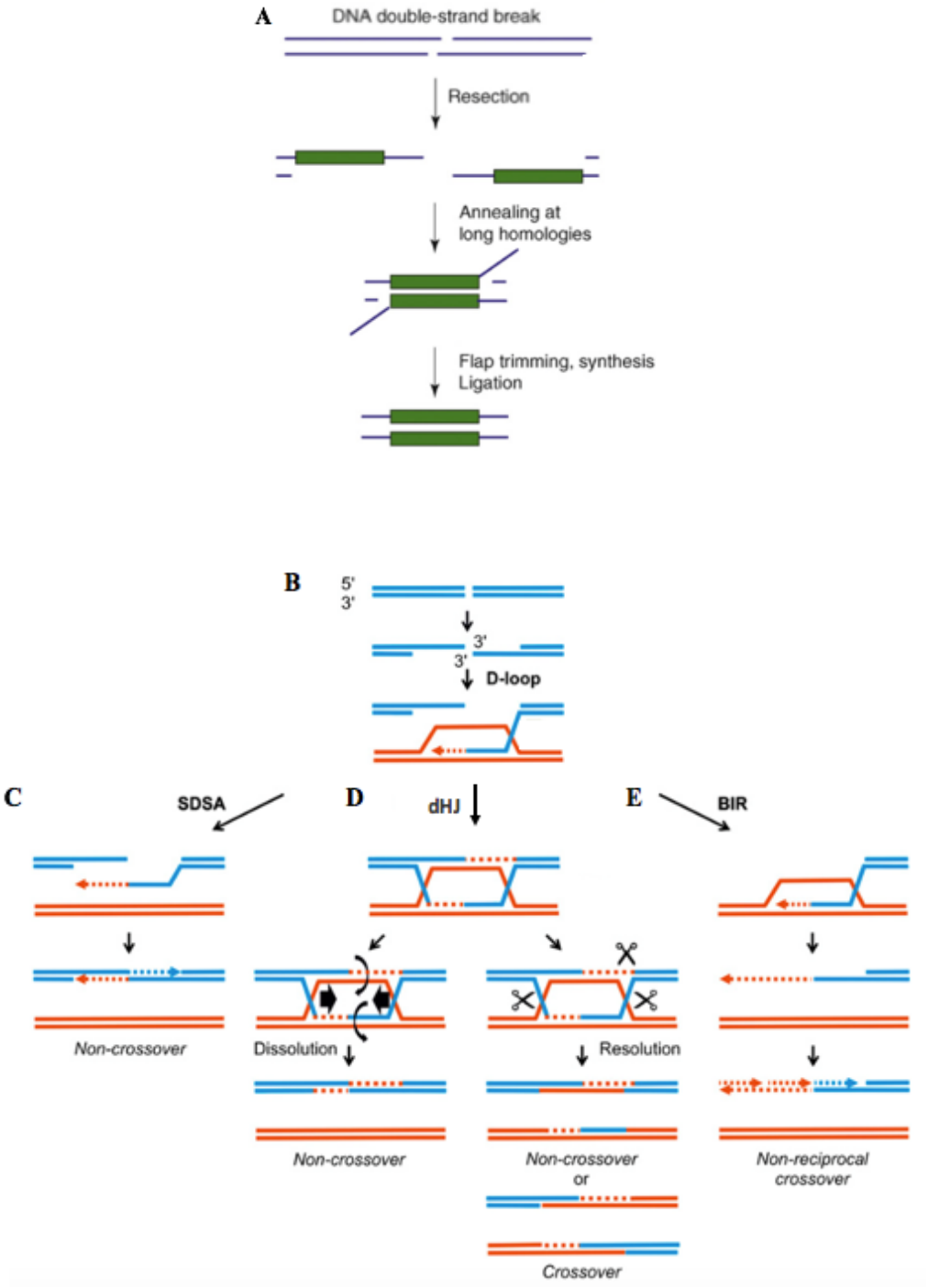

Figure 4. Homologous recombination pathways of DSB repair. (A) During SSA, long homologies (≥ 29 bp) that are exposed after resection anneal, and the intervening non-homologous sequences are removed. Repair is completed by fill-in synthesis and ligation. Figure modified from (39). (B-E) HR pathways involving strand invasion. (B) Following resection, the 3′ ssDNA tail invades the donor chromosome forming a D-loop structure. (C) The SDSA pathway. Following strand invasion and D-loop formation, DNA synthesis initiates from the invading 3′ end. The newly synthesized strand is unwound from the donor template and anneals to the ssDNA on the non-invading end of the break and serves as template for fill-in synthesis of its complementary strand. SDSA always results in a non-crossover (NCO) outcome. (D) The dHJ pathway involves strand invasion and D-loop formation, DNA synthesis from the invading 3′ end, and invasion of the other 3′ end (second-end capture). These processes result in the formation of a double Holliday junction (dHJ) structure that is either dissolved or resolved to generate the repair products. dHJ dissolution results in a NCO outcome, while resolution produces both NCO and CO products. (E) One-ended DSBs are channeled into the BIR pathway. DNA synthesis initiates from the invading 3′ end and proceeds to the end of the donor chromosome. The newly synthesized strand is extruded and serves as template for synthesis of its complementary strand. Figure modified from (40).

The recombination protein Rad52, required for all forms of homologous recombination repair, promotes SSA by facilitating strand annealing of the homologous sequences (reviewed in (38)). As little as 29 bp of homologous sequence is sufficient to stimulate SSA in *S. cerevisiae*, although the efficiency of SSA rises as the length of homology increases (41). Additionally, the role of Rad52 in strand annealing becomes less important with increasing homology length (42), possibly reflecting the ability of longer sequences to spontaneously form more stable DNA duplexes and therefore compensate for absence of Rad52 activity.

Cleavage of the non-homologous sequences is mediated by Rad1-Rad10, a structure-specific 3′ flap endonuclease (43, 44). Although Rad1-Rad10 is ultimately directly responsible for flap cleavage, several other proteins (Msh2, Msh3, Saw1, Slx4) are important for flap cleavage as well (45, 46). The mismatch repair proteins Msh2 and Msh3 form a heterodimer that binds to a variety of branched DNA structures, including dsDNA-ssDNA junctions (47). During SSA, the Msh2-Msh3 heterodimer is thought to stabilize the dsDNA-ssDNA junctions formed after the homologous sequences anneal, thereby allowing the recruitment and function of the other proteins involved in flap cleavage (45).

Saw1, identified in a screen for yeast mutants defective in SSA (46), interacts with Rad1 and promotes Rad1-Rad10 recruitment to the 3′ flaps (46). Flap cleavage by Rad1-Rad10 is also stimulated by the Slx4 protein (48, 49). Slx4 typically interacts with Slx1, a structure-specific endonuclease, to form a complex with a preference for cleaving branched DNA structures (50) such as those that arise during homologous recombination. However, an *slx1*Δ mutant is not defective in SSA, indicating that Slx4 plays a role in 3′ flap cleavage during SSA that is distinct from its shared functions with Slx1 (46). Slx4 is targeted to 3′ flaps by an as yet unknown mechanism, where it interacts with Rad1-Rad10 to stimulate flap cleavage (46). Furthermore, this stimulatory function requires the DNA damage-dependent phosphorylation of Slx4 by Mec1 and Tel1 (49). How Slx4 stimulates flap cleavage by Rad1-Rad10 remains to be determined. It has been proposed that Slx4 may regulate the catalytic activity or substrate specificity of Rad1-Rad10, or could modify DNA substrates to render them more accessible for efficient cleavage (49).

Strand Invasion by the 3′ ssDNA Tail Precedes Other Forms of HR Repair

When the homologous sequence utilized as the template or donor for repair is located on a separate chromosome, the 3′ ssDNA tail invades the donor chromosome (Figure 4B) in a process dependent on Rad52 and on the Rad51 recombinase, a protein with DNA-dependent ATPase activity (reviewed in (38)). Following resection, the 3′ ssDNA tail is bound by the replication protein A (RPA) complex. RPA is thought to stabilize the ssDNA, preventing the formation of secondary structures that could inhibit the subsequent steps of repair (38). Subsequently, Rad52 (51, 52), aided by two other recombination proteins (Rad55 and Rad57) (53), facilitates the replacement of RPA with the Rad51 recombinase. Rad51 binds along the ssDNA, forming a nucleoprotein filament that then catalyzes the homology search and strand invasion (54, 55). Rad54, a homolog of the Swi2/Snf2 family of ATP-

dependent translocases, is required for successful recombination and functions at the postsynaptic stage (after strand invasion by the Rad51 nucleofilament) (56). *In vitro* assays demonstrate that the Rad54 ATPase activity stimulates the dissociation of Rad51 from dsDNA, leading to the suggestion that Rad54 promotes Rad51 turnover during the postsynaptic stage so as to allow subsequent repair steps to occur. Rad51, in an ATPase-dependent manner, also self-regulates its postsynaptic dissociation, although to a lesser extent than Rad54 (57).

During strand invasion, the Rad51-ssDNA nucleofilament anneals with the complementary strand of the donor chromosome, while displacing the non-complementary strand. The resulting structure, consisting of a region of heteroduplex DNA and displaced ssDNA, is termed a displacement loop (D-loop) (Figure 4B), and the events that occur after D-loop formation define three different types of HR pathways (reviewed in (38)). When both ends of the DSB contain sequences with homology to the donor chromosome, repair proceeds by the double Holliday junction (dHJ) or synthesis-dependent strand annealing (SDSA) pathways (38). When only one end of the DSB contains sequences with homology to the donor chromosome, repair proceeds by the break-induced replication (BIR) pathway (38).

Double Holliday Junction (dHJ) and Synthesis-dependent Strand Annealing (SDSA)

The dHJ and SDSA pathways employ either a homologous chromosome or a sister chromatid as the template for repair. These pathways may be accompanied by gene conversion (GC) (reviewed in (38)), a non-reciprocal transfer of genetic information from a donor to a recipient allele such that both loci become identical (58). GC is, in theory, more possible when a homologous chromosome is used as the repair template due to the likelihood that sequence polymorphisms exist near the site of recombination. Although much less likely, a sister chromatid may also contain a different allele at the

repair locus if for example, any mismatched base pairs that occur during DNA replication are inaccurately repaired by the MMR machinery. *S. cerevisiae* preferentially employs a sister chromatid as the repair template (59), a choice thought to be regulated by cohesins (60). The acetylation state of H3 also seems to regulate template choice in *S. cerevisiae* (61).

In the dHJ and SDSA pathways, strand invasion is followed by the initiation of DNA synthesis using the invading 3′ end as primer (reviewed in (38)). The replicative polymerases Polδ and Polε function in DNA synthesis during these modes of repair (reviewed in (38)). However, because dHJ and SDSA involve synthesis of relatively short regions of DNA, none of the other components of the replisome, including the processivity factor PCNA, are involved in DNA synthesis in these pathways (reviewed in (38)). A distinguishing feature of the dHJ pathway, in comparison to the SDSA pathway (Figure 4C), is that the 3′ ssDNA from the other end of the DSB also invades the donor template, a process known as second-end capture (reviewed in (38)) (Figure 4D). Upon completion of DNA synthesis, the free ends are ligated resulting in the formation of a double Holliday junction (dHJ) structure (reviewed in (38)). Once formed, the dHJ may be dissolved or resolved (Figure 4D). Dissolution is catalyzed by a "dissolvasome", consisting of a helicase and a topoisomerase. The helicase (Sgs1 in *S. cerevisiae*) acts by convergently migrating the HJs until they fuse into a hemicatenane (62). The topoisomerase (Top3 in *S. cerevisiae*), aided by a third protein Rmi1, unwinds the hemicatenane resulting in the formation of non-crossover (NCO) products (62). Resolution of dHJs in budding yeast is catalyzed by the Mus81-Mms4 endonuclease (63). Resolution produces both NCO and CO products, depending on which pair of strands is cleaved (64).

As previously noted, the SDSA pathway does not involve second-end capture. Instead, the newly synthesized strand is unwound from the donor template, and anneals to the ssDNA on the non-invading end of the DSB (Figure 4C). Gap fill-in synthesis and ligation complete the repair process. In

contrast to dHJ, SDSA always results in an NCO outcome (reviewed in (38)). In *S. cerevisiae*, HR intermediates accumulate *in vivo* only in an *rmi1* mutant and these intermediates are processed by Mus81-Mms4 (63). In the absence of Sgs1 or of another helicase Srs2, crossover frequencies, measured in an an interchromosomal HR assay, increase 2- to 3-fold (65). Taken together with the observations made in different organisms that crossovers associated with mitotic recombination are rare (66-68), these findings indicate that the SDSA and/or dHJ dissolution pathways process the majority of HR intermediates.

Break-induced Replication (BIR)

One-ended DSBs (Figure 4E) are channeled into the BIR pathway, wherein DNA synthesis from the invading 3′ end proceeds all the way to the end of the donor chromosome (Figure 4E). Replication fork assembly (69), to accommodate long-range synthesis, distinguishes BIR from other HR pathways. While proteins present at an active replication fork are required, mutations affecting two components of the pre-replication complex (the origin recognition complex (ORC) and Cdc6) do not impair BIR in *S. cerevisiae* (69). A fundamental difference between conventional DNA replication and BIR is that the latter involves conservative DNA synthesis, as determined by analysis of incorporation of the thymidine analog 5-bromo-2′-deoxyuridine (BrdU) into newly synthesized DNA during BIR (70, 71). BrdU is preferentially incorporated into both strands of the recipient chromosome, supporting a model in which, following extension of the original replication fork to the end of the chromosome, the invading strand is extruded and subsequently serves as template for synthesis of its complementary strand (70, 71) (Figure 4E).

C-NHEJ

The classical NHEJ pathway, henceforth referred to simply as NHEJ, involves synapsis of the DSB ends, end-processing (in cases where the DSB ends are incompatible and cannot be directly religated), and end-ligation (Figure 5A and 5B). Three main complexes, homologs of which are found

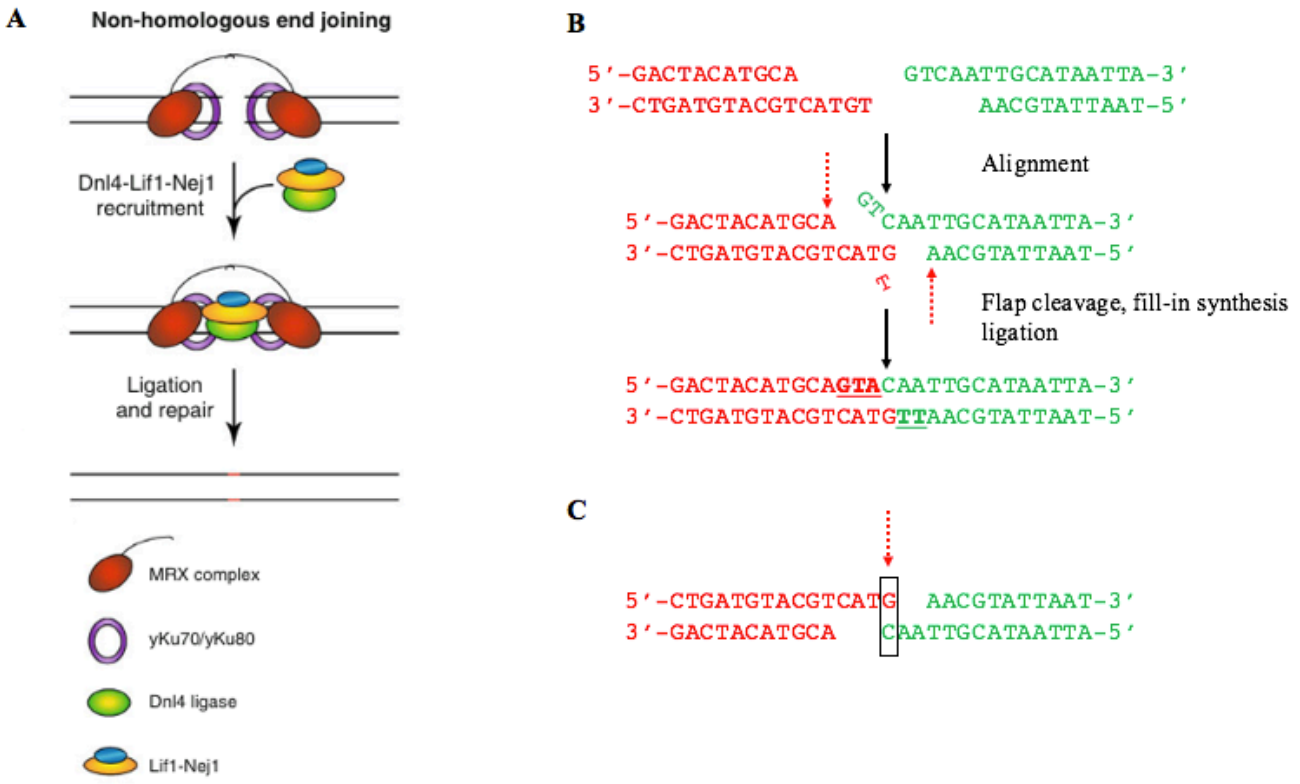

Figure 5. DSB repair by NHEJ. (A) Yku and MRX arrive first at a DSB. The MRX complex bridges the DSB ends, and both Yku and MRX promote recruitment of the ligase complex to the DSB. Figure modified from (37). (B) An example of NHEJ repair involving end-processing of two incompatible ends and showing all of the three possible steps that can occur during end-processing: alignment, flap cleavage, and fill-in synthesis. The nucleotides on both sides of the break are represented by different colors (red and green). The ends align by base pairing between complementary nucleotides and the intervening non-homologous sequences (flaps) are removed. Repair is completed by gap fill-in synthesis and ligation. Dashed red arrows indicate the 3′ ends from which fill-in synthesis initiates. Bold, underlined nucleotides represent filled-in nucleotides. (C) For ends with 3′ overhangs, fill-in synthesis initiates from 3′ ends with relatively unstable template-primer hybrids (dashed red arrow/black rectangle). Such ends are not optimal substrates for replicative polymerases and demonstrate a strong requirement for Pol4 for fill-in synthesis. In comparison, for ends with 5′ overhangs, fill-in synthesis initiates from 3′ ends with relatively stable template-primer hybrids (dashed red arrow in B). As a result, such ends are markedly less dependent on Pol4 for fill-in synthesis than ends with 3′ overhangs.

in mammalian cells, are required for NHEJ in *S. cerevisiae*: the Yku70-Yku80 heterodimer, the MRX complex, and the DNA ligase IV complex (Dnl4-Lif1). Recruitment of these complexes to DSBs is temporally regulated, with Yku70-Yku80 and MRX arriving at approximately the same time, followed by Dnl4-Lif1 (14). As discussed below, interactions among members of each complex facilitate the recruitment and stable retention of the complete NHEJ complex at DSBs.

The yeast Yku70-Yku80 (Yku) heterodimer is a multifunctional complex, with roles in NHEJ (72, 73), telomere length maintenance (72, 74, 75), and telomeric silencing (75). Yku70 and Yku80 were both identified after their mammalian counterparts had already been described (72, 76), and given the established role of mammalian Ku in DSB repair during V(D)J recombination (77, 78) (Section 1.1), several groups sought to examine the role of Yku70 and/or Yku80 in DSB repair. A potential role for Yku70 in NHEJ was uncovered when it was demonstrated that the IR and MMS sensitivities of a *rad52*Δ mutant were further exacerbated by deletion of *YKU70* or *YKU80* (72, 79). *yku* mutants by themselves were not sensitive to the DNA-damaging agents, indicating that Yku functioned in an alternate Rad52-independent pathway for DSB repair (72, 79). Several laboratories, using a plasmid recircularization assay (Figure 3A), demonstrated that this pathway was indeed NHEJ, as deletion of *YKU70* or of *YKU80* resulted in severe (8- to 400-fold) defects in recircularization of linearized plasmids with complementary overhangs (72, 73). A role for Yku in NHEJ was also demonstrated for chromosomal DSBs induced by **HO**mothallic switching (HO) endonuclease. Cell survival following induction of a DSB (at the *MAT*α locus) by HO endonuclease in a strain lacking *RAD52* (to eliminate the HR pathways) was reduced by 8-to 13-fold after deletion of *YKU70* or *YKU80* (73).

Analysis of the repair junctions in plasmids recovered from WT cells revealed that the majority of plasmids (upwards of 90%) were precisely joined, as evidenced by the ability to recleave the plasmid using the restriction enzyme that was originally employed for plasmid linearization (72, 73). In

contrast, the majority of plasmids recovered from *ku70*Δ or *ku80*Δ mutants were imprecisely ligated. These imprecisely joined plasmids contained deletions (ranging in size from 6 to 811 bp) and had been rejoined at short, direct repeats (*i.e.* microhomologies) of 3-16 bp (72, 73). These findings suggested that Yku protected DSB ends from an error-prone repair mechanism (later classified as microhomology-mediated end joining), possibly by protecting DSB ends from resection. Much more is now known about the role of Yku in NHEJ. Yku does indeed prevent resection at DSB ends (80), favoring NHEJ over HR. Yku, through interactions between the C terminus of Yku80 and Dnl4, facilitates DNA ligase IV recruitment to DSBs (81), and also stimulates ligase activity (82). Interestingly, Yku70 is largely responsible for the NHEJ functions of the Yku heterodimer, whereas Yku80 is largely responsible for its functions in telomere maintenance and telomeric silencing (83, 84). In support of these findings, it has been demonstrated that Ku slides onto DNA ends as a preformed ring, with the Ku70 side facing the DNA terminus when bound to a DNA end, and the Ku80 side facing inward, toward the telomere, when bound to telomeric DNA (85).

A role for the MRX complex in NHEJ was first uncovered using a chromosomal DSB repair assay. NHEJ repair of a DSB, induced at *MAT*α by HO endonuclease, was assayed in a strain in which the *HML*α and *HMR***a** loci (Section 1.1) were deleted to eliminate HR repair by gene conversion (86). In this context, DSB survival was reduced by approximately 70-fold in *mre11*Δ*, rad50*Δ, and *xrs2*Δ mutants (86). A constraint imposed on this assay is that DSB survival is contingent on elimination of the HO endonuclease recognition site. As a result, only imprecise repair events are recovered from this assay. In the WT strain, 78% of the events contained a 2 bp insertion (+CA) near the HO cleavage site, while 11% contained a 3 bp deletion (-ACA) near the cleavage site (86). Interestingly, deletion of *MRE11*, *RAD50*, and *XRS2* decreased the +CA events by 5- to 78-fold, whereas the -ACA events were increased by approximately 7-fold, suggesting a role for MRX in promoting insertional events (86).

Although Mre11 possesses nuclease activities, these activities are dispensable for NHEJ. The *mre11-D16A*, *mre11-D56N*, and *mre11-H125N* mutants, all of which lack detectable nuclease activity *in vitro* (87, 88), are not impaired in plasmid recircularization by NHEJ (89). The MRX complex is now believed to facilitate synapsis/end-bridging by keeping the DSB ends in proper alignment for religation by the DNA ligase IV complex (90). A crystal structure of the human Mre11-Rad50 dimer provides the evidence to support this proposed role of the MRX complex. The N and C termini of each Rad50 molecule, which together form a globular DNA-binding "head", are separated by long antiparallel coiled-coil domains. Zinc-hook motifs at the tips of the coiled-coil domains in Rad50 monomers interlock through coordinated binding of a Zn^{2+} ion to facilitate Rad50 dimerization (91). This finding supports a model in which Rad50 molecules bound to both DSB ends interact to bridge the ends and promote NHEJ (Figure 5A).

Mre11 and Xrs2 perform additional functions in NHEJ besides facilitating end-bridging. Mre11 stimulates the ligase activity of Dnl4 (82). Xrs2 promotes recruitment of Dnl4-Lif1 via interactions between residues R32, S47, R48, and K75 in its N-terminal FHA domain, and residues T417 and T387 in the C terminus of Lif1. Mutations of the Xrs2 FHA residues reduce NHEJ by 14- to 27-fold, and mutations of the Lif1 C terminal residues reduce NHEJ by 4- to 10-fold (81). Paradoxically, mutations in MRX also impair DSB repair by homologous recombination (92), suggesting that the DSB repair defects in these mutants may reflect a general function for the complex in checkpoint activation (Section 1.2.2), rather than a specific role in NHEJ or HR. On the other hand, purified MRX stimulates intermolecular ligation by Dnl4-Lif1 *in vitro* (82), suggesting that MRX plays a direct role in NHEJ. Nonetheless, the NHEJ deficiency in MRX mutants could be due in part to a defective checkpoint and also in part to a direct defect in NHEJ.

The Dnl4-Lif1 complex catalyzes the final religation step of NHEJ. Interactions with Yku80 and Xrs2 (see above) promote Dnl4-Lif1 recruitment to DSBs (81, 93), although Dnl4 conversely stabilizes Yku80 at DSBs . Yku binding, assayed by a variant of chromatin immunoprecipitation (ChIP) conducted without the formaldehyde-crosslinking step, was significantly reduced in the absence of *DNL4* or of *LIF1* (15). Like Yku, Dnl4-Lif1 also inhibits DSB resection, thereby suppressing HR (15). Dnl4-Lif1 also promotes the recruitment of the end-processing factors Pol4 and Rad27 (see below) to DSBs and additionally stimulates their end-processing activities (94).

The three complexes discussed above are sufficient for rejoining of DSBs with compatible ends. However, where non-cohesive ends are generated, the ends must be processed before religation can occur, resulting in insertions and/or deletions (1-4 base pairs). End-processing is typically initiated via base pairing between extremely short (0-4 nucleotides) microhomologies on both sides of the break (reviewed in (39)). This "alignment" step generates intermediates that require gap filling and/or flap cleavage (Figure 5B) to generate a ligatable structure. In *S. cerevisiae*, DNA polymerase IV (Pol4), a member of the X family of DNA polymerases that also includes mammalian terminal transferase, Polβ, Polλ, and Polμ, fulfills the gap fill-in function during processing of non-cohesive ends (95, 96). Purified Pol4 does not exhibit nuclease activity *in vitro*, however, suggesting that its activity could be coupled to that of an unidentified nuclease (96).

Two nuclease(s) involved in end-processing during NHEJ have been characterized. The 5′ flap nuclease Rad27 processes most, but not all, 5′ flap joins, suggesting the existence of additional 5′ flap nucleases in *S. cerevisiae* (97). The proofreading 3′-5′ exonuclease activity of Pol2, the catalytic subunit of Polε, processes some of the 3′ flap joins in *S. cerevisiae*, again suggesting the existence of additional 3′ flap nuclease(s) (98). Despite its involvement in 3′ flap cleavage during SSA, the Rad1-Rad10

endonuclease does not appear to be involved in NHEJ, since its absence does not affect the recovery of ligation products resulting from 3′ flap joins (96).

Another factor required for NHEJ in *S. cerevisiae* is Nej1. Nej1 was originally identified as a haploid-specific regulator of NHEJ (99, 100). In haploid cells, Nej1 participates in multiple steps during NHEJ. Nej1 promotes stable binding of Yku to DSBs *in vivo* and stimulates intermolecular ligation by Dnl4-Lif1 *in vitro* (101). Additionally, Nej1 interacts with Pol4 and Rad27, recruiting them to DSBs, and stimulating their end-processing activities (94).

Studies of repair of DSB ends with varying structures (ends with 3′ or 5′ overhangs, or blunt ends) have identified differential requirements for some of the factors discussed above at these ends. Rad27, by virtue of being a structure-specific 5′ flap endonuclease, only processes joins with 5′ flaps. DSBs with 3′ overhangs are strongly dependent on Pol4 for repair, while the absence of Pol4 does not significantly impact NHEJ repair of DSBs with 5′ overhangs (95). Pol4 and other X family DNA polymerases are unique in their ability to successfully prime DNA synthesis from a short, unstable primer-template hybrid, explaining the larger requirement for Pol4 at 3′ versus 5′ overhangs (95) (Figures 5B and C).

MMEJ

DSB repair by MMEJ proceeds via annealing of microhomologies (5-25 nucleotides) (39) flanking the DSB ends (Figure 6A). Often referred to interchangeably with the term alternative non-homologous end joining, MMEJ is genetically distinguishable from NHEJ in that it is Yku-independent. Resection is a requisite for MMEJ since it exposes the microhomologies required for MMEJ (reviewed in (39)). After the homologous sequences anneal, the intervening non-homologous flap sequences are removed by a nuclease. Hence, deletions, the size of which depends on the distance

of the microhomologies from the DSB ends, are a hallmark of MMEJ. Following flap cleavage, gap fill-in (by a DNA polymerase) and ligation complete the repair process (reviewed in (39)) (Figure 6A).

The genetic requirements for MMEJ in *S. cerevisiae* were elucidated using a variation of the HO endonuclease-induced chromosomal DSB repair assay described in Figure 3B (Figure 6B; (102)). The WT strain for this assay contained two inversely oriented HO endonuclease recognition sites separated by a *URA3* marker. Cleavage by HO endonuclease generated a *URA3*-containing fragment

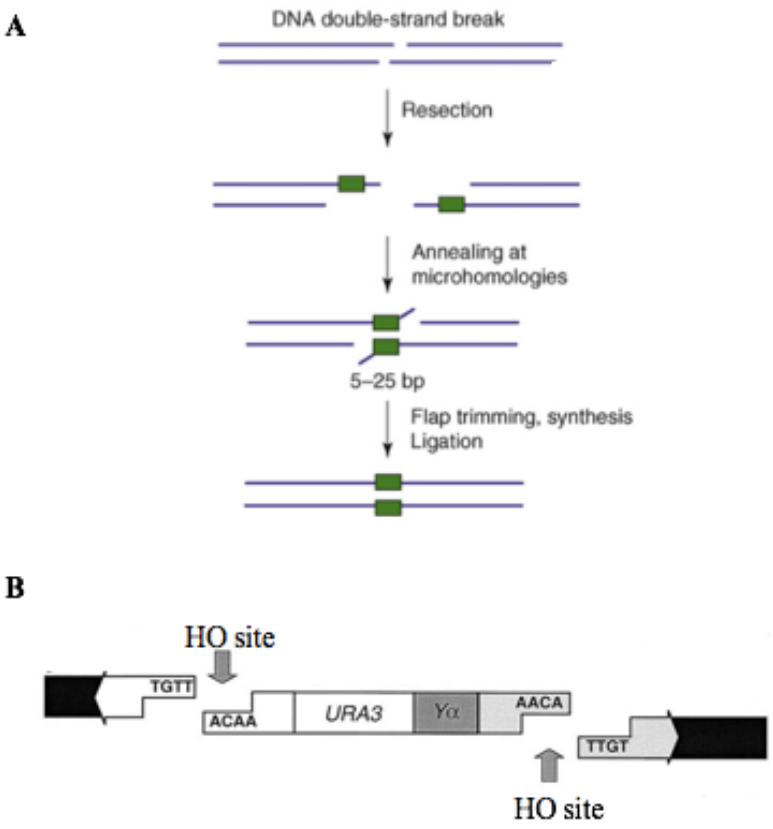

Figure 6. DSB repair by MMEJ. (A) The MMEJ repair pathway. As in SSA, the steps involved in MMEJ are DSB resection, microhomology annealing, flap cleavage, fill-in synthesis, and ligation. In contrast to SSA however, MMEJ utilizes shorter homologies and whether or not Rad52 stimulates the annealing step is still controversial. Figure modified from (39). (B) MMEJ repair assay utilized in *S. cerevisiae*. HO endonuclease introduces DSBs at two inverted HO recognition sites resulting in the generation of ends with incompatible overhangs. In this assay, ~85% of cells repair the breaks by MMEJ. Figure modified from (102).

and overhangs with non-complementary sequences. Of the cells that survived the DSBs, 16% retained the *URA3* marker, presumably by imprecise NHEJ of both HO cleavage sites or from rare instances of non-cleavage by HO endonuclease. The remaining 84% of survivors were ura-, and contained deletions of up to 302 bp. Additionally, 80% of the ura- survivors (thirty-seven of 46 total) had utilized perfect or imperfect microhomologies of 8-10 nucleotides for repair. Given that the majority of survivors repaired the DSBs by MMEJ, this assay system proved extremely useful for dissecting the genetic requirements for MMEJ in *S. cerevisiae*.

MMEJ in *S. cerevisiae* is Yku-independent. In fact, the frequency of MMEJ increases in a *yku70*Δ mutant, with all survivors repairing the DSBs by MMEJ (102). These findings suggest that Yku actually inhibits MMEJ, very likely by its ability to restrict 5′ strand resection at DSBs. In contrast, deletion of either *MRE11* or *RAD50* in the Yku-deficient background severely impaired MMEJ, implicating the MRX complex as an important factor for MMEJ in *S. cerevisiae* (102). In a subsequent study, the requirement for the MRX complex in MMEJ was attributed to the nuclease activity of Mre11 (103). MMEJ was severely compromised in strains expressing the *mre11-H125N* allele that is nuclease-defective but retains the ability to form an intact MRX complex (103). Ku and MRX therefore function antagonistically to regulate the resection step of MMEJ.

In *S. cerevisiae*, the role of Rad52 in the strand-annealing step of MMEJ remains controversial. Whereas some studies demonstrated that MMEJ was not impaired in a *rad52*Δ mutant, other studies revealed a dependence on Rad52 for MMEJ. Interestingly, microhomology length appears to be a contributing factor in whether or not Rad52 is required for MMEJ. Rad52 is required for MMEJ events that utilize ≥ 15 bp of microhomology, but inhibits events utilizing < 15 bp of microhomology (104). These findings suggest that Rad52 plays a complex role in MMEJ, depending on the availability and length of microhomology at DSBs.

As in SSA, flap cleavage during MMEJ is carried out by the Rad1-Rad10 nuclease. MMEJ is strongly impeded, but not completely abolished, in the absence of Rad1 and/or Rad10, indicating that one or more nucleases can catalyze flap cleavage in the absence of Rad1-Rad10 (103). Similarly, gap fill-in synthesis during MMEJ appears to be carried out by several functionally redundant polymerases. Deletion of *POL32* (encoding a subunit of the replicative polymerase Polδ), *POL4*, *RAD30* (encoding the translesion polymerase Polη), and *REV3* (encoding the catalytic subunit of Polζ translesion polymerase) all result in reduced MMEJ efficiency. Moreover, strains carrying deletions of three of these genes exhibit an even greater reduction in MMEJ compared to the single mutants, suggesting functional redundancy among these polymerases in promoting gap fill-in synthesis during MMEJ (103). Finally, the ligation step of MMEJ is only partially dependent on Dnl4-Lif1 indicating that some other ligase, most likely the replicative ligase Cdc9, also functions in MMEJ (103).

In summary, although the MMEJ pathway has several components in common with the NHEJ and HR pathways, MMEJ can be distinguished from NHEJ by its lack of dependence on Ku, and in some cases, from HR, by its lack of dependence on Rad52. Given that MMEJ repair only occurs with considerable frequency in the absence of Ku and/or using assay systems designed to specifically study MMEJ, it may be tempting to speculate that MMEJ, especially given its highly error-prone nature, is a backup mechanism for DSB repair. However, MMEJ is active even in the presence of unperturbed HR and NHEJ pathways, suggesting that MMEJ may be a bona fide, though less used, repair pathway (105, 106).

1.3 Resection is a Major Factor that Regulates DSB Repair Pathway Choice

NHEJ and HR have different repair outcomes: simplistically, the NHEJ pathways are typically referred to as error-prone, whereas HR, specifically by the gene conversion pathway, is typically

referred to as error-free. Complicating this view, however, is the fact that large mammalian genomes contain significant amounts of repetitive sequences. For example, repetitive sequences comprise an estimated 45-50% of the human genome, although this number may be as large as 66-69% (107, 108). For mammalian cells then, DSB repair by HR presents numerous possibilities for the generation of mutations, like translocations and large deletions, if ectopic sequences, rather than the homologous sequences on a sister chromatid or homologous chromosome, are utilized for repair (109). Therefore, for organisms with larger genomes, NHEJ, with its small (1-4 bp) deletions, may be preferred, whereas for organisms with smaller, less repetitive genomes, HR may be the more advantageous choice for repair. Still, the NHEJ and HR repair pathways can co-exist in a cell, begging the question: how does a cell decide between NHEJ and HR?

Several factors have been reported or suggested to contribute to repair pathway choice. Donor availability for HR could be a regulating factor in pathway choice. Yeasts like *S. cerevisiae* preferentially utilize HR for repair , while the repair pathway of choice in mammalian cells is NHEJ. Since *S. cerevisiae* cells actively proliferate under typical laboratory conditions, the homologous templates needed for repair can become available in the S, G_2, and M phases of the cell cycle. Most somatic mammalian cells, on the other hand, spend a majority of their time in the G_0 and G_1 phases of the cell cycle (110) where resection is limited (discussed below), thereby leaving NHEJ as the most likely option for DSB repair. In mammalian cells, repair kinetics have been proposed as another factor regulating pathway choice. The proposed model suggests that NHEJ factors are active at DSBs first, even in G_2 cells (111). Any persistent DSBs then undergo resection and are channeled into the HR pathway (111). Cell type (haploid versus diploid in yeast) (99, 100) and the acetylation/deacetylation state of H3 have been reported to influence pathway choice (61). The structure of the DSB ends also seems to influence pathway choice. A recent publication demonstrated that DSBs with “clean” ends

are preferentially directed to NHEJ, whereas ones with chemically modified "dirty" ends are channeled to HR (112).

Arguably, no other topic has received more attention, especially in recent years, than DSB resection. DSB resection is a complexly regulated process. Nevertheless, a point of consensus is that the NHEJ pathway is favored by little to no resection, while the MMEJ and HR pathways are favored by intermediate and extensive resection, respectively. Next, I review resection and its regulation in *S. cerevisiae*, highlighting along the way the names of the mammalian orthologs of the *S. cerevisiae* proteins. I conclude this section with a review of the fairly recently discovered function of the Rif1 protein in DSB resection and repair.

1.3.1 DSB Resection

DSB resection is a cell cycle-regulated process that occurs to a limited extent in the G_1 phase of the cell cycle when Cdk1 (the master cell cycle regulator in *S. cerevisiae*) activity is low, but occurs more extensively in the S and G_2/M phases when Cdk1 activity is high (113, 114). DSB resection in *S. cerevisiae* is initiated by Sae2 (CtIP in mammalian cells) and MRX (MRN in mammalian cells). Together with Sae2, MRX initiates short-range resection of the 5′ strands (Figure 7). Interestingly, though an endonuclease itself, the role of Sae2 in the initiation of resection at DSBs appears to be stimulation of Mre11 endonuclease activity (115). The Mre11 endonuclease nicks the 5′ strand approximately 300 nucleotides from the DSB end and then its exonuclease activity removes nucleotides in the 3′ to 5′ direction, toward the DSB end (Figure 7) (116). Long-range resection is achieved by the concerted action of two highly processive nucleases Exo1 (EXO1 in mammalian cells) and Sgs1-Dna2 (BLM-DNA2 in mammalian cells), which continue resection from the free 5′ ends generated by the Mre11 endonuclease (Figure 7) (116-118).

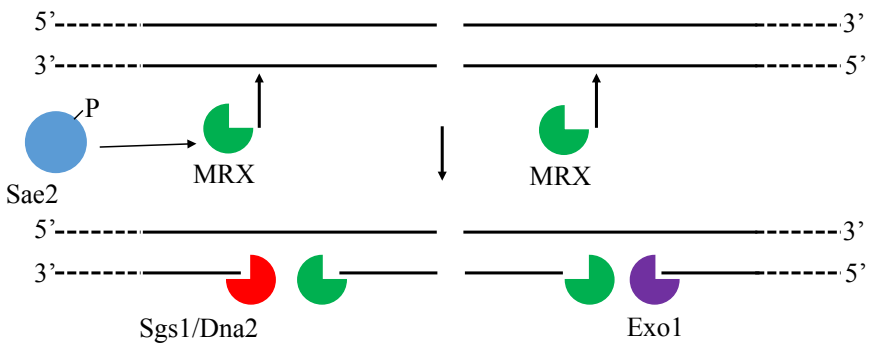

Figure 7. Initiation and Progression of DSB resection in *S. cerevisiae*. Cdk1-phosphorylated Sae2, activates MRX, stimulating its endonucleolytic activity and resulting in the introduction of nicks on the 5′ strand at ~300 nucleotides away from the DSB ends. Resection proceeds by bidirectional processing away from the nicks, with MRX proceeding in the 3′ to 5′ direction towards the DSB ends, and Sgs1/Dna2 and Exo1 proceeding in the 5′ to 3′ direction.

Several proteins regulate DSB resection both at the initiation (short-range) and extension (long-range) stages. Phosphorylation of Sae2 by Cdk1, the master cell cycle regulator in *S. cerevisiae*, promotes DSB resection in G_2/M (119, 120). However, DSB resection is not completely repressed during G_1; ssDNA is still generated during G_1 albeit at much lower levels than during G_2/M . More resection products accumulate in the immediate vicinity of a DSB when *YKU70* or *YKU80* is deleted in G1-arrested cells, indicating that Yku normally inhibits the initiation of resection (80, 121). Moreover, *yku70*Δ cells exhibit a significantly more pronounced accumulation of Exo1, than of Dna2 at DSBs, indicating that Yku primarily inhibits the Exo1-dependent pathway of extensive DSB resection (122).

In the absence of a functional MRX complex, Sgs1-Dna2 becomes essential for the initiation of resection. Mimitou and Symington (2010) (123) measured resection in *rad51*Δ, *rad51*Δ *mre11-nd*, and *rad51*Δ *mre11-nd sgs1*Δ strains. These measurements were made in a *rad51*Δ background to prevent the strand invasion step of HR, thereby stabilizing the 3′ ssDNA and improving its detection. They observed, consistent with a previous report (124), that expression of the nuclease-defective *mre11-nd* (*H125N*) allele did not significantly impair the initiation of resection at the endonuclease-

induced break (123). However, the *mre11-nd* mutant was highly sensitive to IR, suggesting a higher requirement for MRX in the processing of DSBs with "dirty" chemically modified ends such as those generated by IR, versus DSBs with "clean" ends (123). Compared to the *rad51*Δ and *rad51*Δ *mre11-nd* strains, the *rad51*Δ *mre11-nd sgs1*Δ strain exhibited an approximately 2-fold decrease in the accumulation of resection products in the immediate vicinity of the DSB. This finding, combined with their observation that an *mre11-nd exo1*Δ strain was much more resistant to IR than the *mre11-nd sgs1*Δ strain, indicated that Sgs1-Dna2, but not Exo1, can partially fulfill the resection initiation function of the Mre11 nuclease (123). Likewise, Sgs1-Dna2 becomes essential for the initiation of resection when Sae2, which initiates resection together with MRX, is absent (125).

Reflecting yet another level of regulation of resection, Yku (Ku in mammalian cells) and MRX reciprocally antagonize each other's presence at DSBs. Yku reduces the association of MRX with DSBs in G_1 phase and when overexpressed in G_2 phase (80). Conversely, MRX limits Yku association with DSBs (122). However, the dual role for MRX in both NHEJ and HR precludes a model wherein mutually exclusive binding of Yku and MRX to DSBs channels them to either NHEJ or HR.

The checkpoint protein Rad9 (53BP1 in mammalian cells) is another important regulator of DSB resection in *S. cerevisiae*. A role for Rad9 in limiting resection was first reported in 2008 (126). Using a Southern blot approach for measuring the accumulation of resection products, the authors demonstrated that resection products accumulated faster, and at further distances from the DSB, in the absence of *RAD9*. This study therefore implicated Rad9 as an inhibitor of long-range resection. Furthermore, Exo1 was ruled out in this study as the nuclease(s) regulated by Rad9 (126). Seven years later, a role for Rad9 in limiting short-range resection was uncovered (125). The authors used a more sensitive technique, quantitative PCR (qPCR), to measure the kinetics of resection near the DSB. Taking advantage of an *RsaI* restriction enzyme site located at ~ 150 bp from one end of the DSB, the

authors quantified the production of a PCR product generated with primers flanking the *RsaI* site. Resection past the *RsaI* site converts it to ssDNA, rendering it resistant to cleavage and leaving an intact template for PCR amplification with the flanking primers. The converse is the case for when resection is impaired. Short-range resection was impaired, as expected, in a *sae2*Δ mutant relative to the WT strain, and this defect was partially alleviated in a *sae2*Δ *rad9*Δ mutant. Importantly, a *sae2*Δ *rad9*Δ *sgs1*Δ strain exhibited resection levels similar to the *sae2*Δ strain (125). Taken together, the findings from both of these studies indicate that Rad9 limits short-range and long-range resection by inhibiting the Sgs1-Dna2-dependent resection pathway.

1.4 Role of Rif1 in DSB Resection and Repair

Rif1 was first discovered in *S. cerevisiae* in a screen designed to identify interacting partners for the telomere-binding protein Rap1, and was characterized in the same study as a negative telomere length regulatory factor (discussed further in Section 3.4) (127). A little over ten years later, human RIF1 (hRIF1) was identified based on sequence similarity to yeast Rif1 (128). Surprisingly, unlike its yeast ortholog, hRIF1 did not colocalize with telomeres by immunofluorescence, and was not detected in immunoprecipitates of known telomere-binding proteins, including Rap1. hRIF1 did, however, colocalize with damaged telomeres, and also formed foci at IR-induced DSBs (128). This finding was the first indication of a role for hRIF1 in DSB signaling and/or repair. In 2013, almost a decade after yeast RIF1 was identified, publications from several laboratories elaborated on the role of RIF1 in DSB repair. Prior to these studies, the BRCA1 and 53BP1 proteins were reported to promote HR and NHEJ, respectively (129-132). Moreover, several lines of evidence suggested an antagonistic relationship between BRCA1 and 53BP1. BRCA1 excludes 53BP1 from ionizing radiation-induced foci (IRIF), sites of accumulation of DNA damage response proteins, formed in the S phase of the cell cycle (133).

Furthermore, 53BP1 deficiency suppresses the resection and HR defects of BRCA1-deficient cells (134, 135). These findings raised the possibility that 53BP1 inhibits resection, and by extension HR, so as to favor NHEJ. Importantly, expression of a mutant BRCA1 protein containing N-terminal mutations of 28 potential S/TQ phosphorylation sites for the ataxia-telangiectasia mutated (ATM) kinase also suppressed HR defects of BRCA1-deficient cells (136), suggesting additional involvement of one or more 53BP1-interacting proteins in NHEJ. Given that hRIF1 localization to IR-induced DSBs had been previously shown to be dependent on 53BP1 (128), hRIF1 emerged as a likely candidate for a 53BP1-interacting protein with a function in NHEJ. The major findings from the publications that described a role for hRIF1 as an effector for 53BP1 in NHEJ are described below.

In agreement with previous reports, hRIF1 localized to IRIF in an ATM- and 53BP1-dependent manner, as mutation of the S/TQ sites in 53BP1 impaired hRIF1 localization to IRIF. Importantly, these mutations did not impair the formation of 53BP1 IRIF, indicating that hRIF1 was recruited to DSBs via interactions with phosphorylated residues in 53BP1. Furthermore, hRIF1 depletion did not impair 53BP1 IRIF, suggesting that hRIF1 functioned as a downstream effector of 53BP1 (137-141).

To determine whether hRIF1 functioned in NHEJ, several assays were employed, all yielding the same conclusion. hRIF1 depletion reduced antibody class switching (Section 1.1), an NHEJ-dependent process, both *in vivo* in mice and *ex vivo* in a B cell lymphoma cell line (137, 138). NHEJ of deprotected telomeres was also reduced upon hRIF1 depletion (137, 141). Finally, hRIF1-deficient cells exhibited increased sensitivity to bleomycin, similarly to cells lacking the NHEJ factor Ku70 (139).

As had been demonstrated for 53BP1, hRIF1 depletion attenuated the resection defect of BRCA1-deficient cells, as evidenced by increased RPA accumulation at DSBs (137, 140, 141).

Consistent with the increased resection upon hRIF1 depletion, gene conversion, SSA, and MMEJ, processes dependent on resection, were increased upon hRIF1 depletion (139).

Finally, the antagonism between 53BP1 and BRCA1 was shown to be cell cycle-regulated. BRCA1 had been previously reported to exclude 53BP1 from S-phase IRIF. Reciprocal experiments demonstrated that BRCA1 did not form IRIF in G_1 cells (137, 140). However, upon 53BP1 depletion, BRCA1 IRIF formed in G_1 cells (139, 140). Like 53BP1, hRIF1 did not form IRIF in G_2/S cells. However, ectopic hRIF1 IRIF arose in G_2/S cells when BRCA1 or its interacting partner CtIP was depleted (137). The results from these studies led to the development of a model wherein 53BP1/hRIF1 excludes BRCA1/CtIP from DSBs in G_1, thereby inhibiting resection and favoring NHEJ. In G_2/S, BRCA1/CtIP exclude 53BP1/hRIF1 from DSBs, allowing for resection, and consequently HR, to occur (137-141).

Rad9, the *S. cerevisiae* ortholog of 53BP1, also inhibits DSB resection (Section 1.3.1). A point of divergence, however, is that *S. cerevisiae* Rif1, unlike its mammalian counterpart, promotes DSB resection by reducing Rad9 accumulation at DSBs (142). When tested in a SSA assay, a *Scrif1*Δ mutant was defective in SSA repair using two direct repeats located 25 kb apart. *ScRIF1* deletion had no effect, however, when the repeats were located 5 kb apart (142). This observation suggests that ScRif1 promotes DSB repair by HR by promoting resection, and raises the possibility of ScRif1 having a converse role in NHEJ regulation. Whether or not Rif1 regulates NHEJ in *S. cerevisiae* has not yet been addressed up prior to the work presented in this thesis.

1.5 Significance

Rif1 was originally identified in *S. cerevisiae* as a telomere length regulatory protein (127), but in the 25 years since its discovery, additional functions, in DSB repair and DNA replication, have been

attributed to Rif1. In yeast, mice, and humans, Rif1 functions in the temporal regulation of DNA replication (143-145). As discussed above, Rif1 regulates DSB repair pathway choice in mammalian cells, favoring NHEJ over HR. A common thread among these functions of Rif1—telomere regulation, DSB repair, and DNA replication —is that these processes influence genome maintenance, thereby positioning Rif1 as an important regulator of genome maintenance.

While several laboratories have independently reported on the role of mammalian Rif1 in DSB repair (137-141), the role of ScRif1 in DSB repair has not been explored extensively. In 2014, the Longhese lab provided evidence that ScRif1 promotes resection, suggesting that ScRif1 favors HR over NHEJ (142). Our laboratory has undertaken the task of further exploring the role of ScRif1 in DSB repair, and the findings from our studies thus far are presented in Chapter II. I demonstrate that imprecise NHEJ events in WT and *rif1Δ* cells have different mutation signatures, suggesting a role for ScRif1 in regulating the fidelity of NHEJ repair. I also provide evidence that this function of Rif1 is dependent on its protein phosphatase-1 (PP1)-interacting domain. This PP1-interacting domain has also been implicated in replication timing regulation by ScRif1 (146-148), and is seemingly involved in telomere length regulation by ScRif1 (my data, as well as unpublished results from the Shore lab described in a review article published from his lab (149)). It is not yet known whether or not this domain is involved in the regulation of DNA replication timing or DSB repair by mammalian Rif1. Therefore, in addition to revealing an important role for ScRif1 in regulating the fidelity of NHEJ repair, these findings also contribute to our understanding of how Rif1 accomplishes its diverse functions, by revealing, for the first time, an involvement of the PP1-interacting domain in a DSB repair function of Rif1.

CHAPTER II

SACCHAROMYCES CEREVISIAE RIF1 REGULATES THE FIDELITY OF NHEJ REPAIR[1]

2.1 Introduction

Cellular DNA is constantly exposed to genotoxic agents both from endogenous and exogenous sources, resulting in the formation of DNA lesions. Among the numerous types of DNA lesions are base oxidations and deaminations, bulky DNA adducts, interstrand crosslinks, mismatched bases, single-strand breaks, and double-strand breaks (DSBs) (5). DSBs are the most cytotoxic lesions: just one unrepaired DSB can have lethal consequences for a cell (150). Aberrant DSB repair gives rise to mutations and/or gross chromosomal rearrangements (GCRs), the consequences of which can include genomic instability and carcinogenesis (151). Therefore, to ensure genomic integrity and cell survival, DSBs must be repaired in a timely manner and with high fidelity.

Eukaryotic cells have evolved two main pathways for DSB repair: homologous recombination (HR) and non-homologous end joining (NHEJ). Homologous recombination uses a homologous sequence as template for DSB repair. Nucleolytic resection of the 5′ strands of the DSB is crucial to the success of HR since it exposes the 3′-ended single-stranded DNA required to initiate homology search and subsequently complete repair. There are four subtypes of homology-dependent repair (HDR), all dependent on the protein Rad52: the error-free double Holliday junction (dHJ) and synthesis-dependent strand annealing (SDSA) pathways, and the less conservative break-induced replication (BIR) and single-strand annealing (SSA) pathways (38).

[1] The work presented in this chapter are my contributions towards ongoing work in our lab aimed at elucidating the role of yeast Rif1 in DSB repair.

In contrast to HDR, classical NHEJ (c-NHEJ) involves religation of the DSB ends, with little to no end processing. A second subtype of NHEJ known as alternative non-homologous end joining (alt-NHEJ) or microhomology-mediated end joining (MMEJ) involves base pairing between 5-25 nucleotides of microhomology, exposed by resection, on each side of the break. Consequently, MMEJ results in deletions of up to a few hundred base pairs (39). These pathways are genetically distinct: c-NHEJ requires the Ku70/Ku80 (Ku) heterodimer (72, 73), whereas MMEJ is Ku-independent (102, 103). The fidelity of NHEJ depends on the kinds of DSB ends generated. DSBs with cohesive overhangs require no modifications prior to religation, whereas incompatible ends must be processed first to generate ligatable structures (152). Numerous studies indicate that the requirements for factors involved in end-processing may differ depending on the structure of the DSB ends (95, 96, 153-155). Some of these studies have, however, yielded contradictory findings that were suggested to arise from differences in the types of assays used (plasmid-based versus chromosomal-based NHEJ assays) (153-155).

Although the HR and NHEJ pathways both operate in eukaryotic cells, one pathway is preferentially used over the other. For instance, HR is the predominant pathway in the budding yeast *Saccharomyces cerevisiae*, whereas NHEJ is typically the pathway of choice in mammalian cells. Sister chromatids are the preferred templates for HR repair (59), and as such, HR is largely confined to the S and G2 phases of the cell cycle during which sister chromatids are available for repair. Much attention has been paid to how eukaryotic cells regulate DSB repair pathway choice. In mammalian cells, RIF1 has emerged as a critical factor that regulates the choice between HR and NHEJ. RIF1 is recruited to DSBs via an interaction with 53BP1, and in a manner dependent on ATM-mediated phosphorylation of 53BP1 (137-141). RIF1 and 53BP1, acting in the same pathway, limit accumulation of the resection- and HR-promoting factors BRCA1/CtIP at DSBs in the G_1 phase of the cell cycle, and consequently

limit DSB resection (137-141). Analogously, BRCA1/CtIP inhibit RIF1/53BP1 accumulation at DSBs in the S and G_2 phases of the cell cycle, supporting a model in which competition for DSB ends by 53BP1/RIF1 and BRCA1/CtIP determines which pathway, HR or NHEJ, is used to repair the break (137-141).

In stark contrast to its mammalian homologue, *S. cerevisiae* Rif1 promotes resection, interestingly by limiting the accumulation of the 53BP1 homolog Rad9 (142). DSB resection is a two-step process in which Mre11-Rad50-Xrs2 (MRX) and Sae2 initiate resection, removing approximately 300 nucleotides from the 5′ strand (short-range resection) (115, 116), followed by further (long-range) resection mediated by the Exo1 and Sgs1-Rmi1-Top3-Dna2 nucleases (116-118). In *S. cerevisiae*, Rad9 inhibits both short- and long-range resection by forming a physical barrier, via oligomerization, that blocks nucleolytic resection (125, 126, 156). Consistent with its role in antagonizing Rad9 recruitment to DSBs, *S. cerevisiae* Rif1 promotes DSB repair by the SSA pathway (142). An inference that could be made from the finding that *S. cerevisiae* Rif1 promotes homology-dependent DSB repair is that it conversely inhibits NHEJ. This hypothesis has not, however, been directly tested.

In yeast and mammalian cells, Rif1 regulates the temporal pattern of replication initiation. In budding yeast (144), fission yeast (157), and mammalian cells (143, 145), Rif1 exerts a global, genome-wide effect on replication timing, with late-replicating origins firing earlier and early-replicating origins firing later in *rif1* cells. In *S. cerevisiae*, Rif1 inhibits DNA replication initiation by interacting with and directing protein phosphatase-1 to reverse Cdc7-Dbf4 (DDK)-mediated phosphorylation of Mcm4, a component of the pre-replication complex (146, 147).

In both yeast and mammalian cells, Rif1 is also involved in chromatin organization at the nuclear periphery (145, 158, 159). In *S. cerevisiae*, this function of Rif1 is independent of its role in replication timing (144). In mammalian cells, however, Rif1 controls replication timing through regulation of

chromatin organization (145, 159). In human cells, whereas Rif1-bound replication domains are resistant to DNase I digestion, consistent with co-locolization of these replication domains with the nuclear membrane, Rif1-bound ionizing radiation-induced foci (IRIF), formed after DSBs, are DNase I-sensitive and therefore not associated with the nuclear membrane (145). Therefore, Rif1 appears to play distinct roles in DNA replication and DSB repair.

Here, we have investigated a role for *S. cerevisiae* Rif1 in DSB repair by NHEJ. We provide evidence that Rif1 regulates the fidelity of NHEJ repair of a DSB induced by the CRISPR/Cas9 nuclease. Whereas WT repair junctions only consist of deletions (median = 7 nucleotides), *rif1*Δ junctions contain both deletions (median = 2 nucleotides) and Pol4-dependent insertions, most commonly of a T nucleotide. Finally, we present evidence that this function of Rif1 is mediated by its protein phosphatase 1-interacting domain, but does not require its interaction with Rap1 or Rif2.

2.2 Results

2.2.1 The fidelity of NHEJ is altered in the absence of *S. cerevisiae* Rif1

To address the role of *S. cerevisiae* Rif1 in DSB repair, we utilized the CRISPR/Cas9 system to induce a DSB at the *CAN1* locus and measured the frequency of survival following DSB induction. Strains utilized in this assay contain two plasmids, one carrying the Cas9 gene under control of a galactose-inducible promoter (160), and the other constitutively expressing the guide RNA targeting *CAN1* (gRNA CAN1.Y) (160). Growth on media containing galactose induces expression of the Cas9 nuclease, which in turn creates a blunt-ended DSB at the *CAN1* locus. When plated to media containing galactose, 3.00±0.95% of WT cells survived the Cas9-induced DSB (Figure 8A). This value is significantly lower than the previously reported value of ~80% (160). The reason for this discrepancy

is currently unknown, but differences in strain background may account for the observed differences in DSB survival frequencies.

Deletion of *RIF1* reduced survival modestly (by about 3-fold), but reproducibly among four independent *rif1*Δ isolates (Figure 8A). The frequency of survival in the *rif1*Δ strains ranged from 0.78-1.01%, but these minor differences were not statistically significant (p=0.90) by ANOVA with post-hoc Tukey HSD (Figure 8A). Next, we sequenced the region spanning the predicted Cas9 cleavage site (henceforth referred to as the repair junction) from fifteen galactose-resistant survivors of the WT (*RIF1*) strain and fifteen survivors of a *rif1*Δ strain. All of the WT repair junctions contained deletions ranging from 3 to 216 bp, with a median deletion size of 7 bp (Figure 8B). Mutations at the repair junction were expected because only those cells that incur a mutation at the target site become resistant to persistent cleavage by Cas9. Furthermore, the observation that 15/15 survivors contained mutations and that none of the clones appeared to contain mixed sequences is consistent with efficient cleavage that prevents the growth of "escapers." Sequencing of the repair junctions from *rif1*Δ isolates revealed a dramatically different repair signature from that observed in WT cells. Eight of 15 *rif1*Δ repair junctions contained deletions of only 1-3 bp, with a median deletion size of 2 bp (Figure 8B). Additionally, 40% of the repair junctions (six out of 15) contained insertions, mostly of a T nucleotide (Figure 8B), unaccompanied by deletion.

In the WT strain, most survivors contained deletions of 25 bp or fewer, with microhomologies of 1-5 nucleotides evident at the site of repair (Figure 8B), observations consistent with repair by NHEJ. To verify that the Cas9-induced DSB was repaired primarily by NHEJ, we assayed DSB repair in strains lacking Yku80 and Lif1 (required for NHEJ), Rad1 (required for MMEJ), and Rad52 (required

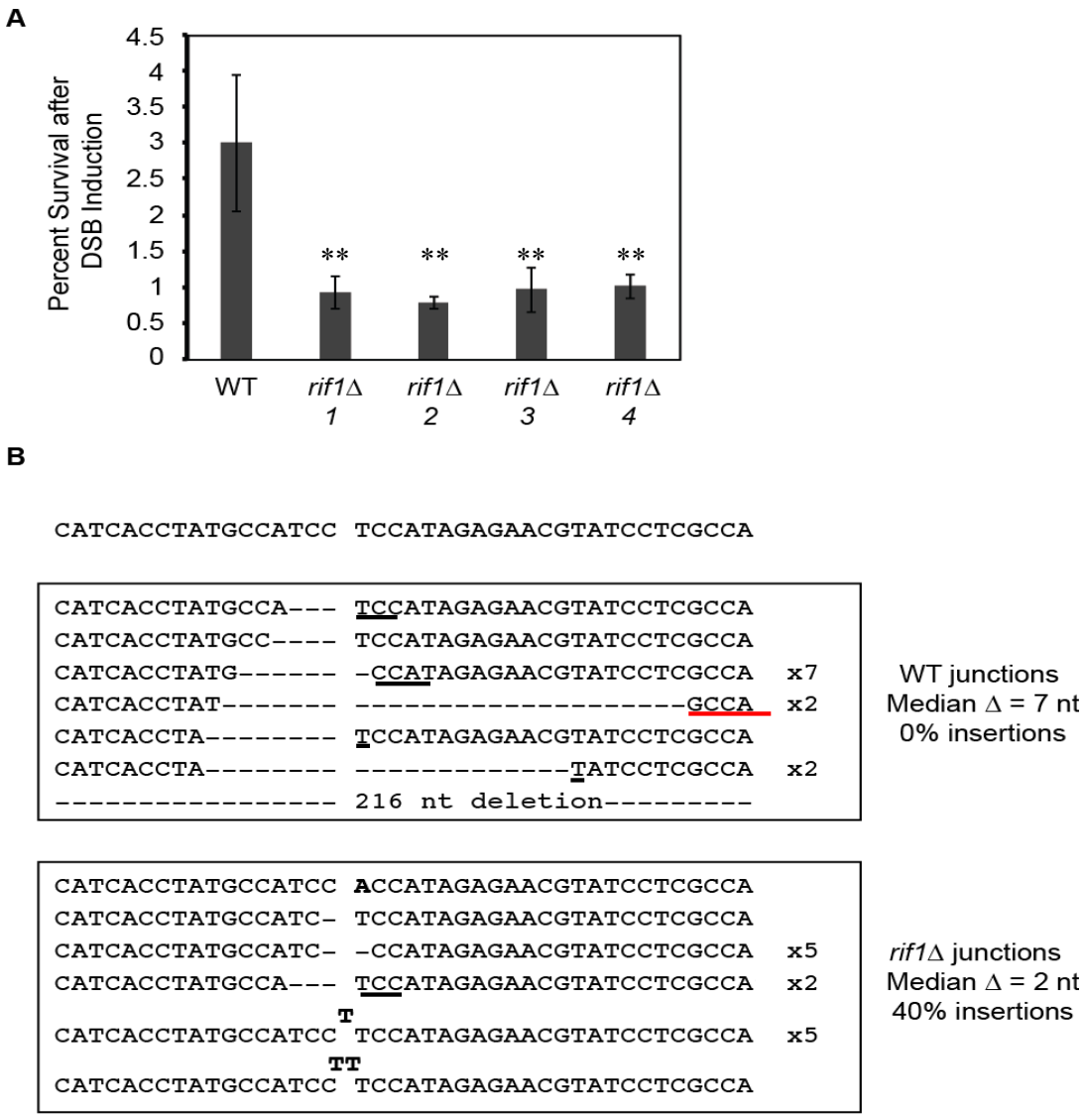

Figure 8. Rif1 regulates the fidelity of NHEJ repair.
(A). DSB survival rates in WT and *rif1*Δ cells. Data represent the average of 3 independent experiments and error bars represent standard deviations. **The indicated mutants are significantly different from WT ($p<0.01$) by ANOVA with post-hoc Tukey HSD.
(B). Repair junctions from the WT and *rif1* strains. The top sequence shows the original WT sequence with a gap representing the Cas9 cleavage site. The boxed sequences show the mutagenic repair junctions in WT and *rif1*Δ cells. Dashes represent deletions and staggered, bolded nucleotides represent insertions. For repair junctions that had multiple occurrences, the number of times that junction was isolated is indicated to the right of the sequence. Underlined sequences represent microhomology that was likely utilized for repair. There was no discernible microhomology for the WT isolate in which no nucleotide is underlined. For the sequence underlined in red, there is an additional nucleotide of microhomology that is not shown.

for all forms of HR). Deletion of *RAD52* (p=0.86) or *RAD1* (p=0.78) did not significantly change the frequency of survival following DSB induction (Figure 9A and B). In contrast, deletion of *YKU80* reduced survival by 63-fold (Figure 9C), indicating that the majority of survivors repaired the DSB by NHEJ. Deletion of *LIF1*, which encodes for a component of the primary NHEJ ligase machinery (Dnl4/Lif1) recapitulated our finding with *yku80*Δ, reducing survival by 17-fold (Figure 9D). However, the smaller fold reduction in the *lif1*Δ mutant compared to the *yku80*Δ mutant suggests that during NHEJ repair of DSBs that require end-processing, another ligase can catalyze the final ligation step in the absence of Dnl4/Lif1.

Deletion of *RIF1* caused a further reduction in survival in the *rad52*Δ and *rad1*Δ backgrounds (Figure 9A and B) (2.4 fold and 2.8 fold, respectively), but not in the absence of *YKU80* or *LIF1* (Figure 9C and D), placing Rif1 in the NHEJ pathway of DSB repair. Taken together, these data indicate that Rif1 regulates the fidelity of NHEJ in *S. cerevisiae*.

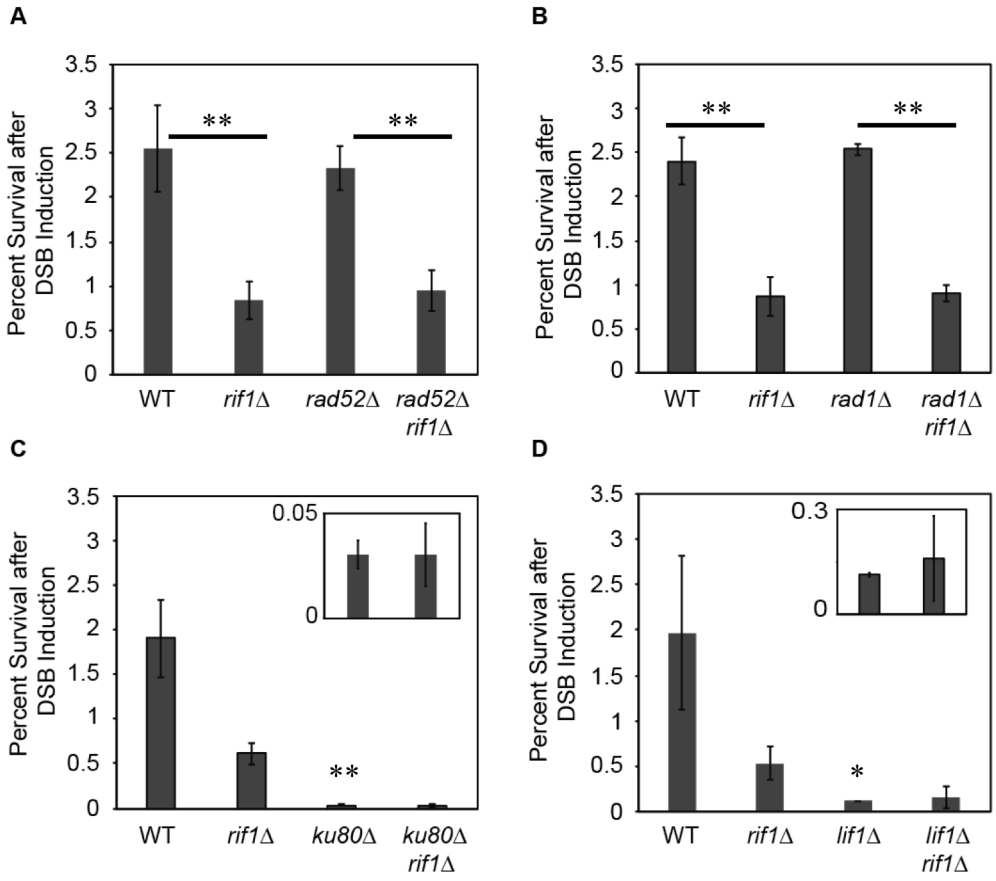

Figure 9. Rif1 functions in the NHEJ pathway of DSB repair.
(A-D) DSB survival frequencies in HR (*RAD52* and *RAD1*) and NHEJ (*KU80* and *LIF1*) mutants. Data represent the averages of 3 independent experiments and error bars represent standard deviations. Insets are included for the NHEJ mutants (C and D) because the scales used in the larger images do not permit proper visualization of the extent of survival in those strains. A-B: **p<0.01 by ANOVA with post-hoc Tukey HSD. C-D: Given the clear lack of an effect following deletion of *RIF1* in the NHEJ mutant strains, statistical comparisons were made only between the WT and *ku80*Δ or *lif1*Δ strains. *p<0.05, **p<0.01 by Student's t-test.

2.2.2 Repair junction insertions that occur in the absence of Rif1 are Pol4-dependent

Given the unique insertional signature of the *rif1*Δ mutant compared to the WT strain, we tested for a potential involvement of DNA polymerase IV (Pol4), an end-processing factor known to participate in gap-filling during NHEJ (95, 96). Consistent with its known function in NHEJ, deletion

of *POL4* led to a 4-fold reduction in survival after DSB induction (Figure 10A). The repair junctions in the *pol4*Δ mutant contained larger deletions compared to the WT strain and this difference was significant (Figure 10B). Similar to fission yeast (161), the *pol4*Δ strain exhibited slightly increased use of microhomology, in particular, of imperfect microhomology, compared to the WT strain (Figure 10C and D).

Deletion of *RIF1* in the *pol4*Δ background did not cause further change in DSB survival (p=0.63, by ANOVA with post-hoc Tukey HSD) (Figure 10A), suggesting an involvement of Pol4 in the Rif1 pathway of NHEJ repair. Pol4 was absolutely required for the insertions that we observed in the *rif1*Δ mutant (Figure 8B) as insertions were never observed in the *pol4*Δ *rif1*Δ repair junctions (Figure 10B). However, the "small deletion" (1-3 bp) phenotype characteristic of the *rif1*Δ mutant persisted in the *pol4*Δ *rif1*Δ strain (Figure 10B), indicating the involvement of other factor(s) in generating this phenotype in the absence of Rif1. As the *pol4*Δ *rif1*Δ strain did not exhibit a similar mutation signature compared to the *pol4*Δ strain (Figure 10B), these data indicate that Rif1's function in regulating NHEJ fidelity is only partially dependent on Pol4.

2.2.3 The end-processing factors Rad27, Tdp1, and Srs2 are not involved in the Rif1-dependent NHEJ pathway

Next, we tested whether several factors implicated in end-processing during DNA repair affect the deletion size generated after Cas9 cleavage in the *RIF1* or *rif1Δ* backgrounds. Rad27 is a 5′ flap endonuclease that has been reported to catalyze 5′ flap cleavage during NHEJ (97). Another protein of interest, Tdp1, has differing roles during NHEJ depending on the nature of the DSB ends. Tdp1 affects neither the frequency nor the fidelity of NHEJ at DSB ends with 3′ overhangs (153). In the absence of *TDP1*, more insertions occur at ends with 5′ overhangs, but the frequency of end-joining is unchanged

(153). *TDP1* deletion improves the frequency of joining of blunt ends, but does not affect the fidelity of joining at those ends. In our assay, deletion of *RAD27* decreased survival after DSB induction only by 1.6-fold (p=0.03 by ANOVA with post-hoc Tukey HSD), whereas deletion of *TDP1* had no effect on DSB survival (p=0.90 by ANOVA with post-hoc Tukey HSD) (Figure 11A and B). The *rad27*Δ *rif1*Δ and *tdp1*Δ *rif1*Δ double mutants exhibited reduced survival after DSB induction compared to the *rad27*Δ and *tdp1*Δ single mutants respectively (Figure 11A and B), suggesting that neither Rad27 nor Tdp1 functions in the Rif1-dependent NHEJ pathway. The lack of strong involvement of Rad27 strongly suggests that repair of the Cas9-induced DSB primarily proceeds by way of intermediates containing 3′ overhangs or 3′ flaps expected to be generated after 5′ strand resection from an initial blunt break.

The Rad1-Rad10 endonucleases, together with the Srs2 helicase, cleave the long 3′ flaps generated during SSA (43, 44, 162), and are candidates for the end-processing factors that cleave the shorter 3′ flaps generated during NHEJ. However, consistent with a previous report (163) and with our finding that Rad1 does not play a significant role in repair of the Cas9-induced DSB (Figure 9B), deletion of *SRS2* did not significantly change cell survival after DSB induction (p=0.12 by ANOVA with post-hoc Tukey HSD) (Figure 11C).

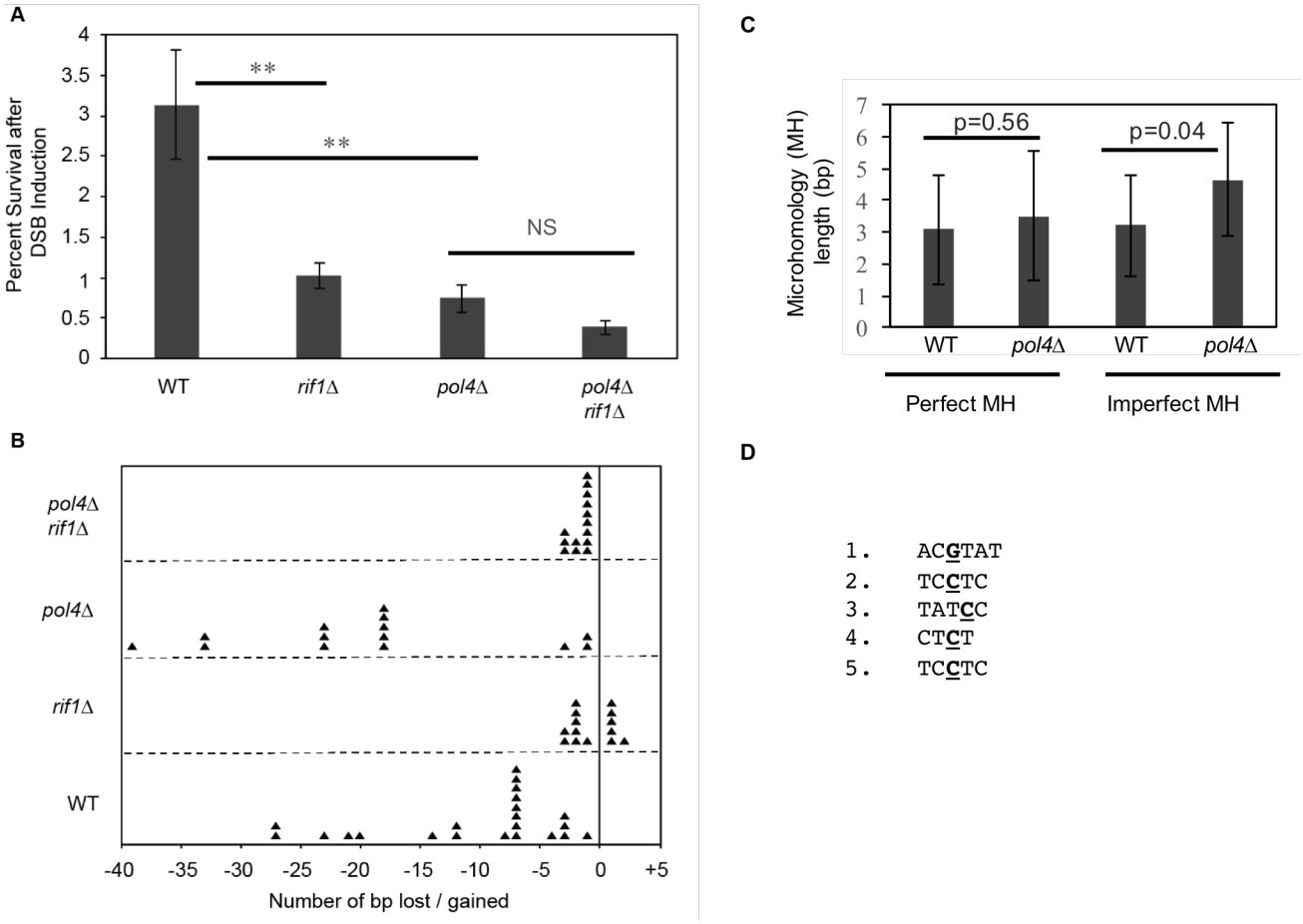

Figure 10. DSB repair junction insertions that occur in the absence of Rif1 are Pol4-dependent.
(A) DSB survival frequencies in WT, *rif1*Δ, *pol4*Δ, and *pol4*Δ *rif1* strains. Data represent averages from 3 independent experiments and error bars represent standard deviations. **p<0.01 by ANOVA with post-hoc Tukey HSD. NS = not significant.
(B) Mutation signatures in WT, *rif1*Δ, *pol4*Δ, and *pol4*Δ *rif1* strains. Each triangle represents an independent repair event. The type of event (deletion or insertion) is indicated by the position relative to the central axis. Deletions are indicated to the left and insertions to the right. The numbers on the X-axis indicate the sizes of the insertions and deletions. The Kolmogorov-Smirnov test was used for pair-wise comparisons among the four strains and a Bonferroni correction was performed to account for the multiple comparisons. Except for the *rif1*Δ and *pol4 rif1*Δ pairing, the mutation signatures of all other strain pairs were significantly different (for each pair-wise comparison, p was < the Bonferroni-adjusted alpha level of 0.0083).
(C) Average lengths of microhomologies (MH) in WT and *pol4*Δ strains. For each strain, the same data set (13 WT isolates and 14 *pol4*Δ isolates) were analyzed to determine the average MH length, either without the inclusion of uncomplementary nucleotides (Perfect MH) or allowing for only one mismatch (imperfect MH). Error bars represent standard deviations. Data were analyzed by unpaired Student's T test.
(D) Imperfect microhomologies utilized in the *pol4*Δ strain. The underlined and bolded nucleotides represent the mismatches.

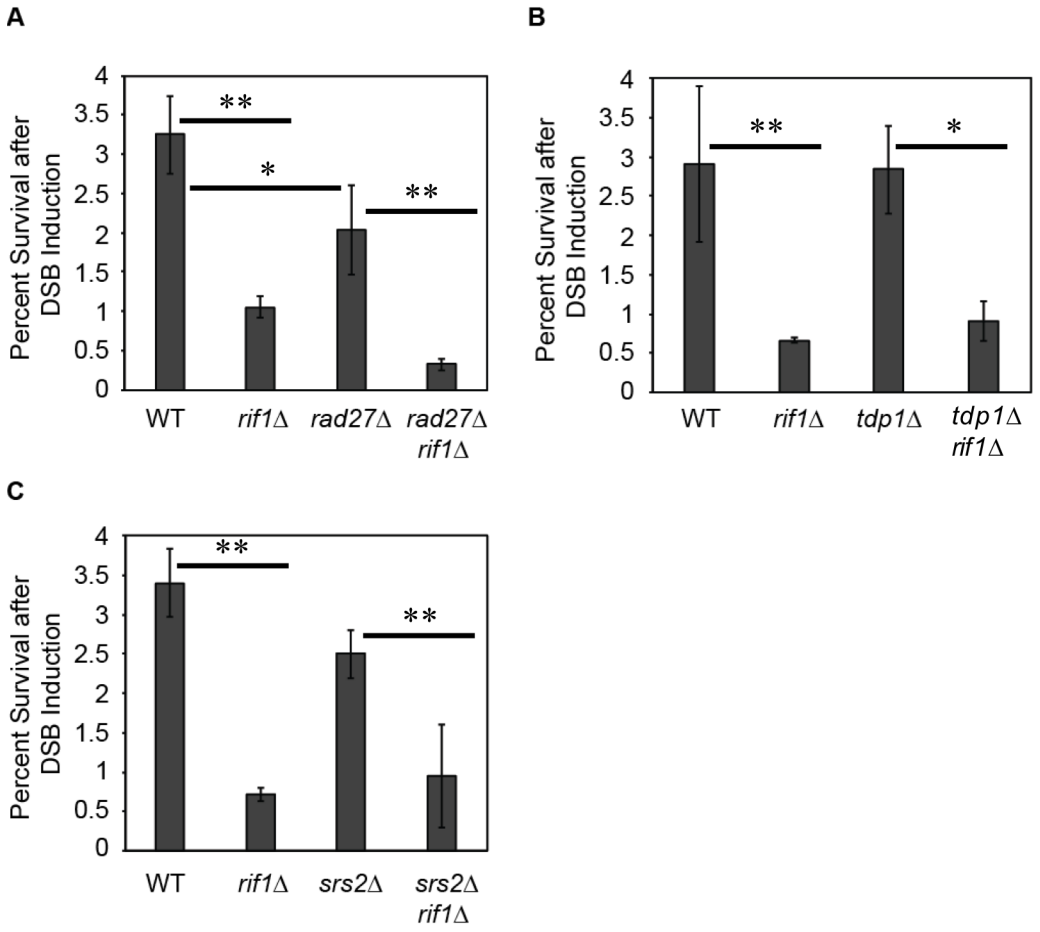

Figure 11. End-processing factors Srs2 and Tdp1 do not affect DSB survival of a Cas9-induced DSB. DSB survival frequencies in strains carrying deletions of genes with known roles in end-processing (*RAD27*, *TDP1*, and *SRS2*). Data represent averages from 3 independent experiments and error bars represent standard deviations. *p<0.05, **p<0.01 by ANOVA with post-hoc Tukey HSD.

2.2.4 Rif1 and Rad9 have partially overlapping functions in the regulation of NHEJ fidelity

S. cerevisiae Rif1 promotes DSB resection by limiting the accumulation of the checkpoint protein Rad9, an inhibitor of both short- and long-range resection (125, 126), at DSBs (142). Given that the deletions in the *rif1*Δ strain were smaller than in the WT strain, as would be expected if more Rad9

accumulated at the DSB in the absence of Rif1, we addressed a possible role for the checkpoint protein Rad9 in promoting these small deletions. In a *rad9*Δ strain, survival was reduced 4.5-fold after DSB induction ($p<0.01$), and deletion of *RIF1* did not cause a further change in survival in the *rad9*Δ strain ($p=0.85$), suggesting a potential involvement of Rad9 in the Rif1-dependent NHEJ pathway (Figure 12A). We sequenced the repair junctions from thirty-six *rad9*Δ and thirty-six *rad9*Δ *rif1*Δ survivors. In twenty-two out of 36 *rad9*Δ isolates, resection proceeded past at least one of the primers utilized for amplification of the repair junction (data not shown). This result is consistent with increased long-range resection expected in a *rad9*Δ strain. The remaining fourteen *rad9*Δ isolates exhibited a phenotype similar to the *rif1*Δ strain (Figure 12B). Nine junctions contained small (2-3 bp) deletions, three contained an insertion, and the last two were mixed (insertion and deletion) junctions that resulted in net insertions of 1 bp (Figure 12B). The *rad9*Δ *rif1*Δ mutant had a similar mutation signature as the *rad9*Δ mutant: fourteen out of 36 junctions were unamplifiable, indicative of extensive resection. Of the remaining twenty-two isolates, eleven contained small (1-3 bp) deletions, and eleven contained 1-2 bp insertions (Figure 12B). Although the *rif1*Δ mutant does not fully recapitulate the repair defects of the *rad9*Δ mutant, deletion of *RIF1* in the *rad9*Δ background does not cause any considerable changes in repair (Figure 12A and B), suggesting that Rif1 and Rad9 have partially overlapping functions in end-processing during DSB repair.

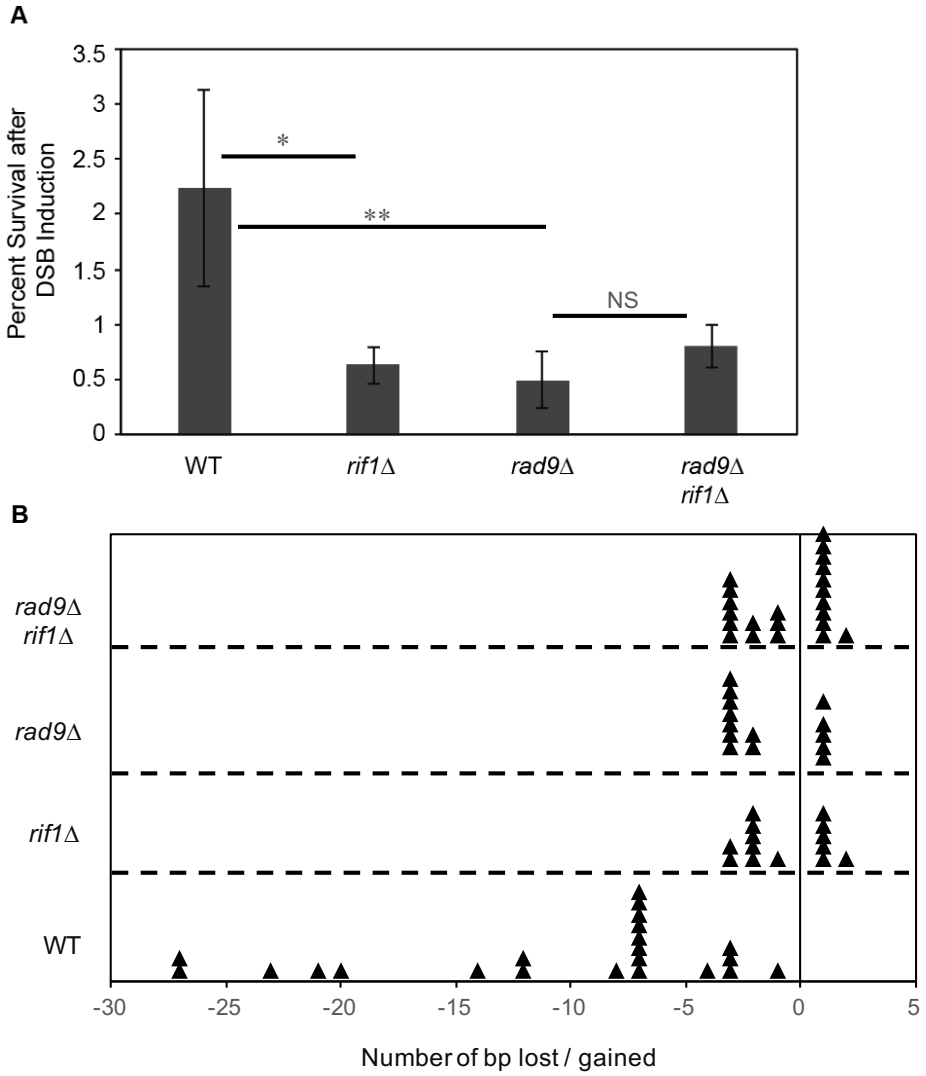

Figure 12. Rad9 and Rif1 have partially overlapping functions in the regulation of NHEJ fidelity.

(A) DSB survival frequencies in WT, *rif1*Δ, *rad9*Δ, and *rad9*Δ *rif1* strains. Data represent averages from 3 independent experiments and error bars represent standard deviations. *p<0.05, **p<0.01 by ANOVA with post-hoc Tukey HSD. NS = not significant.

(B) Mutation signatures in WT, *rif1*Δ, *rad9*Δ, and *rad9*Δ *rif1*Δ strains. Each triangle represents an independent repair event. The type of event (deletion or insertion) is indicated by the position relative to the central axis. Deletions are indicated to the left and insertions to the right. The numbers on the X-axis indicate the sizes of the insertions and deletions. WT and *rif1*Δ data are the same as those shown in Figure 10B. The Kolmogorov-Smirnov test was used for pair-wise comparisons among the four strains, and a Bonferroni correction was performed to account for the multiple comparisons. Each of the mutant strains exhibited a significantly different mutation signature compared to the WT strain (for each pair-wise comparison, p was < than the Bonferroni-adjusted alpha level of 0.0083). Excluding the larger deletions that occur in the *rad9*Δ strains (data not shown), the mutant strains did not differ significantly from each other in their mutation signatures (for each pair-wise comparison, p was > than the Bonferroni-adjusted alpha level of 0.0083).

2.2.5 Rif1's function in NHEJ is independent of its role in telomere maintenance

We next addressed whether Rif1's function in NHEJ is separable from its function in telomere maintenance. Rif1 executes its role in telomere length regulation as part of a complex containing two other proteins, Rif2 and the telomere-binding protein Rap1 (127, 164). At telomeres, Rap1, Rif1, and Rif2 form a protective array that caps the chromosome ends and that is stabilized by multiple interactions among the three proteins (165). Deletion of *RIF2* did not affect survival following DSB induction (Figure 13B), suggesting that Rif1's function in NHEJ is independent of its function in telomere maintenance. We took a more direct approach to verify that Rif1 plays a role in NHEJ independent of its role in telomere maintenance by assaying DSB repair in a strain in which the last 565 amino acids of Rif1, containing its Rap1-interacting motifs (Figure 13A), were deleted (*rif1-C*Δ). Deletion of the Rif1 C terminus reduced survival after DSB induction, although the decrease was less pronounced than typically seen in the *rif1*Δ strain (compare WT vs *rif1-C*Δ in Figure 13B to WT vs *rif1*Δ in preceding figures). Sequencing of the repair junctions in the *rif1-C*Δ strain also revealed a modest, but insignificant, change in the repair signature, compared to the WT strain, with the appearance of slightly smaller deletions and a few insertions ($p=0.048$, higher than the Bonferroni-adjusted alpha level of 0.0083) (Figure 13C).

The Rif1 C terminus contains a tetramerization domain (CTD), in addition to the Rap1-binding motif (RBM) (Figure 13A) (165). To address more specifically whether the Rap1-binding motif or the tetramerization domain contribute to the *rif1-C*Δ phenotype, we mutated the RBM and CTD separately. Mutation of the RBM did not cause a significant change in either cell survival after DSB induction (Figure 13B) or in the repair signature ($p=0.883$, compared to WT) (Figure 13C), indicating that Rif1's function in NHEJ is independent of its interaction with Rap1, and therefore of its function in telomere

length regulation. Mutation of the CTD did, however, reduce DSB survival significantly (Figure 13B) and caused a modest, though insignificant, change in repair signature compared to WT cells (p=0.051, higher than the Bonferroni-adjusted alpha level of 0.0083) (Figure 13C), indicating that this domain plays at least a partial role in mediating Rif1's functions in DSB repair.

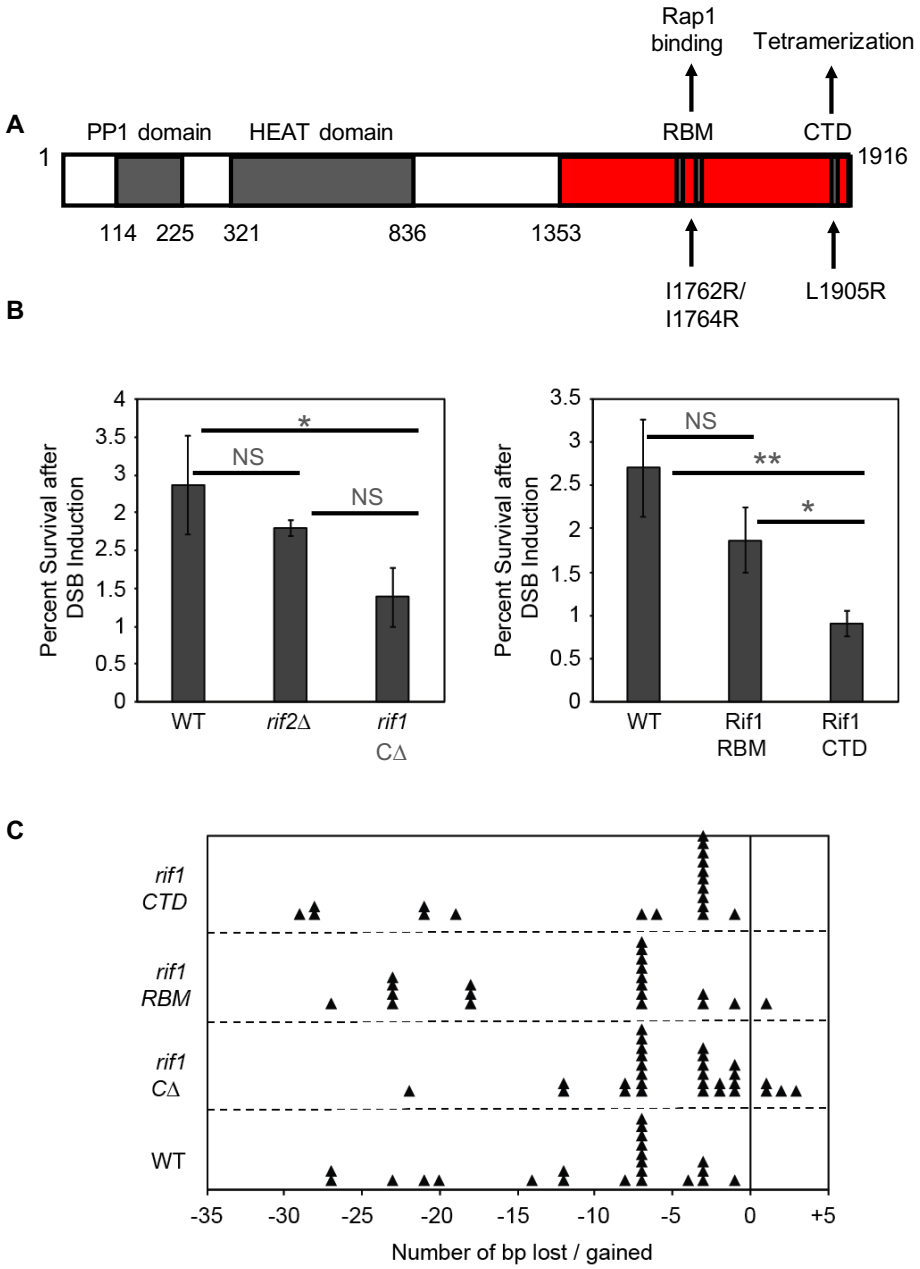

Figure 13. Regulation of NHEJ fidelity by Rif1 is independent of its telomere functions.
(A) Schematic representation of *S. cerevisiae* Rif1, showing the RBM and CTD mutations. In the *rif1-C*Δ strain, the last 565 amino acids (1353-1917, shown in red) are deleted.
(B) DSB survival frequencies in WT, *rif2*Δ, *rif1C*Δ, *rif1RBM*, and *rif1CTD* strains. Data represent averages from 3 independent experiments and error bars represent standard deviations. *p<0.05, **p<0.01 by ANOVA with post-hoc Tukey HSD. NS = not significant.
(C) Mutation signatures in WT, *rif1*Δ, *rif1C*Δ, *rif1RBM*, and *rif1CTD* strains. Each triangle represents an independent repair event. The type of event (deletion or insertion) is indicated by the position relative to the central axis. Deletions are indicated to the left and insertions to the right. The numbers on the X-axis indicate the sizes of the insertions and deletions. WT data are the same as those shown in Figure 10B. The Kolmogorov-Smirnov test was used for pair-wise comparisons among the four strains and a Bonferroni correction was performed to account for the multiple comparisons. Of note, the p value for the WT vs *rif1-C*Δ comparison was 0.048, and p value for the WT vs *rif1 CTD* comparison was 0.051. Following the Bonferroni correction, however, none of the strains differed significantly from each other in their mutation signatures (for each pair-wise comparison, p was > the Bonferroni-adjusted alpha level of 0.0083). See text for more details.

2.2.6 The role of Rif1 in NHEJ repair is mediated by its phosphatase-interacting domain

To determine which other domain(s) of Rif1 are involved in its NHEJ function, we constructed strains in which either the Rif1 HEAT domain or Rif1 protein phosphatase 1-interacting domain was deleted. Similar to the *rif1*Δ strain (see WT vs *rif1*Δ in preceding figures), deletion of either the HEAT or the protein phosphatase 1-interacting domains decreased DSB survival and changed the repair signatures compared to WT cells (Figure 14A and C). The Rif1 HEAT domain is predicted to contain the DNA binding domain of Rif1, although the specific residues involved in DNA binding are yet to be mapped (149). Protein phosphatase 1-interacting domains bind to and recruit protein phosphatase 1 (PP1) for the targeted dephosphorylation of specific substrates. The specific residues in Rif1 that mediate binding to PP1 have been mapped in *S. cerevisiae* (147). To verify the role of the PP1-interacting domain of Rif1 in NHEJ, we mutated the residues in Rif1 responsible for PP1 binding. The resulting strain, *rif1-pp1bs* (147), exhibited reduced DSB survival (Figure 14C), and a similar repair signature as the *rif1*Δ strain (compare *rif1 pp1bs* in Figure 14C to *rif1*Δ in Figure 10B). These findings implicate the Rif1 PP1-interacting domain as the domain of Rif1 that mediates its role in NHEJ.

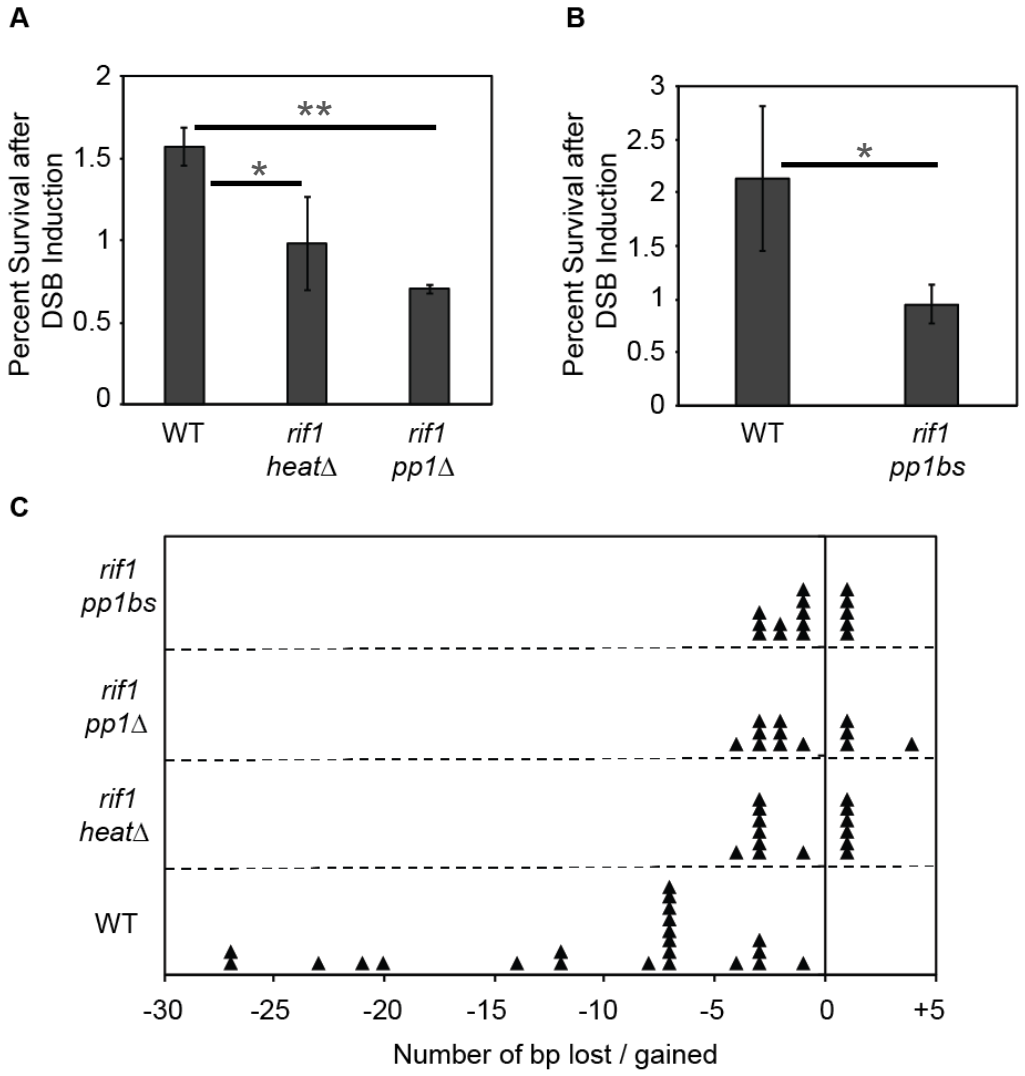

Figure 14. Regulation of NHEJ fidelity by Rif1 is mediated by its PP1-interacting domain.
(A-B) DSB survival frequencies in WT, *rif1 heat*Δ, *rif1 pp1*Δ, and *rif1 pp1bs* strains. Data represent averages from 3 independent experiments and error bars represent standard deviations. The amino acid changes in the *rif1 pp1bs* strain are: K114A, V116A, I147A, I148A, I223A, L224A, V318A, and W320A (147). A: *p<0.05, **p<0.01 by ANOVA with post-hoc Tukey HSD. B: *p<0.05 by unpaired Student's T test.
(C) Mutation signatures in WT, *rif1 heat*Δ, *rif1 pp1*Δ, and *rif1 pp1bs* strains. Each triangle represents an independent repair event. The type of event (deletion or insertion) is indicated by the position relative to the central axis. Deletions are indicated to the left and insertions to the right. The numbers on the X-axis indicate the sizes of the insertions and deletions. WT data are the same as those shown in Figure 10B. The Kolmogorov-Smirnov test was used for pair-wise comparisons among the four strains and a Bonferroni correction was performed to account for the multiple comparisons. Each of the mutant strains exhibited a significantly different mutation signature compared to the WT strain (for each pair-wise comparison, p was < the Bonferroni-adjusted alpha level of 0.0083). The mutant strains did not differ from each other in their mutation signatures (for each pair-wise comparison, p was > the Bonferroni-adjusted alpha level of 0.0083).

2.3 Conclusions and Future Directions

Rif1 was initially identified in *S. cerevisiae* and characterized as a negative regulator of telomere length homeostasis (127). However, the telomere function of Rif1 does not appear to be conserved as mammalian RIF1 does not play a role in telomere maintenance. Mammalian RIF1 does, however, have a clearly established role in DSB repair. At DSBs, RIF1 inhibits resection by acting as a downstream effector of 53BP1, thereby channeling breaks into the NHEJ pathway of DSB repair (137-141). In contrast to its mammalian counterpart, *S. cerevisiae* Rif1 has been reported to promote resection and DSB repair by SSA (142). However, whether or not ScRif1, by virtue of promoting resection, conversely inhibits NHEJ has yet to be determined. The goal of this study was to address whether or not ScRif1 plays a role in NHEJ.

We show here that WT and *rif1*Δ cells exhibit different mutation signatures following imprecise NHEJ repair of a Cas9-induced DSB (Figure 8B). In our assay conditions, the Cas9 nuclease is under control of a galactose-inducible promoter, and cells are grown continuously on media containing galactose. Therefore, a restriction imposed by the conditions of our assay is that cells must incur mutations in the guide RNA target site so as to prevent further cleavage by Cas9. Consequently, the survival frequencies in our assay reflect the rate at which cells experience mutations during repair, although cells that survive under our assay conditions may undergo one or more rounds of precise repair that cannot be detected prior to acquiring mutations. The majority of DSBs generated in cells have chemically modified "dirty" ends that require end-processing before repair. In fact, in human cells, an estimated 60% of NHEJ events proceed by way of intermediates that use 1-2 bp microhomologies flanking the break site (166). Therefore, although our assay does not address whether Rif1 regulates error-free NHEJ, it may better reflect the conditions under which cellular DSBs are

repaired.

Previous reports indicated that Yku has no effect on, or may even inhibit, rejoining of blunt-ended linearized plasmids (153, 167). In stark contrast, we observed a strong reduction (63-fold) in survival of a Cas9-generated DSB in a *yku80*Δ strain (Figure 9C). Similarly, while Tdp1 has been previously reported to increase the frequency of end-joining of blunt-ended linearized plasmids (153), we did not observe any changes in DSB survival in a *tdp1*Δ strain compared to WT (Figure 11B). One possible reason for these disparities may be that in contrast to the plasmid recircularization assay, in which the survival frequencies reflect both precise and imprecise repair, the survival frequencies in our assay reflects the rate at which cells incur mutations. However, cells may make multiple attempts at repair and/or successfully undergo precise repair before incurring mutations. Although these processes cannot be detected in our assay, the rates at which they occur may influence the frequency with which cells acquire mutations and survive the DSB. In *S. cerevisiae*, Yku recruits Nej1 and Dnl4-Lif1 to DSBs (81, 101). In turn, Nej1 and Dnl4-Lif1 form a complex that recruits the end-processing factors Pol4 and Rad27 to DSBs (94). In the absence of Yku and therefore of Nej1 and Dnl4-Lif1 at DSBs, Cdc9, the only other ligase in *S. cerevisiae*, may substitute, albeit at low frequency, for the ligase activity of Dnl4, but not for its role in recruitment of end-processing factors. In this context, Cdc9 is expected to stimulate precise ligation of the DSB, resulting immediately in cell survival in a plasmid-based experimental context. In our assay, however, the repair-cleavage cycle that occurs as a result of precise repair, combined with the reduced recruitment of end-processing factors, would effectively decrease DSB survival. Since we observe a 63-fold reduction in DSB survival in a *yku80* mutant (Figure 9C), compared to a 4-fold and 1.6-fold decrease, respectively, for a *pol4*Δ mutant (Figure 10B) and a *rad27*Δ mutant (Figure 11A), it is tempting to speculate that Yku, with Nej1, and Dnl4-Lif1 may function as a scaffold for recruitment of Pol4, Rad27, and additional factors involved in end-processing.

In the absence of Rif1, we observed smaller deletions at repair junctions (Figure 8B), compared to WT cells. A second phenotype of the *rif1*Δ strain was the appearance of repair junctions containing insertions (Figure 8B). These insertions were Pol4-dependent as they completely disappeared in the absence of Pol4 (Figure 10B). How might these Pol4-dependent insertions arise in the absence of Rif1? Pol4 is phosphorylated by the Tel1 kinase in a damage-dependent manner and this phosphorylation modulates its function in NHEJ (168). One possibility to address in future experiments is that Rif1, through protein phopshatase-1, modulates Pol4 phosphorylation status, affecting its function at DSBs during NHEJ. An alternative possibility is that the decreased rate of resection in the *rif1*Δ strain (142) allows Pol4 to quickly gain access to the DSB ends, even before resection begins, and to incorporate nucleotide(s). Analysis of the phosphorylation status of Pol4 in WT versus *rif1*Δ strains, and ChIP to measure Pol4 recruitment to DSBs in WT versus *rif1*Δ strains should distinguish between the two scenarios above.

In an attempt to elucidate the cause of the "small deletion" phenotype seen in the *rif1*Δ strain, we tested the effect of deletion of *RAD9* on NHEJ repair. Rif1 has been reported to promote resection in *S. cerevisiae* by limiting the accumulation of the resection inhibitor Rad9 at DSBs (142). Rad9 inhibits both short- and long-range resection of the 5′ strands at DSBs (125, 126). We hypothesized that deletion of *RAD9* would result in deletions similar to or larger than those found in WT cells (Figure 8B) and that this phenotype would be epistatic to the *rif1*Δ phenotype. In both the *rad9*Δ and *rad9*Δ *rif1*Δ strains, we recovered two types of events: unamplifiable junctions (data not shown) that are presumably the consequence of extensive resection, as expected to occur in the absence of Rad9 (126), and amplifiable junctions containing smaller insertions and deletions (Figure 12B). In the *rad9*Δ strain, the unamplifiable junctions constitute 38.9% of the junctions recovered, compared to 61.1% in the *rad9*Δ *rif1*Δ strain. This difference is on the threshold of significance (chi-squared contingency test,

p=0.059), suggesting that Rif1 may inhibit this class of events, independently of Rad9. More repair junctions from the *rad9*Δ and *rad9*Δ *rif1*Δ strains should be obtained and statistically analyzed to reach a more definitive conclusion. Furthermore, it will be interesting to elucidate the nature of these events, which could fall into one or more of three classes: MMEJ/SSA events that retain the chromosome terminus, and *de novo* telomere additions or translocations that result in loss of the chromosome terminus. The location of the junction breakpoints can be mapped by PCR using primers starting from the cleavage site and extending outward. This analysis should distinguish the MMEJ/SSA events from the *de novo* telomere addition and translocation events. For events involving loss of the chromosome terminus, Southern blotting can be employed to determine whether they are telomere additions or translocations.

When we analyzed the amplifiable junctions (repaired by NHEJ) in the *rad9*Δ strain, we found that contrary to our prediction that the deletions in this strain would be similar in size to or larger than those in the WT strain, the *rad9*Δ strain, like the *rif1*Δ strain, contained smaller deletions (2-3 bp) and even insertions (1 bp), suggestive of those ends having undergone limited resection (Figure 12B). In the *rad9*Δ background, absence of Rif1 appeared to partially suppress the deletion events, leading to the appearance of more insertions (Figure 12B), although more junctions will need to be analyzed to justifiably make this conclusion. These findings suggest that Rif1 and Rad9 may have partially overlapping functions in regulating the fidelity of NHEJ repair.

We also performed experiments to address which domain(s) of Rif1 mediate its NHEJ repair function. Deletion of the protein phosphatase-1-interacting domain phenocopies the *rif1*Δ mutant (Figure 14), indicating that this region is important for Rif1's function in DSB repair. We have not determined yet whether Pol4 catalyzes the insertions that occur in the *rad9*Δ strain. Pol4-dependency, despite the presence of *RIF1*, would favor the hypothesis (discussed above) that Pol4 has increased

access to the DSB ends in the absence of *RIF1*, rather than the alternative hypothesis that Rif1 directly inhibits Pol4 function by regulating its phosphorylation status.

Deletion of a C-terminal region of Rif1 (*rif1-C*Δ), containing a Rap1-binding motif and a tetramerization domain (165), caused a significant decrease in DSB survival (Figure 13A). The mutation signature in the *rif1-C*Δ strain (Figure 13B), consisting mostly of deletions ranging from 1-7 bp and a few insertions, may be different from that in the WT strain (p=0.048, although this value is higher than the Bonferroni-adjusted alpha level of 0.0083). Mutation of the Rap1-binding motif in the Rif1 C terminus had no significant effect on DSB survival (p=0.086) or on the mutation signature (p=0.883) compared to WT cells (Figure 13; *rif1 RBM*), indicating that Rif1's function in NHEJ is independent of its interaction with Rap1, and therefore separable from its function in telomere maintenance. Interestingly, mutation of the Rif1 tetramerization domain (Figure 13; *rif1 CTD*) significantly reduced DSB survival compared to the WT strain. The mutation signature in the *rif1 CTD* strain also may be different from that of the WT strain (p=0.051, although this value is higher than the Bonferroni-adjusted alpha level of 0.0083). More specifically, the median deletion size in the *rif1 CTD* strain was 3 nucleotides compared to 7 nucleotides for the WT strain. This phenotype is not identical to that of a *rif1*Δ strain (see Figure 10B), however, suggesting that Rif1's function in DSB repair by NHEJ is partly dependent on its tetramerization domain.

In pair-wise comparisons to the WT strain, the mutation signature of either the *rif1-C*Δ strain or *rif1 CTD* strain was significantly different from WT or on the threshold of significance (p=0.048 and p=0.051 for *rif1-C*Δ and *rif1 CTD* respectively). However, because Bonferroni corrections were performed to account for the repeated use of the same WT repair junction dataset for comparisons to multiple strains, these p values were higher than the Bonferroni-adjusted alpha level. These experiments may need to be repeated so as to obtain independent WT datasets for comparison to each

of these strains, so as to increase statistical power and allow for making a more definitive conclusion on the role of the Rif1 C-terminal region, specifically of the tetramerization domain, in NHEJ repair.

The Rif1 C-terminus contains partially overlapping binding domains for Rap1 and Dbf4, a component of the Dbf4-dependent kinase (Cdc7-Dbf4) complex (147). Dbf4 binds to and phosphorylates Rif1, preventing its interaction with protein phosphatase-1 (PP1) (147). Preliminary data from our laboratory indicates that the *rif1 CTD* mutation compromises both Rif1 tetramerization and its interaction with Dbf4 (Friedman KL; unpublished data). Accordingly, in the context of DSB repair, in which the Rif1 PP1-interacting domain plays an important role (Figure 14), deletion of the Rif1 C-terminus or mutation of the Rif1 CTD might be expected to increase the interaction between Rif1 and PP1, causing a more "WT-like" phenotype. However, in those strains, we observed phenotypes more indicative of reduced Rif1 function (Figure 13C). A possible explanation for this finding is that the protein(s) targeted by Rif1-PP1 during DSB repair requires dynamic regulation of its phosphorylation status for proper function, and that either constitutive phosphorylation or dephosphorylation causes a deviation from its normal function.

During DNA replication, Rif1 prevents the initiation of DNA replication by directing protein phosphatase-1 to dephosphorylate and inactivate Mcm4, a component of the pre-replication complex (146, 147). In contrast to DSB repair, where deletion of the Rif1 C-terminus causes a phenotype indicative of reduced Rif1 function (Figure 13), deletion of the Rif1 C-terminus causes a more "WT-like" phenotype in the context of DNA replication (147), suggesting that Rif1-PP1 may have distinct mechanisms of action during DSB repair and DNA replication. This interpretation is based on the assumption that the Db4-interacting motif of Rif1 does indeed affect the interaction between Rif1 and protein phosphatase-1 in the context of DSB repair. The residues on Rif1 that are targeted for phosphorylation by Dbf4 have been mapped (147) and can be mutated to determine whether there is a

functional interaction between the Rif1 CTD and protein phosphatase-1-interacting domains during DSB repair.

CHAPTER III

INTRODUCTION: TELOMERES, TELOMERASE, AND DSB REPAIR BY D*E NOVO* TELOMERE ADDITION

Overview

In this chapter, I present an in-depth review of telomeres and telomerase as a prelude to the next section on DSB repair by *de novo* telomere addition. Seminal works that contributed to our current understanding of the structure and function of telomeres and telomerase are discussed, culminating in a review of the structure and function of telomeres and telomerase in *Saccharomyces cerevisiae*. In section three, I review *de novo* telomere addition, a DSB repair pathway that is rarely utilized, but nonetheless has serious implications for genome stability and human health. I discuss our current understanding, prior to the work in this thesis, of the factors that regulate *de novo* telomere addition in *S. cerevisiae*.

3.1 The Discovery of Telomeres, Structures that Distinguish Natural Chromosome Ends from Broken Ends

In the 1920's, Dr. Hermann Muller treated fruit flies with X-rays to gain insight into the hereditary unit, the gene. Among the repair products of the broken chromosomes were inversions, translocations, and deficiencies (deletions). He noted, however, that terminal deficiencies, deletions in chromosomes that extended all the way to the chromosome terminus, rarely occurred. Dr. Muller postulated that the repaired chromosomes resulted from the rejoining of broken ends and that rejoining never occurred between "originally free ends." He coined the term "telomere", a combination of the Greek words *telos* (end) and *meros* (part), for the "free ends" (169).

Prior to Dr. Muller's publication, the idea that natural chromosome ends were structurally and functionally distinct from broken DNA ends had already been put forth by Dr. Barbara McClintock. While studying X-ray-induced mutagenesis in *Zea mays*, she made similar observations as Muller, noting the absence of rejoining between "a piece of one chromosome" and "the end of another [intact chromosome]" (170). In later experiments, Dr. McClintock would go on to recover chromosomes with terminal deletions, but only after she irradiated young maize embryos soon after the first zygotic division (171). Her findings indicated that some broken ends could be "healed" and stabilized, leading her to propose, in 1939, the existence of a regulated mechanism for the maintenance of chromosome ends (172).

3.2 The End-replication Problem

The elucidation, in the 1950s and 1960s, of the linear nature of eukaryotic chromosomes and of the mechanism of DNA replication suggested a new problem, the end-replication problem, which in turn spurred models of the process by which telomeres were replicated. The original concept of the end-replication problem, independently proposed by Dr. Alexey Olovinkov and Dr. James Watson in the early 1970s (173, 174), was based on the knowledge that DNA replication proceeds only in the 5′ to 3′ direction and requires primed synthesis from a short RNA oligonucleotide. It posits that removal of the terminal RNA primer on the lagging strand creates an unreplicated 5′ gap that traditional replicative DNA polymerases cannot fill.

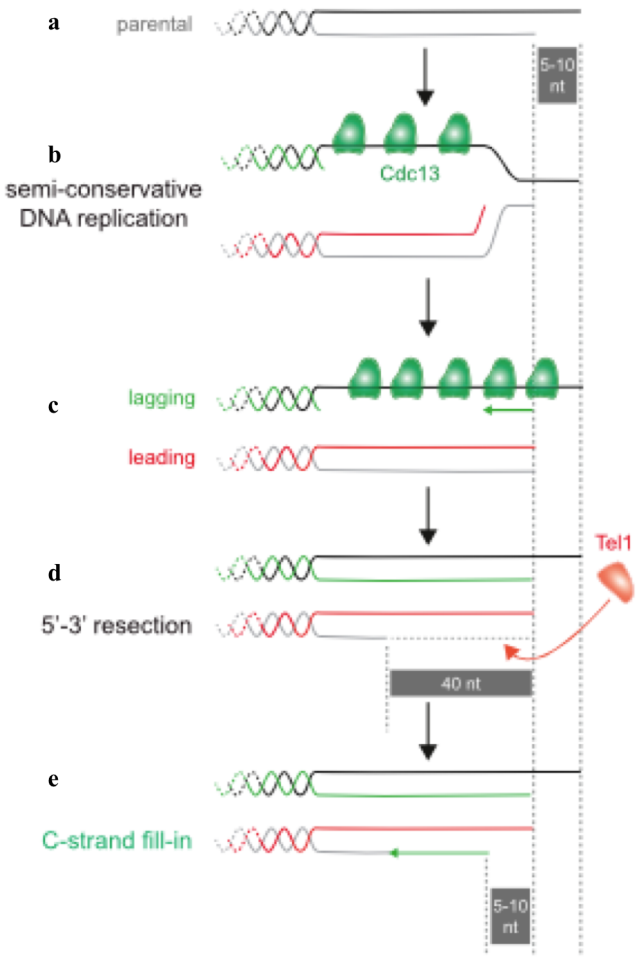

Figure 15. The revised end-replication problem. The original end-replication problem posits that telomere shortening is a consequence of removal of the last RNA primer from the lagging strand after DNA replication. In the revised model, removal of the last primer from the lagging strand simply regenerates the telomeric 3' overhang present on the parental chromosome (a). Leading strand replication (b) generates a blunt-ended intermediate (c) that must be processed by nucleolytic resection of the C-rich strand in an effort to generate a 3' overhang (d). The lagging strand machinery fills in the resected C-strand, and removal of the last primer (represented by the distance between the first and second vertical dashed lines) results in telomere shortening (e). Figure modified from (175).

The implication was that unless another mechanism existed to fill in this gap, subsequent cycles of cell division would lead to loss of a substantial portion of the chromosome ends.

The end-replication problem would be revised later to accommodate the discovery that telomeres terminate in 3′ overhangs (Figure 15). On the lagging (3′) strand, removal of the terminal RNA primer would simply regenerate the 3′ overhang. On the leading (5′) strand, however, replication would proceed to the terminus, generating a blunt-ended intermediate. To create a 3′ overhang, the 5′ strand would need to be nucleolytically resected, resulting in loss of terminal telomere sequences (Figure 15). The revised end-replication problem therefore posits a leading, rather than a lagging, strand problem (reviewed in (176, 177)), and experimental evidence in support of this hypothesis was obtained only fairly recently (175).

In the following section, I review key studies that contributed to our current knowledge of how telomeres solve the end-replication problem. These studies, performed in *Tetrahymena thermophila*, provided significant insight into the structure of telomeric DNA and revealed the existence of an enzymatic activity, telomerase, responsible for telomere maintenance.

3.3 Elucidation of Telomere Structure and Discovery of Telomerase: A Microscopic Ciliate Reveals Big Secrets

In 1978, Drs. Elizabeth Blackburn and Joseph Gall reported the structure of telomeric DNA in *Tetrahymena thermophila* (178). The single-celled ciliate has two nuclei: a mitotically dividing micronucleus, and a polyploid, amitotically dividing macronucleus, the latter of which facilitated the purification of telomeres. The macronucleus contains multiple copies of each of approximately 270 acentromeric, autonomously replicating pieces (ARPs) or minichromosomes generated from fragmentation of the micronuclear genome. The smallest minichromosome, at 21 kb, contains the ribosomal RNA gene, and is maintained at approximately 10,000 copies per macronucleus (reviewed in (179)). The relatively small size and abundance of the rDNA minichromosomes facilitated the

purification and analysis of their telomeres at a time when DNA sequencing technology was in its infancy.

The key findings presented by Drs. Blackburn and Gall are as follows: the terminal fragments of *T. thermophila* rDNA molecules contain a variable number (between 20 and 70) of repeats of the hexanucleotide sequence CCCCAA/TTGGGG, and are heterogeneous in length, ranging in size from 360 bp to 520 bp. Additionally, the CA-rich strand was determined to be oriented 5′ to 3′ toward the center of the molecule (178). Still, the question remained: how were these telomeres maintained?

In 1983, Dr. Blackburn received a letter in which Dr. McClintock reported that she had isolated a maize mutant that was defective in telomere healing at broken chromosome ends (180). Reasoning that a mutant meant the existence of a gene possibly encoding an enzymatic activity that maintained telomeres, Dr. Blackburn sought to identify this activity in *T. thermophila*. In 1985, Dr. Blackburn and Dr. Carol Greider, then a graduate student in the Blackburn laboratory at the University of California, Berkeley, published their discovery of this activity in *T. thermophila* (181). This finding would galvanize the field of telomere biology and ultimately garner them (and Dr. Jack Szostak, for his independent studies) the 2009 Nobel Prize in Physiology or Medicine.

Using an *in vitro* primer extension assay that entailed incubation of cell-free extract from *T. thermophila* with a synthetic primer containing *Tetrahymena* telomeric sequence $(TTGGGG)_4$, Drs. Blackburn and Greider demonstrated that an enzymatic activity in *T. thermophila* elongated the primer, adding nucleotides in a recurring six-base pattern. This activity was specific to telomeric DNA and was independent of DNA polymerase Polα, since treatment of the extract with aphidocolin, an inhibitor of Polα, did not inhibit primer elongation. The enzyme also appeared to be DNA template-independent, as treatment of the extract with micrococcal nuclease (to digest endogenous *Tetrahymena* DNA) did not inhibit primer elongation. Moreover, the telomere terminal transferase, so-called because its

apparent template-independence was reminiscent of the terminal transferase enzyme, added *Tetrahymena* telomeric repeats onto a primer containing yeast telomeric sequence. The reciprocal finding, that *Tetrahymena* telomeres could be maintained in yeast cells and that yeast telomeres were added onto the *Tetrahymena* telomeres, was made the previous year (182). These findings pointed to a conservation of at least some aspects of telomere biology among eukaryotes.

Two years after their discovery, Drs. Greider and Blackburn reported purification of the enzyme (183). They renamed the enzyme telomerase and demonstrated that telomerase was a ribonucleoprotein, as treatment of the enzyme with proteinase K or with RNaseA eliminated enzymatic activity (183). By 1989, the telomerase RNA was partially purified and sequenced (184). The purified RNA contained the sequence CAACCCCAA, which was complementary to the *Tetrahymena* TTGGGG repeats and could therefore serve as a template for telomere synthesis. To verify that this was the case, purified telomerase was co-incubated with a 20-nucleotide antisense oligonucleotide that was complementary to a region of the telomerase RNA adjacent to and including the CAACCCCAA sequence, and with RNaseH, a ribonuclease that specifically degrades the RNA strand within RNA-DNA hybrids. Analysis of telomerase post-incubation revealed that the telomerase RNA was cleaved by RNaseH at several positions within the CAACCCCAA sequence, resulting in inhibition of telomerase activity (184). Furthermore, in another study from the Blackburn laboratory, published in 1990, mutation of the CAACCCCAA sequence resulted in corresponding changes in the sequences of newly synthesized telomeric DNA *in vivo* (185). These studies therefore established telomerase as a reverse transcriptase, and this finding would hold true for other eukaryotic species including *S. cerevisiae*.

In Section 3.4 below, I present an extensive review of the structure and function of telomeres and telomerase in *S. cerevisiae*. The functions attributed to telomeres, protection of chromosome ends

from nucleases and distinguishing chromosome ends from DSBs, are mediated by telomere-binding proteins. I discuss the telomeric functions of telomere-binding proteins in *S. cerevisiae*, as well as the discoveries and functions of telomerase components in *S. cerevisiae*. I conclude the section with a review of the regulation of both telomere-binding proteins and telomerase in *S. cerevisiae* as a means of controlling telomere replication. Furthermore, to illustrate the conservation of telomere biology in eukaryotes, I present a brief review of the structure and function of human telomeres in Section 3.5.

3.4 Telomeres and Telomerase in *S. cerevisiae*

3.4.1 Telomere Structure and Function

Telomeres have several important functions. Telomere-binding proteins form a "telomere cap" that protects chromosome ends from nucleolytic degradation, and serves to distinguish natural chromosome ends from internal DSBs (186). Telomeres also control gene expression by the silencing of nearby genes, a phenomenon known as telomeric silencing or telomere position effect (TPE) (187). *S. cerevisiae* telomeric DNA contains 300 ± 75 bp of $TG_{1\text{-}3}/AC_{1\text{-}3}$ repeats, and terminates in a short 3′ overhang, a 12 to 15-nucleotide G-rich tail (188). Telomere-binding proteins, rather than the telomeres themselves, mediate the telomere functions described above.

The major telomere-binding protein in *S. cerevisiae* is the sequence-specific dsDNA-binding protein Rap1 (Figure 16). Rap1 is a multifunctional protein, so much so that it was "identified" several times (189, 190) and acquired many names before the name Rap1 was adopted. The name was proposed by Dr. David Shore and Kim Nasmyth who showed that Rap1 could bind to both silencer and activator sequences and named it **R**epressor/**A**ctivator Site Binding **P**rotein (189). At non-telomeric sites in the genome, Rap1 functions as a transcriptional regulator, mostly of ribosomal protein genes (191, 192).

Telomeric DNA contains high affinity Rap1 binding sites, on average, one every 20 bp (188). Rap1 binds to telomeric DNA *in vivo* as demonstrated by chromatin immunoprecipitation and by fluorescence microscopy experiments that provided evidence of Rap1 co-localization with telomeric DNA (193-195). Several attempts have been made to define the consensus binding sequence for Rap1 (191, 192, 196, 197), although Lieb *et al.* and Rhee *et al.* took a more comprehensive approach by utilizing a ChIP-seq and ChIP-exo approach, respectively, for genome-wide analysis of Rap1 binding sites. From their analysis, Lieb *et al*. derived a 13 bp Rap1 consensus sequence (5′-ACACCCRYACAYM-3′) consisting of two hemi-sites (ACACC and ACAYM) separated by a 3 bp spacer sequence (191). However, thermodynamic mapping of Rap1 binding sites revealed that Rap1 makes contacts with three additional bases immediately 5′ to the consensus sequence (198). Further demonstrating the complexity of Rap1 binding to its sequences, Rhee *et al.* identified four consensus sequences for Rap1, one of which is utilized exclusively at telomeres, while another is selectively utilized at ribosomal protein genes, which form the majority of non-telomeric Rap1-binding sites (192).

The double-Myb DNA binding domain of Rap1, located in the central region of Rap1, is required for all functions of the protein (199). An N-terminal region, containing a BRCT domain, can be deleted without generating any obvious phenotypes (199, 200), while the C-terminal domain of Rap1 mediates its telomeric functions, through interactions with the silencing proteins Sir3 and Sir4 (200) and with the telomere length regulatory proteins Rif1 and Rif2 (127, 164) (Figure 16).

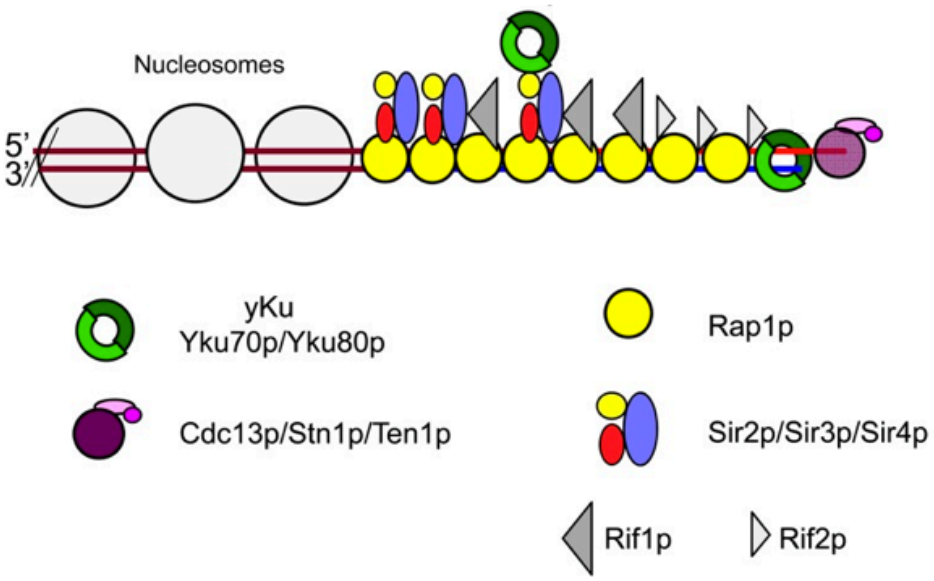

Figure 16. *S. cerevisiae* telomeres. Rap1 bound to the double-stranded telomeric repeats recruits the silencing proteins Sir2, Sir3, and Sir4, and the telomere length regulatory proteins Rif1 and Rif2 to telomeres. Cdc13 interacts with the single-stranded 3' overhang. The association of Yku with telomeres occurs both through direct end-binding by Yku and by Sir4-mediated recruitment. Figure modified from (188).

The C terminus of Rap1 interacts with the silencing protein Sir4 to mediate telomeric silencing or TPE (200). TPE is initiated by Rap1-mediated recruitment of Sir4 to telomeres (201). Sir4, in turn, recruits other silencing proteins Sir2 and Sir3 to facilitate the spreading of TPE, up to 2-4 kb from the telomere. Sir2, a histone deacetylase, is purported to play a major role in TPE spreading by deacetylation of the amino terminal tails of histones H3 and H4, thereby allowing Sir3 and Sir4 to bind to neighboring nucleosomes (188, 201).

The Rap1 C terminus also contains four binding surfaces, three of which are non-overlapping, for the telomere length regulatory proteins Rif1 and Rif2. Multiple interactions between Rap1 and Rif1, and between Rap1 and Rif2 facilitate the formation of a higher-order "velcro-like" structure (165) that regulates telomere length (127, 164), prevents telomeric fusions (202, 203), and protects telomeres from nucleolytic degradation (121, 204). Telomere length in *S. cerevisiae* is inversely proportional to the number of Rap1-bound Rif1 and Rif2 molecules present at telomeres—when targeted adjacent to

telomeres, the Rap1 C terminus, Rif1, and Rif2 molecules are "counted" together with the endogenous telomeres and telomere length decreases proportionately to the number of targeted molecules (205, 206). One mechanism by which Rif1 and Rif2 restrain telomere lengthening involves inhibition of a Yku80-Sir4 telomere lengthening pathway (207). Yku80 had been shown to interact with Sir4 (bound to telomeres through Rap1), as shown by yeast two-hybrid experiments (83). Hass *et al.* proposed that Rif1 and Rif2 inhibit the Yku80-Sir4 telomere lengthening pathway by competitive inhibition of Sir4 binding to Rap1 (207). Rif2 additionally inhibits telomere lengthening by reducing the accumulation of the checkpoint kinase Tel1 at telomeres (208). Tel1 is recruited to telomeres by the MRX complex (18), although Tel1 in turn appears to promote the stable binding of MRX at telomeres (208). MRX and Tel1 function in the same pathway for telomere maintenance (209) and are required for efficient recruitment of telomerase to telomeres (210). Deletion of *RIF1* and/or *RIF2* also results in increased TPE, suggesting that the Rif proteins compete with the Sir proteins for Rap1 binding (127, 164).

Rap1 also inhibits NHEJ at telomeres by three pathways, one involving Rif2, a second involving Sir4, and a third independent pathway (202). Taking advantage of the shortened, deprotected telomeres in a *tel1*Δ strain, Marcand *et al.* found that fusions between the deprotected *tel1*Δ telomeres increased in the absence of Rif2 and Sir4, and in cells expressing a conditional allele of Rap1 [*rap1*-(Δ)] that reduces Rap1 levels. Telomere fusions were higher in *tel1*Δ *rif2*Δ *sir4*Δ cells than in either *tel1*Δ *rif2*Δ or *tel1*Δ *sir4*Δ cells, indicating that Rif2 and Sir4 inhibit NHEJ independently. Likewise, telomere fusions occurred with higher frequency in *tel1*Δ *rif2*Δ *sir4*Δ *rap1*-(Δ) cells than in *tel1*Δ *rif2*Δ *sir4*Δ cells, indicating that Rap1 additionally inhibits telomere fusions in a Rif2- and Sir4-independent manner (202).

Rif1 and Rif2 also function in limiting telomere resection, albeit by different mechanisms. Rif2 limits telomere resection by inhibiting MRX/Tel1 accumulation at telomere (208), whereas Rif1 limits

Exo1-dependent resection specifically at telomeres in which the capping function of Cdc13 (see below) is compromised (204).

The Yku heterodimer, which is required for NHEJ (Section 1.2.3: C-NHEJ), is paradoxically, also present at telomeres (Figure 16), structures at which the DNA damage checkpoint and NHEJ are inhibited. There are at least two modes of recruitment of Yku to telomeric DNA. Yku associates directly with the terminal telomeric region in a Sir4-independent and sequence-independent manner (211), and with the internal subtelomeric region in a Sir4-dependent manner (83). Yku promotes telomere lengthening, as deletion of either *YKU70* or *YKU80* results in telomere shortening (75) and protects telomeres from exonucleolytic degradation by Exo1 (121). Lastly, Yku promotes TPE, as yeast cells lacking Yku70 or Yku80 are severely defective in TPE (75). Deletion of *RIF1* and/or *RIF2* restores TPE in *yku* mutant cells, suggesting that Yku regulates TPE by affecting the competition between the Rif and the Sir proteins for the Rap1 C terminus (212).

A third DNA-binding protein, Cdc13, binds to the terminal G-rich tail of telomeres (Figure 16). Cdc13 plays a large role in telomere capping and this capping function is essential for cell viability. Cdc13 forms a protein complex, with two other essential proteins Stn1 and Ten1, that protects telomeres from nucleolytic degradation (213-215). In addition to its capping function, Cdc13 also recruits telomerase to telomeres. The telomerase recruitment function of Cdc13 is further elaborated in Section 3.4.2 below.

3.4.2 Telomerase Structure and Function

S. cerevisiae telomerase consists minimally of a reverse transcriptase Est2, the telomerase RNA TLC1, and the accessory subunits Est1 and Est3. Est1, the first component to be described, was identified using a genetic screen designed to identify yeast mutants that were defective in telomere

function (216). The screen was based on the ability of yeast cells to convert, at a low frequency, a circular plasmid containing inverted repeats of *Tetrahymena* telomeres into a linear plasmid, stabilized by the addition of yeast telomere repeats onto the *Tetrahymena* telomeres. The two telomeric repeats were separated by a *URA3* gene that would be lost as a consequence of linearization of the plasmid and elongation of the *Tetrahymena* telomeres. Cells carrying the stabilized linear plasmid could be identified by their ability to grow on medium containing 5-Fluoroorotic acid (5-FOA), a drug that is toxic to *URA3*-expressing cells. Therefore, mutants that were defective in plasmid linearization, telomere elongation, or telomere protection would display a reduced frequency of 5-FOA resistance.

To conduct the screen, yeast cells containing the plasmid described above were mutagenized with ethyl methansulfonate (EMS). From the seven thousand colonies that were screened, 32 mutants were identified that exhibited reduced 5-FOA resistance and one of these had shortened chromosomal telomeres. The affected gene was cloned and sequenced, and named *EST1* (**E**ver **S**horter **T**elomere **1**) because *est1* mutants exhibited progressively shorter telomeres when cultured for many generations. In addition to the shortened telomere phenotype, *est1* mutants also exhibited increased chromosome loss and a progressive reduction in viability termed senescence (216).

Five years after this report, the telomerase RNA TLC1 (**T**elomerase **C**omponent **1**) was identified (217). This discovery, coupled with the fact that nuclear extract prepared from *est1Δ* cells still had telomerase activity *in vitro*, suggested that there were more gene(s) to be identified that were involved in telomere elongation. Capitalizing on the chromosome loss phenotype displayed by *est1* mutants (above), Lendvay *et al.* performed another genetic screen to identify additional activities responsible for telomere elongation in *S. cerevisiae* (218). The authors first screened for mutations with increased chromosome loss rates, as observed for the original *est1* strain. This approach allowed the researchers to screen through a total of 350,000 colonies. Mutants with increased chromosome loss

were then subjected to the plasmid linearization assay (above) to identify 19 mutants that displayed chromosomal telomere shortening and senescence. These mutants mapped to four genes: the previously identified *EST1*, *EST2*, *EST3*, and *EST4*. The sole *est4* mutant turned out to be allelic to the gene encoding the telomere-binding protein *CDC13* (218).

Studies published in 1997 began to shed some light on the functions of the *S. cerevisiae* telomerase protein components. Using reverse genetics techniques, Lingner *et al.* cloned and sequenced the gene encoding the p123 subunit of *Euplotes aediculatus* telomerase (219). By conducting a BLAST search of protein databases, Lingner *et al.* demonstrated that p123 was homologous to yeast Est2. Est2 had been previously cloned and sequenced (218), although at the time its sequence gave no immediate insight into its function. Furthermore, given the fact that both *T. thermophila* and *S. cerevisiae* telomerases utilized RNA templates for the synthesis of telomeric DNA (184, 217) and that both p123 and Est2 co-purified with their respective telomerase RNAs (219, 220), Lingner *et al.* tested the possibility that p123 and Est2 provided the reverse transcriptase activities in their respective telomerases. Indeed, alignment of the amino acid sequences of p123 and Est2 with those from known reverse transcriptases revealed the presence of reverse transcriptase motifs in both Est2 and p123 (219). Mutations of conserved residues within these motifs, including three absolutely conserved aspartate residues, resulted in phenotypes (telomere shortening and senescence) that were indistinguishable from those of an *est2Δ* strain, thereby identifying Est2 as the *S. cerevisiae* telomerase reverse transcriptase.

Another report from 1997 demonstrated that Est1 and Est3, though required for telomere lengthening *in vivo*, were dispensable for telomerase activity *in vitro*, suggesting that they played regulatory roles *in vivo* (221). Work done in the lab of Dr. Victoria Lundblad provided the first indication that Est1 plays a regulatory role in telomerase recruitment (222). In this study, expression of Est2 as a fusion protein with the the DNA binding domain (DBD) of the telomeric 3' overhang-

binding protein Cdc13 (Est2-Cdc13$_{DBD}$) in *est1Δ* cells allowed for stable telomere maintenance. Because the Est2-Cdc13$_{DBD}$ fusion, expected to be constitutively bound at telomeres, bypasses the requirement for Est1 in telomere maintenance, these results suggest that Est1 plays an important role in telomerase recruitment, possibly via an interaction with Cdc13 (222).

In support of an interaction between Est1 and Cdc13, and a role for this interaction in telomere maintenance, the *in vivo* telomere replication defects of a charge-swap mutant of Cdc13 (Cdc13^{E252K}) are suppressed by a charge-swap mutation in Est1 (Est1^{K444E}), suggesting a role for glutamate-252 of Cdc13 and lysine-444 of Est1 in mediating a physical interaction between Cdc13 and Est1 (223). *In vitro* binding assays have confirmed a direct physical interaction between Cdc13 and Est1 (224). Furthermore, while Est1 does not bind efficiently to telomeric ssDNA in gel shift assays, it binds to, and forms a tertiary complex, with a Cdc13-telomeric ssDNA complex (224). The glutamate-252 residue that mediates the interaction with Est1 (223) is not situated within the Cdc13^{DBD} (see paragraph above). Importantly, Est1 is unable to form a tertiary complex with a Cdc13^{DBD}-telomeric ssDNA complex confirming the importance of the Cdc13-Est1 interaction for recruiting Est1 to telomeric ssDNA (224). While, as expected, the Cdc13^{E252K} mutation reduces telomerase recruitment *in vivo* (225), Est1, unexpectedly, interacts equally well with WT Cdc13^{E252} and with mutant Cdc13^{E252K} *in vitro* (224). To reconcile these findings, it has been proposed that the Est1-Cdc13^{E252K} complex may be defective *in vivo*, such that Est1 cannot interact stably with other telomerase subunits at telomeres leading to telomerase dissociation (224).

Expression of Est2 as a fusion protein with Cdc13$_{DBD}$ does not bypass the requirement for Est3 in telomere maintenance in *est3Δ* cells, suggesting that Est3's primary role in telomere maintenance is unrelated to telomerase recruitment (222). Est3 may, however, have a role in stimulating telomerase activity via a direct interaction with the Est2 reverse transcriptase (226).

3.4.3. Regulation of Telomere Replication

Cell cycle regulation of telomerase

In an effort to understand how telomerase function is regulated, Diede *et al.* devised an ingenious assay for this purpose (227). The WT strain for this assay contained an ectopic construct, consisting of an HO endonuclease recognition sequence inserted immediately adjacent to an 81 bp telomeric "seed" sequence, integrated on chromosome VII in *S.cerevisiae*. The HO endonuclease gene was placed under the control of a galactose-inducible promoter, allowing for temporal control of HO endonuclease induction. HO endonuclease expression was induced by exposing cells to galactose, resulting in cleavage and exposure of the telomeric seed. The researchers monitored the telomeric seed by Southern blotting and found that the seed was efficiently elongated; by 4 hours after HO endonuclease induction, approximately 90% of cells had added a new telomere to the end of the telomeric seed. Importantly, telomere elongation was dependent on telomerase, as cells lacking the telomerase RNA TLC1 were profoundly defective in elongating the telomeric seed.

To address whether telomerase function was cell cycle-regulated, they performed this assay in synchronized cells. Whereas G_2/M-arrested cells efficiently elongated the telomeric seed, G_1-arrested cells did not. Importantly, the inability of G_1-arrested cells to elongate the telomeric seed was not due to a lack of telomerase activity in those cells because as demonstrated using an *in vitro* assay, telomerase purified from G_1 cells elongated a synthetic primer containing yeast telomeric sequences as effectively as telomerase purified from G_2/M-arrested cells.

The finding that telomere elongation by telomerase did not occur *in vivo* in G_1 cells, despite the presence of active telomerase in these cells, suggested that telomerase was not recruited, or at least

not efficiently recruited, to telomeres in G_1 cells, and spurred numerous studies aimed at addressing whether telomerase recruitment to telomeres was cell cycle-regulated.

Chromatin immunoprecipitation proved to be a useful technique for this purpose, allowing for examination of the association of telomerase components with telomeres throughout the cell cycle. Much of the findings discussed here are the result of work done in the laboratory of Dr. Virginia Zakian. By arresting cells in G_1 and then releasing them into the cell cycle, the association of telomerase components with telomeres could be monitored as cells progressed through the cell cycle.

Est2, the reverse transcriptase, and TLC1, the telomerase RNA, are both telomere-bound in G_1. As cells progress into S phase, Est2 and TLC1 association with telomeres decreases, until the late S phase when a second peak of association with telomeres is detected (228). In G_1, Est2 association with telomeres is dependent on an interaction between Yku80 and the telomerase RNA TLC1 (84, 188). An additional component to this Yku-TLC1 recruitment pathway has recently been described. In the absence of Sir4, a component of the subtelomeric silencing complex, telomeres shorten to the same extent as in cells in which the interaction between Yku80 and TLC1 has been disrupted (84, 207), suggesting that Sir4, itself bound to telomeres via an interaction with the telomere-binding protein Rap1, recruits Yku-TLC1 to telomeres. However, these mutants do not display an *est* phenotype (progressive telomere shortening and senescence) suggesting that the association of telomerase with the telomere during G_1 is not crucial for telomere maintenance (188, 207).

Est1 and Est3 display similar telomere association profiles. Both proteins predominantly associate with telomeres in late S phase, although Est3 shows minor association during G_1 phase (228, 229). Est1 protein levels are cell cycle-regulated—Est1 protein levels are low in G_1 phase, as a result of protein degradation, but peak in late S/G_2 phase (230). Est1 degradation during G_1 phase is

proteasome-dependent (230), and involves at least two E3 ubiquitin ligases, Ufd4 and the anaphase-promoting complex (APC) (231, 232).

Peak telomere associations of all four components of telomerase (Est1, Est2, Est3, and TLC1) coincide during late S/G2 phase, when abundant Est1 levels permit the assembly of a complete, active telomerase holoenzyme (228-230). However, Est1 abundance levels alone do not account for cell cycle regulation of telomerase function, as stabilization of Est1 in G_1 phase by inhibition of the proteasome still does not permit telomere elongation (230).

Telomerase preferentially elongates short telomeres

During any given cell cycle, telomerase does not act at every telomere, but rather preferentially elongates the shortest telomeres in the cell. The MRX (Mre11-Rad50-Xrs2) complex and Tel1, which are important for efficient telomerase recruitment, as well as Rif2 and Pif1, are critical determinants of this preference (233-237). In WT cells, telomerase binds preferentially to short telomeres, but this preference is lost in cells lacking Tel1 or in cells expressing a mutant of Xrs2 that is defective at recruiting Tel1 to telomeres (236). Consistent with the role of Rif2 in limiting Te11 accumulation at telomeres (208), telomerase also loses its binding preference in cells lacking Rif2 (234), indicating that reduced association of Rif2 with short telomeres marks those telomeres for elongation (234, 236).

Pif1, a helicase that inhibits telomere lengthening by displacing telomerase from telomeres (238, 239), has also been implicated in delineating which telomeres are elongated by telomerase. In *pif1* mutant cells, as in *tel1Δ* cells, telomerase is no longer recruited preferentially to short telomeres (235). Unlike MRX/Tel1, however, Pif1 is preferentially recruited to long telomeres (235), indicating that preferential elongation of short telomeres is achieved in at least two ways: exclusion of telomerase

from long telomeres by Pif1 and Rif2, and preferential recruitment of telomerase to short telomeres by MRX and Tel1 (233-237).

3.5. Structure and Function of Human Telomeres

Much of telomere and telomerase biology is conserved among eukaryotic species, including in humans. Human telomeres contain 10 - 15 kb of double-stranded TTAGGG/CCCTAA repeats and terminate in an approximately 150-200-nucleotide long G-rich 3' overhang (reviewed in (240)). Telomeres are bound by a six-member protein complex (TRF1, TRF2, TIN2, TPP1, RAP1, POT1) (Figure 17) called shelterin that is in many ways functionally analogous to the Rap1-Rif1-Rif2 complex in *S. cerevisiae* (reviewed in (241)). In contrast to ScRap1, however, hRAP1 is dependent on TRF2 for localization to telomeres (242) and is not involved in telomere length regulation (243). Rather, the role of ScRap1 in telomere length regulation is fulfilled by TRF1-TRF2 in human cells. The shelterin proteins are organized such that TRF1 and TRF2 are bound to the double-stranded telomere repeats and POT1 is bound to the G-rich tail. TPP1 and TIN2 link TRF1 and TRF2 to 3' overhang-bound POT1, while RAP1 is recruited to the complex via an interaction with TRF2 (reviewed in (241)) (Figure 17).

In human cells, overexpression of TRF1 causes telomeres to shorten, indicating that TRF1 is a negative regulator of telomere elongation (244). In agreement with this conclusion, overexpression of a dominant-negative mutant of TRF1 that perturbs the localization of endogenous TRF1 to telomeres results in telomere elongation (244). TRF2, like TRF1, inhibits telomere elongation by telomerase when overexpressed, indicating a role in negative regulation of telomerase (245). TRF2 plays additional roles in telomere-end protection. A dominant-negative allele of TRF2 that inhibits binding of endogenous TRF2 to telomeres causes increased telomere fusions by NHEJ (246), as a result of loss

of the telomeric 3' overhang (246). Finally, TRF2, but not the other shelterin proteins stimulates, *in vivo*, the formation of telomere loops (t-loops) (247), protective structures formed when the 3' overhang invades the duplex telomeric sequence (reviewed in (241)). The NHEJ inhibitory and end-protection functions of TRF2 have been proposed to be a consequence of its role in t-loop formation (247).

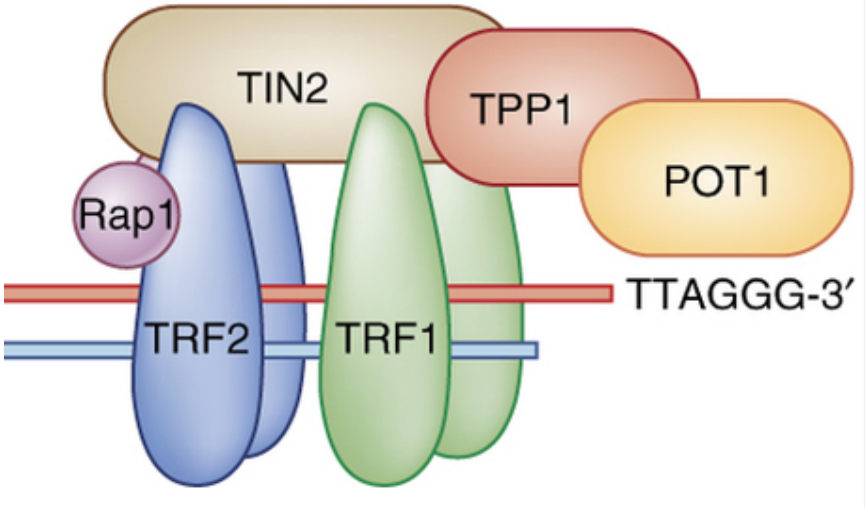

Figure 17. The human shelterin complex. Human shelterin is a six-member protein complex consisting of TRF1, TRF2, RAP1, TIN2, TPP1, and POT1. TRF1 and TRF2 interact with the double-stranded telomeric repeats, whereas POT1 binds to the terminal 3' overhang. TIN2 and TPP1 serve as bridging proteins within the complex, linking dsDNA-bound TRF1 and TRF2 to POT1 bound at the 3' overhang. Figure modified from (248).

In human cells, depletion of POT1 causes only a very slight increase in telomere fusions (<2-fold (249) compared to a 10-100-fold increase in cells in which TRF2 has been inhibited (246)), indicating that POT1 does not play a significant role in preventing NHEJ at human telomeres (249). However, POT1 is required for maintenance of the telomeric 3' overhang, as overhang lengths are decreased in POT1-depleted cells (249). POT1, together with TPP1, also promotes telomerase recruitment to telomeres (250), and stimulates telomerase repeat addition processivity (RAP) (251). Repeat addition processivity defines the number of telomeric repeats that telomerase can synthesize before dissociating from the telomere (252). Telomerase recruitment and stimulation of RAP by the

TPP1-POT1 complex requires a TEL patch on the surface of TPP1 consisting of a cluster of mostly acidic amino acid residues (253). The corresponding residues in human telomerase reverse transcriptase (hTERT) that mediate telomerase interaction with TPP1 have recently been described (254). Schimdt *et al.* showed that mutation of two basic residues in the telomerase essential N-terminus (TEN) domain of hTERT reduces TPP1-POT1 stimulation of telomerase RAP *in vitro* and causes defective telomere maintenance *in vitro*. A charge-swap mutation in the TPP1 TEL patch, rescued the telomere maintenance and telomerase RAP defects of the hTERT mutant, indicating that a direct interaction between the TPP1 TEL patch and the hTERT TEN domain is required for telomerase recruitment and TPP1-POT1 stimulation of telomerase RAP. Importantly, the hTERT mutant was not defective in telomerase activity *in vitro*, indicating that the telomerase maintenance and telomerase RAP defects are primarily due to loss of the interaction with TPP1 (254).

3.6 Human Diseases Associated with Dysfunctional telomeres

In 1961, Dr. Leonard Hayflick demonstrated that cells have a replicative limit (255), challenging the previously held notion that cells could proliferate indefinitely under optimal culture conditions. Dr. Alex Carrel proposed the latter hypothesis in 1912 after growing chick heart fibroblasts continuously in culture for three months (256). These cells proliferated continuously in culture for a total of 34 years; however, we now understand that the culture medium was prepared daily from chick embryo extract likely contaminated with stem cells, providing a renewable source of heart cells for the culture (240, 257).

Since Dr. Hayflick's discovery, tremendous progress has been made in understanding the molecular mechanisms of cellular aging, and it is now widely accepted that telomere length is a primary determinant of cellular replicative lifespan. In normal human somatic cells, TERT expression is

transcriptionally repressed and as a consequence, telomere length progressively decreases with successive cell cycles until cells reach their replicative limit and senesce (reviewed in (240)). The timing of replicative senescence is dependent on a number of factors including initial telomere length, the rate of telomere shortening, and the length of the shortest telomere in the cell (reviewed in (240)). Senescence, the first block to oncogenesis, is triggered by cell cycle checkpoints (reviewed in (240)). However, cells with dysfunctional checkpoints may continue to divide until they reach the second block to oncogenesis, a stage referred to as crisis that is marked by extreme telomere loss, extensive chromosomal instability, and cell death by apoptosis (240). Still, a very small proportion of cells, approximately 1 in 10^6 to 10^7 escape crisis and become immortalized by re-activating telomerase expression or using a recombination-based ALT (**A**lternative **L**engthening of **T**elomeres) mechanism for telomere maintenance (reviewed in (240)). Telomerase activity has been identified in approximately 90% of cancers (reviewed in (240)). Somatic mutations in the TERT promoter have been identified in many cancer types, accounting for one potential source of telomerase activity in cancer cells (reviewed in (240)). However, it is possible that cancer cells may arise from the clonal selection of pre-existing telomerase-positive cells during carcinogenesis (reviewed in (258)).

Telomere attrition is correlated with many aging-related diseases. These so-called telomeropathies, examples of which are dyskeratosis congenita (DKC), idiopathic pulmonary fibrosis (IPF), Werner Syndrome (WS), and Bloom Syndrome (BS), are caused by defects in the telomere maintenance machinery or in DNA repair proteins that contribute to telomere maintenance, and in some cases, show clear patterns of familial inheritance (reviewed in (240)). Telomeropathies share overlapping phenotypes—such as growth deficiencies, immunodeficiencies, and increased cancer predisposition—that may present at different times during the lifetime of an individual or with varying degrees of penetrance, even among individuals with identical mutations (reviewed in (240)). Genetic

anticipation, a phenomenon in which the age of onset decreases and disease severity increases in later generations, is also common in telomeropathies, and is influenced by a number of factors, including the types of disease-causing mutations and environmental factors (reviewed in (240)). Another source of genetic anticipation is the inheritance by each successive generation of unusually short telomeres from preceding generations, as has been observed in families with DKC (259, 260).

Potential therapeutic avenues for targeting telomeres and telomerase are being explored for cancers and aging diseases. The varying types of therapies in development for cancers include, but are not limited to, therapies aimed at inhibiting telomerase activity and immunotherapies aimed at stimulating immune system-driven killing of cancer cells (reviewed in (261)). Also being explored are therapies that directly mimic or interfere with telomeres. These therapies have the potential added benefit of targeting both telomerase-expressing cancer cells and ALT cancer cells that maintain their telomeres by a telomerase-independent recombination mechanism (reviewed in (261)). Conversely, therapies in development for aging diseases include compounds that upregulate telomerase activity, and androgens that stimulate *TERT* expression (reviewed in (262)). However, these therapies must be designed to allow for regulated telomerase expression and/or activity so as to prevent carcinogenesis (reviewed in (262)).

Although endogenous telomere dysfunction is a contributing factor to the pathological conditions discussed above, aberrant telomerase activity at internal sites of DNA damage can also contribute to disease pathologies in humans. This process, known as *de novo* telomere addition, is the focus of the next section.

3.7 *De Novo* Telomere Addition

Telomerase action is not limited to chromosome ends. At chromosomal DSBs, telomerase can add telomeric repeats to one or both ends of the break, resulting in stabilization of the centromere-containing chromosome fragment. This process is referred to as telomere healing or *de novo* (new) telomere addition. *De novo* telomere addition is accompanied by terminal deletions because the acentromeric fragment, whether or not it is "healed" by telomerase, cannot be maintained in the cell. Dr. Muller's and Dr. McClintock's observations of terminal deletions (Section 3.1; (169, 172)) resulting from irradiation of fruit flies and maize, respectively, represent probably the first documented examples of *de novo* telomere addition. *De novo* telomere addition has now been observed in many other organisms. Macronucleus formation in *T. thermophila* (see Section 3.3) is accompanied by telomere addition to the ends of chromosomal fragments derived from the micronucleus genome. In the parasitic nematode *Ascaris suum*, somatic differentiation of early embryonic cells is accompanied by chromatin diminution, a process in which about a quarter of the genome is eliminated (263). During chromatin diminution, specific chromosomal sites are targeted for cleavage, and the resulting DSBs are healed by *de novo* telomere addition (263). *De novo* telomere addition also occurs in human cells and in *S. cerevisiae* (discussed extensively below). Nonetheless, spontaneous *de novo* telomere additions that are not associated with developmental events are rare events. In *S. cerevisiae*, for example, spontaneous *de novo* telomere additions are estimated to occur at a frequency of approximately 3.5×10^{-10} (264).

De novo telomere addition has dire consequences for genome stability and cell viability. In haploid cells, terminal deletions that cause loss of one or more essential genes result in cell death, and in diploid cells, *de novo* telomere addition is one mechanism by which loss-of-heterozygosity (LOH) can arise (reviewed in (265)). Given the implications for *de novo* telomere addition in chromosome

stability and cell survival, a significant amount of research has been directed towards elucidating the regulation of *de novo* telomere addition. As the majority of these studies have been conducted in *S. cerevisiae*, I will next discuss the two most common types of assays utilized for *de novo* telomere addition studies in *S. cerevisiae*, before launching into a review of the mechanisms regulating *de novo* telomere addition in *S. cerevisiae*.

3.7.1 *De Novo* Telomere Addition Assay Systems

The most common assay systems for studies of *de novo* telomere addition at spontaneous DSBs and at experimentally induced DSBs are illustrated in Figure 18A and B, respectively. The gross chromosomal rearrangement (GCR) assay (264) (Figure 18A) allows for the isolation of GCRs (large deletions, translocations, *de novo* telomere additions) that occur within an ~ 11.5 kb non-essential region on the left arm of *S. cerevisiae* chromosome V (ChrV-L). GCR events result in loss of the counterselectable markers (*CAN1* and *URA3*) located distal to the GCR region. Expression of *CAN1* confers sensitivity to the drug canavanine, while expression of *URA3* confers sensitivity to the drug 5-Fluoroorotic acid (5-FOA). Cells that incur GCR events can therefore be isolated as canavanine-resistant (CAN^R) and 5-FOA-resistant ($5\text{-}FOA^R$) colonies following plating to medium containing both drugs, and the approximate site at which a genomic rearrangement occurred can be determined by PCR amplification using multiple sets of primers arrayed along the target region. CAN^R $5\text{-}FOA^R$ isolates are further subjected to Southern blotting to identify the isolates that incurred *de novo* telomere addition events, by looking for the characteristic smear pattern of telomeric sequences.

Most of our current knowledge on *de novo* telomere addition and its regulation in *S. cerevisiae* resulted from studies of telomere addition at HO endonuclease-induced DSBs. The more common

variant of this assay employs HO endonuclease to create a DSB (on ChrVII-L) that may or may not be preceded by a short telomeric seed on the centromere-proximal side of the break (Figure 18B). The HO

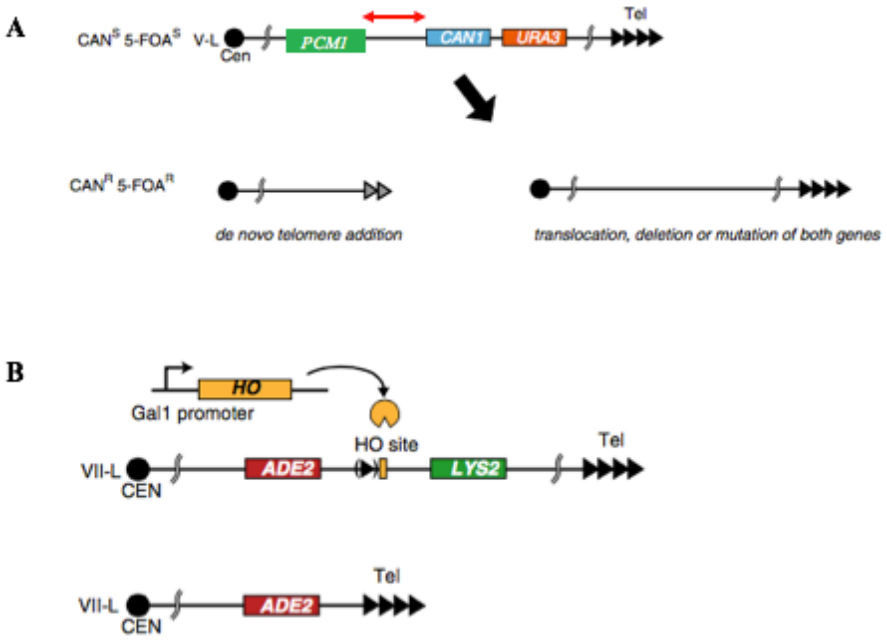

Figure 18. *De novo* telomere addition assay systems. (A) The GCR assay system for analysis of *de novo* telomere addition events resulting from spontaneously occurring DSBs. *CAN1* and *URA3* serve as counterselectable markers for the isolation of GCR events (*de novo* telomere additions, translocations, large deletions etc.) that occur within an 11.5 kb GCR region on chromosome V represented by the double-ended red arrow. See text for more details. (B) An inducible DSB assay system for studying *de novo* telomere additions in *S. cerevisiae*. Plating of cells to media containing galactose induces expression of HO endonuclease, which subsequently introduces a DSB adjacent to a telomeric seed sequence. See text for more details. Figures A and B modified from (265).

endonuclease-induced DSB assay system has already been discussed (Figure 3B). The *LYS2* gene on the telomere-proximal side of the HO endonuclease site serves as a marker for the identification of surviving colonies that underwent telomere healing at the DSB. While WT *S. cerevisiae* cells cannot survive on media containing the glutamate analog α-aminoadipate (α-aa) as the sole nitrogen source, *lys2* mutant cells gain the ability to utilize α-aa (266). Therefore, cells that repair the DSB by *de novo* telomere addition lose *LYS2* and can grow on medium containing only α-aa as the sole nitrogen source. Telomere addition in these isolates is then verified by Southern blotting. For the assays depicted in

Figure 18, although the *URA3* and *LYS2* genes are utilized for the identification of cells that have undergone *de novo telomere* addition and lost the end of the chromosome, any counter-selectable marker may serve this purpose.

Next, I discuss the *cis*- and *trans*-acting requirements, revealed through the use of these assays, for *de novo* telomere addition in *S. cerevisiae*.

3.7.2 Factors Affecting *De Novo* Telomere Addition in *S. cerevisiae*

Presence or Absence of Telomeric Seed Sequences

Although telomere additions can, and do, occur at sites with little TG sequences (267), in other cases, relatively long TG-rich (telomere-like) tracts have been observed near telomere addition target sequences. In a study of *de novo* telomere additions that occurred after HO endonuclease-induced generation of a DSB on an engineered extra copy of *S. cerevisiae* chromosome VII, a number of the telomere healing target sites were located 37-49 bp distal to a 35 bp stretch of telomere-like sequence (268).

Similar observations were made in a study of *de novo* telomere additions that occurred after HO endonuclease-induced generation of a DSB on *S. cerevisiae* chromosome III. In this assay, a *T. thermophila* telomeric seed sequence $(T_2G_4)_{13}$ was inserted approximately 10 kb centromere-proximal to an HO endonuclease site located at the *MATα* locus on chromosome III (269). Despite the presence of about 10 kb of intervening sequence (that contained short TG sequences at which telomeres could theoretically be added) between the HO site and the $(T_2G_4)_{13}$ repeats, all of the *de novo* telomere addition events occurred in sequences within 100 bp of the seed. The $(T_2G_4)_{13}$ repeats were themselves not targets for telomere addition, but they were absolutely required for telomere addition. No *de novo*

telomere additions were observed in a strain in which the $(T_2G_4)_{13}$ repeats were not inserted on chromosome III. Moreover, the telomere addition target sites were considerably shorter than the $(T_2G_4)_{13}$ repeats; the most commonly used target site was a 9 bp (GGGTGTGGT) sequence. These findings suggested that the relatively longer $(T_2G_4)_{13}$ repeats stimulated *de novo* telomere addition at the shorter target sequences (269).

Similar findings were reported in studies in which a telomeric seed, composed of *S. cerevisiae* telomeric DNA, is placed immediately adjacent to the HO endonuclease site (Figure 18B). The 81 bp telomeric seed (TG_{81}) greatly stimulates *de novo* telomere addition following HO cleavage (227). However, the new telomeres are often added at the 3′ TTGT overhang of the HO endonuclease recognition site, rather than within the TG_{81} seed itself, suggesting that the telomeric seed possesses an ability to stimulate *de novo* telomere addition at the target site (270).

What property of these telomeric seeds might account for their ability to stimulate *de novo* telomere addition? One possibility is that the telomeric seeds recruit telomere-binding proteins that confer the seeds with their stimulatory abilities. In support of this idea, tethering a Gal4 DNA binding domain-Yku70 (GBD-Yku70) fusion protein to Gal4 upstream activating sequences (UAS) inserted adjacent to a non-telomeric DSB greatly stimulates *de novo* telomere addition (271). A similar effect is observed when Cdc13 is tethered adjacent to the DSB (271). The Yku70 and Cdc13 stimulatory effects are dependent on their ability to interact with TLC1 and Est1, respectively, indicating that their telomerase recruitment functions are required to promote telomere addition (271).

Cdc13 recruitment to DSBs is negatively regulated by the checkpoint kinase Mec1. Mec1-dependent phosphorylation of Cdc13 at serine 306 reduces Cdc13 accumulation at DSBs (272). Reflecting yet another level of regulation of *de novo* telomere addition by the DNA damage checkpoint, Mec1 phosphorylates Pif1, and this phosphorylation is proposed to promote its ability to remove

telomerase from DSBs, as an unphosphorylatable Pif1 mutant still accumulates at DSBs, but is defective at repressing telomerase (273).

Length of the Telomeric Seed

As discussed in Section 3.5, telomerase recruitment to endogenous telomeres is regulated as a function of endogenous telomere length. Similar studies, using the assay depicted in Figure 18B, have been carried out to elucidate how *de novo* telomere addition is regulated as a function of the telomeric seed length. Results from these studies suggest that, as at endogenous telomeres, the Rap1-Rif1-Rif2 complex is involved in the regulation of *de novo* telomere addition at or near telomeric seed sequences. When a TG_{81} seed is placed adjacent to an HO endonuclease-induced DSB (henceforth referred to as TG_{81}-HO), telomere addition occurs rapidly after HO endonuclease induction. After HO induction, telomere addition is detectable, though weakly, by 2 hours after induction, and is strongly detectable by 4 to 6 hours after induction (227). In contrast, in strains containing longer TG seeds (TG_{162}-HO and TG_{250}-HO), the TG seeds remain stable and are not elongated even by 6 hours of HO induction (208, 274).

In a TG_{81}-HO strain, deletion of *RIF2*, but not *RIF1*, increases telomere addition after HO induction (208, 227, 275). Similarly, deletion of *RIF2* and to a much lesser extent, *RIF1*, permits telomere addition in a TG_{162}-HO strain (208). Tethering Rif1 or Rif2 adjacent to a DSB reduces Tel1 accumulation at the break whereas tethering Rap1 adjacent to a DSB reduces Mre11 accumulation at the break (208). These data suggest a mechanism whereby Rap1, Rif1, and Rif2 inhibit telomere addition at DSBs, and possibly at endogenous telomeres too, by preventing the recruitment of the telomere maintenance proteins Mre11 and Tel1 (208). However, Rap1 also appears to play a role in telomere length regulation that is independent of its interaction with Rif1 and Rif2 as tethering Rap1

adjacent to a DSB reduces Mre11 accumulation at the break, even in the absence of Rif1 and Rif2 (208).

In contrast to the studies discussed above, other publications have reported a role for Rap1 in stimulating *de novo* telomere addition at or near both short and long telomeric seeds. When transformed *in vivo*, a linearized plasmid containing telomeric seeds at its ends can only be stably maintained in the cell if the telomeres are elongated. Lustig and colleagues demonstrated that a 41 bp telomere seed containing three Rap1 binding sites (two non-overlapping and one overlapping) and which was tested and shown to bind Rap1 in a gel shift assay, was effectively elongated *in vivo* (276). After transformation with the plasmid carrying the WT telomeric seed at its ends, 92% of the recovered transformants contained plasmids whose ends had undergone telomere addition (276). In contrast, after transformation with plasmids carrying telomeric seeds containing mutated Rap1 sites or only one Rap1 site at their ends, only 17-23% of recovered transformants contained plasmids that had undergone telomere addition (276). These data suggested that Rap1 stimulated *de novo* telomere addition at the telomeric seeds. However, Rap1 and Cdc13 bind to similar sequences at telomeres, and since a role for Cdc13 was not tested in this study, it remains possible that the stimulatory effect of the telomeric seed observed in this study was conferred either in full or in part by Cdc13 binding.

In another publication, Rap1's role in *de novo* telomere addition was tested using an assay system in which the left telomere of chromosome VII was truncated by homologous recombination at the *ADH4* locus (277). Effectively, the ~15 kb terminal region of the left arm of chromosome VII starting with ADH4 was replaced with an ~3 kb construct that contained, beginning with the most centromere-proximal sequence and moving outward, *ADH4*, *URA3*, telomeric or non-telomeric sequences expected to bind Rap1, and a terminal 29 bp TG sequence. *De novo* telomere addition was assayed by counterselecting $URA3^{+}$ transformants on 5-FOA to identify those in which the *URA3* gene

had been silenced by TPE (section 3.5: "The Rap1-Rif1-Rif2 Complex") as a result of elongation of the 29 bp TG sequence to form a stable telomere. A strain in which the terminal 29 bp TG sequence was preceded by a 275 bp TG tract (with a 50 bp polylinker separating the short and long TG tracts), formed *de novo* telomeres 50 times more efficiently than a control strain lacking the long TG tract (277). A similar result was obtained from a strain in which the 29 bp TG sequence was preceded by 6 non-telomeric Rap1 binding sites from the *TEF2* promoter (277).

To verify that Rap1 stimulated telomere addition in this scenario, the researchers targeted GBD-Rap1 C terminus fusion proteins to Gal4 UAS sites inserted near the 29 bp TG sequence. A strain in which a Rap1 C terminus protein, consisting of the last 175 amino acids of Rap1 (residues 653-827), was targeted adjacent to the 29 bp TG sequence formed *de novo* telomeres 36 times more efficiently than the control strain (277). Taken together, these data suggested that internally bound Rap1 molecules, specifically Rap1 C terminus molecules, stimulated *de novo* telomere addition at the short terminal TG tract. Nonetheless, this study did not address a role for Cdc13 in their experimental setup. Therefore, it remains possible that both Rap1 and Cdc13 regulate *de novo* telomere addition in that experimental context.

3.8 Significance

Much of our knowledge of the requirements for *de novo* telomere addition in *S. cerevisiae* has been derived from studies of telomere addition at artificial telomeric seed sequences of defined lengths placed immediately adjacent to a DSB. Such artificial sequences may not be fully representative of endogenous sites of *de novo* telomere addition as endogenous sites are expected to vary in length, as well as in their location relative to DSB sites. Part of my thesis work has been focused on elucidating

the requirements for *de novo* telomere addition at endogenous sites of *de novo* telomere addition, referred to henceforth as **S**ites of **R**epair-associated **T**elomere **A**ddition (SiRTAs).

The results from these studies are detailed in chapter IV. I provide evidence that *de novo* telomere addition at an endogenous SIRTA located on chromosome V in *S. cerevisiae* requires a bipartite structure, wherein Cdc13 binding to a stimulatory (Stim) sequence promotes telomere addition at a separate target (Core) sequence. A newly identified SiRTA on chromosome IX also exhibits this bipartite structure.

CHAPTER IV

ENDOGENOUS HOTSPOTS OF *DE NOVO* TELOMERE ADDITION IN THE YEAST GENOME CONTAIN PROXIMAL ENHANCERS THAT BIND CDC13[2]

4.1 Introduction

Chromosomes in the budding yeast *Saccharomyces cerevisiae*, as in all eukaryotes, terminate with specialized nucleoprotein structures called telomeres. *S. cerevisiae* telomeric DNA consists of ~250-350 bp of TG_{1-3}/AC_{1-3} repeats and a short (~10 bp) terminal G-rich 3' overhang (176). Because the conventional DNA replication machinery cannot fully replicate chromosome ends, telomeres shorten with each cell division cycle. In most eukaryotes, telomere shortening is counteracted by the enzyme telomerase, a ribonucleoprotein complex that uses an intrinsic RNA subunit as the template for telomeric DNA synthesis. Associated with telomeric DNA are proteins that protect chromosome ends from nucleolytic resection and prevent chromosome end-to-end fusions by distinguishing natural chromosome ends from ends generated by DNA double strand breaks (DSBs) (186). These protective functions make telomeres essential for the maintenance of genome integrity and cell viability.

In *S. cerevisiae,* optimal telomere length requires a balance between positive and negative regulatory mechanisms mediated by telomere-binding proteins including Cdc13 and Rap1 (188). Cdc13, a telomere sequence-specific single-strand DNA binding protein, recruits telomerase to telomeres during the S/G2 phase of the cell cycle through interaction with Est1, a subunit of the

[2] The work presented in this chapter has been published in: **Obodo UC, Epum EA, Platts MH, Seloff J, Dahlson NA, Velkovsky SM, Paul SR, Friedman KL.** 2016. Endogenous hotspots of *de novo* telomere addition in the yeast genome contain proximal enhancers that bind Cdc13. Mol Cell Biol **36:**1750-1763. For the data in this chapter, contributions by each author are duly noted in the figure legends.

telomerase holoenzyme [reviewed in (188)]. Rap1 binds to the double-stranded telomeric repeat, forming a telomere length regulatory complex through interactions of its C-terminal domain with Rif1 and Rif2 (127, 164). Regulation occurs through a counting mechanism in which telomere length is inversely proportional to the number of Rif1 and Rif2 molecules present at a telomere (205, 206).

Cells experience insults to their genome from endogenous and exogenous sources, including reactive oxygen species, radiation, and chemical mutagens (278). DSBs resulting from these sources pose an enormous threat to genome stability and cell viability since failure to repair DSBs can cause chromosome rearrangements and/or chromosome loss. Eukaryotic cells utilize two main pathways for DSB repair: a homologous recombination (HR) pathway that uses a sister chromatid or homologous chromosome as template for DSB repair, and a non-homologous end joining (NHEJ) pathway in which broken DNA ends are directly ligated (279). Inaccurate repair of DSBs can give rise to gross chromosomal rearrangements (GCRs), large-scale changes in chromosome structure that include interstitial deletions, chromosome end-to-end fusions, and translocations (280). Direct action of telomerase at DSBs results in yet another type of GCR, *de novo* telomere addition, in which all genetic information distal to the DSB is lost (281).

In yeast, either Cdc13 or Rap1 can stimulate *de novo* telomere addition. Cdc13 appears to facilitate telomerase recruitment to DSBs in a manner similar to its role at endogenous telomeres (271). Following DSB induction by HO endonuclease, Cdc13 and Est1 are both recruited to an artificial telomere seed (~ 80 bp TG tract) inserted adjacent to the HO site and artificial tethering of Cdc13 adjacent to the break is sufficient to stimulate *de novo* telomere addition (271). Est1 recruitment depends on its interaction with Cdc13, although the converse is not true (271). In contrast to its negative regulatory role at endogenous telomeres, Rap1 stimulates *de novo* telomere addition at artificial chromosomal (277, 282) or extrachromosomal termini containing short telomere-like sequences (276).

While informative about mechanisms of telomerase recruitment, the vast majority of these studies utilize artificial sequences to facilitate the formation of *de novo* telomeres. Cdc13 and/or Rap1 could stimulate *de novo* telomere addition at endogenous intrachromosomal TG-rich sequences with the potential to bind one or both proteins. However, a potential role for Cdc13 or Rap1 at such sequences has not been directly addressed.

Given that *de novo* telomere addition at intrachromosomal TG-rich sequences has the potential to influence genome stability, we sought to identify the *cis*- and *trans*-acting factors required for *de novo* telomere addition at such endogenous sequences. Here, we investigate the requirements for *de novo* telomere addition at an 84 bp Site of Repair-associated Telomere Addition, located 35 kb from the left telomere of chromosome V (SiRTA 5L-35). As previously described (84), the majority of telomere additions at SiRTA 5L-35 occur within a 23 bp TG-rich sequence, which we refer to as the "Core" sequence.

We find that a separate TG-rich sequence located centromere-proximal to the Core, and which itself is infrequently targeted for telomere addition, is required for high levels of telomere addition at the Core (referred to here as the "Stim" sequence). Using two different approaches to differentially target Cdc13 or Rap1 to SiRTA 5L-35, we show that it is likely the ability of Cdc13 to bind the Stim sequence that promotes telomere addition at SiRTA 5L-35. SiRTA 5L-35 therefore has a bipartite structure in which Cdc13 binding to an upstream sequence stimulates telomere addition at a neighboring target site. Finally, we report the identification of a new SiRTA located 44 kb from the left telomere of chromosome IX and show that SiRTA 9L-44 has a similar bipartite structure as SiRTA 5L-35.

4.2 Results

4.2.1 An internal telomere-like sequence on chromosome V in *S. cerevisiae* is a target of *de novo* telomere addition

In *S. cerevisiae*, a short sequence within the *NPR2* gene on the left arm of chromosome V (chrV-L) incurs a high frequency of *de novo* telomere addition relative to flanking sequences (84). To determine the magnitude of this effect in our strain, we utilized an assay (264) in which *CAN1* and *URA3* are utilized to select GCR events within a 12 kb region on chrV-L between *CAN1* and the first essential gene (Figure 19A). Independent liquid cultures were plated on medium containing canavanine (CAN) and 5-fluoroorotic acid (5-FOA), drugs toxic to cells expressing *CAN1* and *URA3*, respectively. A single surviving colony was isolated from each culture for analysis. As previously shown (84, 264), nearly all cells resistant to both drugs lost DNA sequences distal to *CAN1*. The approximate location of each rearrangement was determined by multiplex PCR using primer pairs spanning the 12 kb region (Figure 20) and each chromosome rearrangement was subsequently classified as "telomere addition" or "other" using Southern blot analysis to detect the characteristic "smear" generated by heterogeneous telomeric repeats.

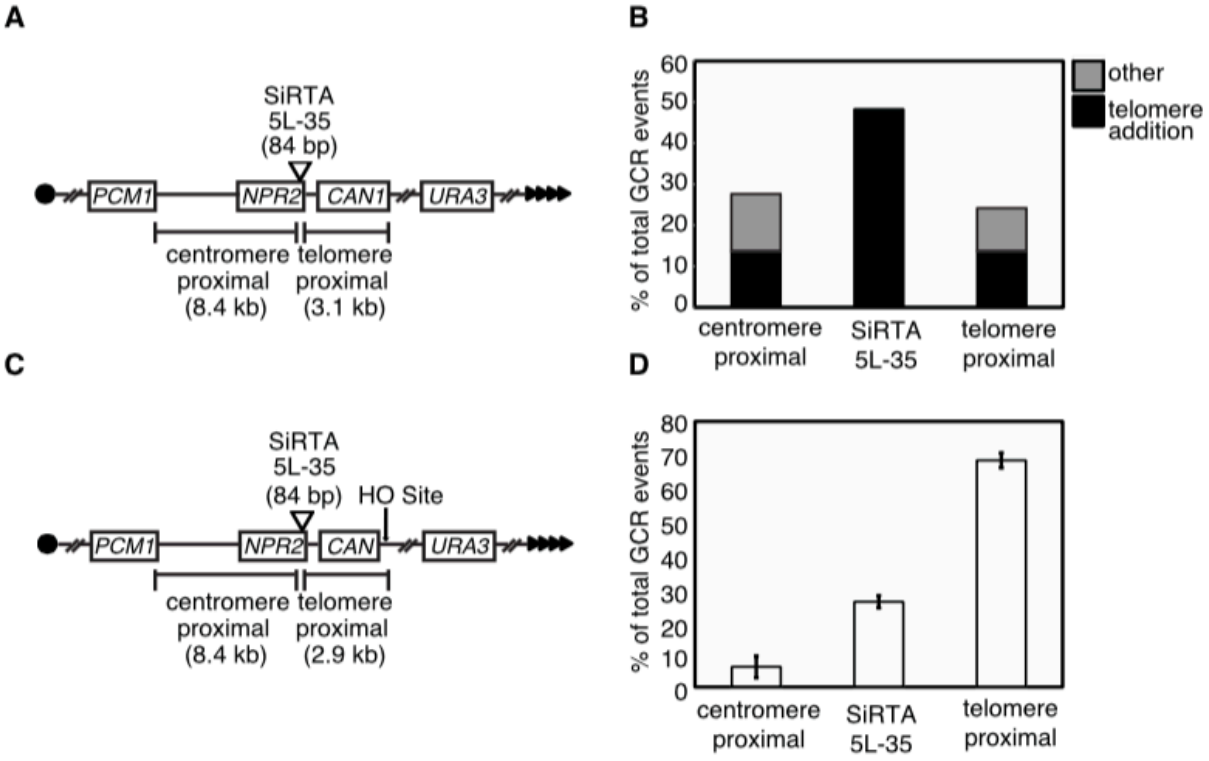

Figure 19. SiRTA 5L-35 incurs a high frequency of *de novo* telomere addition relative to flanking sequences.

(A) Schematic of chromosome V GCR assay system. Filled triangles represent the terminal telomeric repeats. Throughout the manuscript, chromosome arms are diagrammed with the telomere to the right. This convention places the 3' terminus upon which telomerase directly acts on the top strand of DNA.

(B) Distribution of spontaneously occurring GCR events in the WT strain. GCR events were mapped by multiplex PCR (Figure 20) to one of the three regions indicated in (A). The type of event (telomere addition or "other") was determined by Southern blot. A total of 29 events were analyzed. The enrichment of GCR events within the 84 bp SiRTA relative to the expected frequency (assuming random distribution of GCR events across the 11.5 kb target region) was significant by Fisher's Exact Test ($p<0.001$).

(C) Schematic of chromosome V HO-inducible GCR assay system. Expression of the HO endonuclease is induced by growth on media containing galactose and the site of HO cleavage is indicated (arrow).

(D) Distribution of HO-endonuclease-induced GCR events in the WT strain. Data are from three independent experiments and ~ 30-40 GCRs per experiment. Error bars represent standard deviation.

Contributing authors: UCO, MHP, SMV, SRP.

A

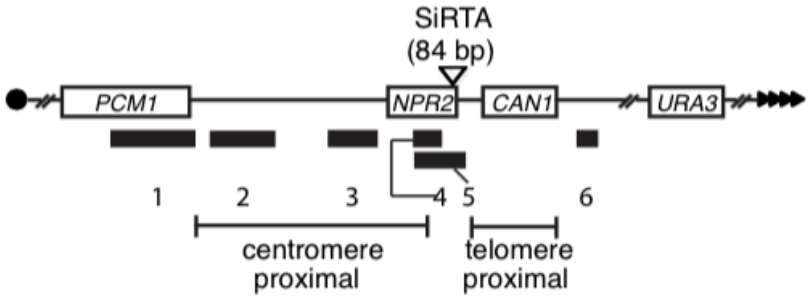

B

PCR product (size in bp)	Primer sequences
1 (620)	5'-CGATGAAGGTTGATTACGAGC-3'
	5'-GAAGGCTCCTATAAAGAACG-3'
2 (508)	5'-CGAGGTCACGGACACATATACC-3'
	5'-CGAGTGTAAATAGAGTATTTTCTAAC-3'
3 (415)	5'-GAAAATCGACATAATAAGAGTAGATTTCC-3'
	5'-GATTTGCGATAGCGTCGCTGCC-3'
4 (341)	5'-CTTAGTTTAGAAATTTTGGCAATG-3' *
	5'-GAAAAGGATACAAAGGATATGAG-3'
5 (452)	5'-CTTAGTTTAGAAATTTTGGCAATG-3' *
	5'GTTTTCTTCGATTTGAAGGTGTTGG-3'
6 (242)	5'-GAGTTTGCTAGATTCATAAAAGCC-3'
	5'-CCGATAATGTCTGAGTTAGGTGAG-3'

* Shared primer

Figure 20. Multiplex PCR analysis of spontaneous GCR events.
(A) Schematic of chromosome V GCR region showing approximate locations and relative expected sizes of PCR products. A GCR event within SiRTA 5L-35 is denoted by the presence of products 1-4 and the absence of products 5 and 6.
(B) Primer sequences used for multiplex PCR analysis. The expected size of each PCR product is indicated.

Three PCR primers were designed to detect GCR formation within an 84 bp TG-rich sequence encompassing the telomere addition hotspot within *NPR2* (Figure 20; PCR products 4 and 5). To reflect the propensity for *de novo* telomere addition, we refer to this sequence as the Site of Repair-associated Telomere Addition 35 kb from the left telomere of chromosome V (SiRTA 5L-35). Similar to previous reports (84), 48.3% (14 of 29) of GCR events occurred in SiRTA 5L-35. The remaining events were split evenly between the regions centromere- and telomere-proximal to SiRTA 5L-35 (Figure 19B). In

every case, GCR events within SiRTA 5L-35 involved *de novo* telomere addition, whereas GCRs in the flanking regions consisted of both telomere additions and other chromosome rearrangements (Figure 19B). Given that the 84-bp SiRTA 5L-35 comprises less than 1% of the total region analyzed, this sequence incurs a remarkably high frequency of *de novo* telomere addition.

To eliminate concern that telomere addition arises from a propensity for DNA breakage within or near this region, we utilized a second approach in which a site-specific DNA break is introduced ~3 kb distal to SiRTA 5L-35. The strain utilized (283) contains a single recognition site for the yeast homothallic switching endonuclease (HO endonuclease) within the *CAN1* gene (Figure 19C). Homologous sequences on chromosome III are deleted to eliminate repair by gene conversion. The HO endonuclease gene is expressed from a galactose-inducible promoter such that growth on media containing galactose results in a DSB ~3 kb distal to SiRTA 5L-35 (Figure 19C). Most cells accurately repair the DSB, resulting in a cleavage-repair cycle that culminates in cell death. However, approximately 0.1% of cells survive as a result of mutations at the HO site that prevent further cleavage. These cells have incurred small insertions or deletions or have lost all DNA distal to the HO site. The latter are identified by selection on 5-FOA for cells lacking the distal *URA3* marker (Figure 19C). We refer to cells that survive on galactose and have lost the *URA3* marker (gal^R $5\text{-}FOA^R$ colonies) as GCR events. The propensity for GCR formation to occur at SiRTA 5L-35 is expressed in two ways: 1) as the overall rate at which GCR formation occurs within SiRTA and 2) as the fraction of GCR events that occur within SiRTA. In both cases, values are the average (with standard deviation) of at least three independent experiments with 25-35 GCR events analyzed per experiment.

A

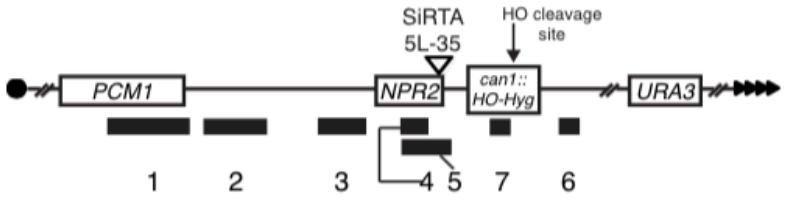

PCR product (size in bp)	Primer sequences
7 (168)	5'-GGCGCTTTGGCTTACATGG-3' 5'-GCGTACGAAGCTTCAGCTGG-3'

Centromere-proximal events amplify 1, 1-2, or 1-3
SiRTA 5L-35 events events amplify 1-4
Telomere-proximal events amplify 1-5
HO adjacent events amplify 1-5 and 7

B

Event type	Total events (n)	telomere addition (n)	Other (n)	% telomere addition
Cen-proximal	3	0	3	0
SiRTA 5L-35	18	17	1	94.4%
Tel-proximal	12	7	5	58.3%
HO adjacent	36	27	8	75%

Total = 69

Figure 21. Multiplex PCR analysis of GCR events.
(A) Schematic of chromosome V in the strain utilized for HO cleavage. PCR products 1-6 are identical to those shown in Figure 20. The reverse primer for PCR product 7 is located within 60 bp of the HO cleavage site.
(B) Characterization of 69 GCR events resulting from two independent HO cleavage assays. The approximate location of each event was determined by PCR as indicated in (A). Southern blot analysis was used to classify each event as "telomere addition" or "other."
Contributing authors: UCO.

By PCR analysis (see Figure 21A), 25.7±1.9% of GCR events following HO cleavage occurred within SiRTA 5L-35, 68.3±2.3% occurred between the HO cleavage site and SiRTA 5L-35, and the remainder occurred in the centromere-proximal region between SiRTA 5L-35 and the first essential gene (Figure 19D). We analyzed a subset of events (69 from two independent assays) by Southern blot. 94.4% (17 of 18) events that mapped to SiRTA 5L-35 involved *de novo* telomere addition (Figure 21B). Events that occurred distal to SiRTA 5L-35 fell into two classes. The majority of distal events

(36 of 48) occurred at or immediately adjacent to the HO cleavage site (within 60 base pairs) and of those, 75.0% involved *de novo* telomere addition. In contrast, only 12 events occurred within the 3 kb separating the HO site from SiRTA 5L-35 and 58.3% of those events involved *de novo* telomere addition (Figure 21B). *De novo* telomere addition events at SiRTA 5L-35 are mediated by telomerase since deletion of *RAD52* to eliminate recombination-mediated telomere maintenance (284) did not reduce the fraction of GCR events occurring at SiRTA 5L-35 (Figure 22).

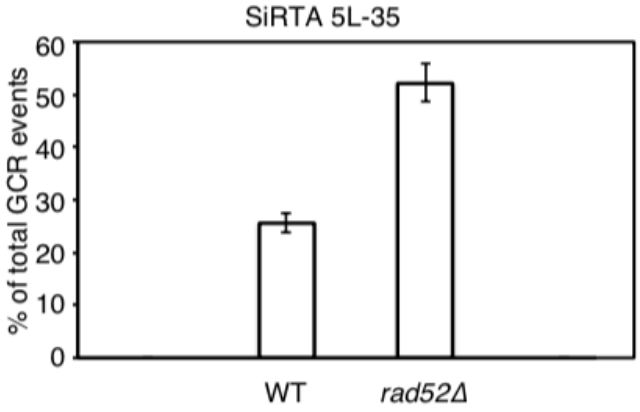

Figure 22. *De novo* telomere addition at SiRTA 5L-35 is *RAD52*-independent.
Percentage of HO endonuclease-induced GCRs occurring in SiRTA 5L-35 in the WT and *rad52*Δ strains. Data are from 3 independent experiments and ~ 30-40 GCRs per experiment. Error bars represent standard deviation. WT data are the same as those shown in Figure 19D.
Contributing authors: UCO.

4.2.2 A sequence internal to the direct target of telomere addition is required for high levels of *de novo* telomere addition at SiRTA 5L-35

To identify sequences required to direct high levels of *de novo* telomere addition at SiRTA 5L-35, we cloned and sequenced fourteen telomere addition events following HO cleavage. Telomere addition occurred at seven different sites, four of which were used more than once (Figure 23A). All fourteen events were independent as reflected in the divergent telomere sequences added to each

(Figure 24). 57.1% (8/14) of the telomere additions occurred within the original 23 bp TG-rich sequence defined by Stellwagen *et al.* (84). Interestingly, very few events occurred at the centromere-proximal end of SiRTA 5L-35, despite the telomere-like nature of that sequence (Figure 23A).

To determine which sequences contribute to the high rate of *de novo* telomere addition, we created a series of mutations diagrammed in Figure 23A. Mutation of the 23-bp TG-rich sequence in which telomere addition frequently occurs (each base mutated to its complement) decreased the overall frequency of GCR events at SiRTA 5L-35 by 16-fold (Figure 23B, mutation a) and reduced the percentage of total GCR events mapping to SiRTA 5L-35 from 25.7±1.9% to 4.8±2.5 % (Figure 25). In contrast, mutation of the neighboring sequence (mutation b) did not significantly change the overall rate of GCR formation (Figure 23B), with 20.3±3.7% of the GCR events mapping to SiRTA 5L-35 (Figure 25). To address a potential role for the TG-rich sequence at the centromere-proximal end of SiRTA 5L-35, we mutated this 18 bp region to adenine (mutation c). Although this sequence is rarely the direct target of telomere addition, the effect on the rate of GCR formation within SiRTA 5L-35 was nearly as pronounced as that seen when the target sequences themselves were mutated (Figure 23B; compare mutations a and c) and only 5.6±2.1% of total GCR events mapped to SiRTA 5L-35 (Figure 25). Furthermore, only 3 of 5 of those events involved *de novo* telomere addition (data not shown). While this sequence enhances telomere addition at SiRTA 5L-35, it is insufficient to support high levels of *de novo* telomere addition since a strain containing only the centromere-proximal sequences (mutation d) underwent a low rate of GCR formation within SiRTA 5L-35 with a small fraction of GCR events at SiRTA 5L-35 (4.4±1.9%; Figures 23B and 25).

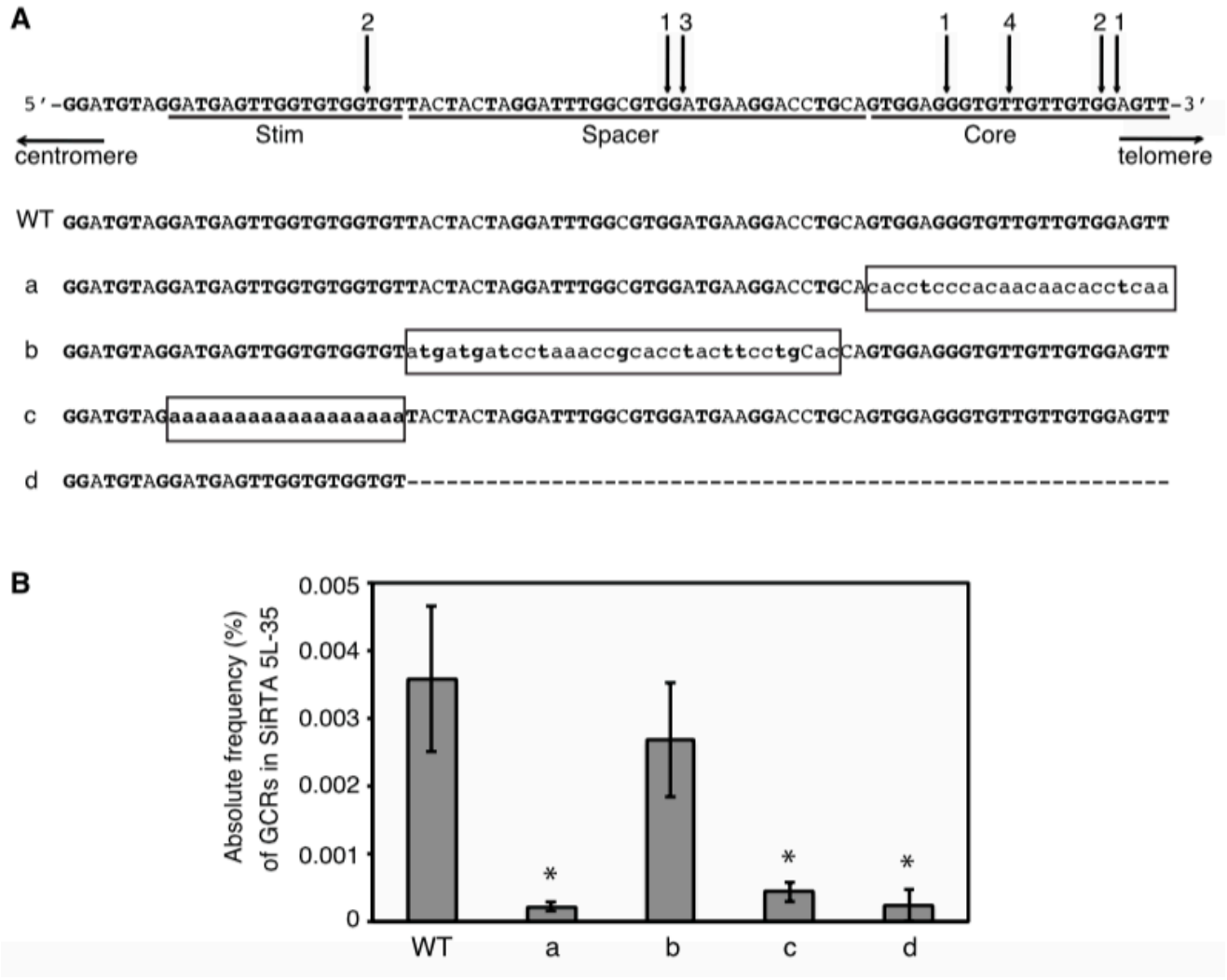

Figure 23. High rates of telomere addition at SiRTA 5L-35 require two separable sequences.
(A) Top schematic: Sequence of SiRTA 5L-35 with arrows indicating sites of *de novo* telomere addition. The most 3' chromosomal nucleotide with identity to the cloned *de novo* telomere is indicated. Individual cloned sequences are shown in Figure 24. Numbers above arrows indicate the number of independent telomere addition events mapped to each site. Stim, Spacer, and Core are defined in the text. Bottom schematic: Mutations created in SiRTA 5L-35. Uppercase letters represent unchanged nucleotides, lowercase letters enclosed in box represent mutated nucleotides, and dashed line indicates deleted nucleotides.
(B) Core and Stim sequences contribute to the formation of GCR events within SiRTA 5L-35. The frequency (%) at which GCR events occur within SiRTA 5L-35 following induction of HO endonuclease expression on media containing galactose is shown for the WT strain and for the mutant strains as depicted in (A). Average of three independent replicates is shown with standard deviation. *Indicated mutants are significantly different from WT ($p<0.05$) by ANOVA with post-hoc Tukey HSD.
Contributing authors: KLF, UCO, JS, NAD.

We conclude that high levels of telomere addition at SiRTA 5L-35 require a bipartite structure in which one sequence serves as the primary, direct target of telomere addition (the SiRTA Core; defined by mutation a), while the other sequence (SiRTA Stim; defined by mutation c) stimulates telomere addition within or near the Core sequence. The spacer between these sites makes no sequence-specific contribution to the stimulation of *de novo* telomere addition.

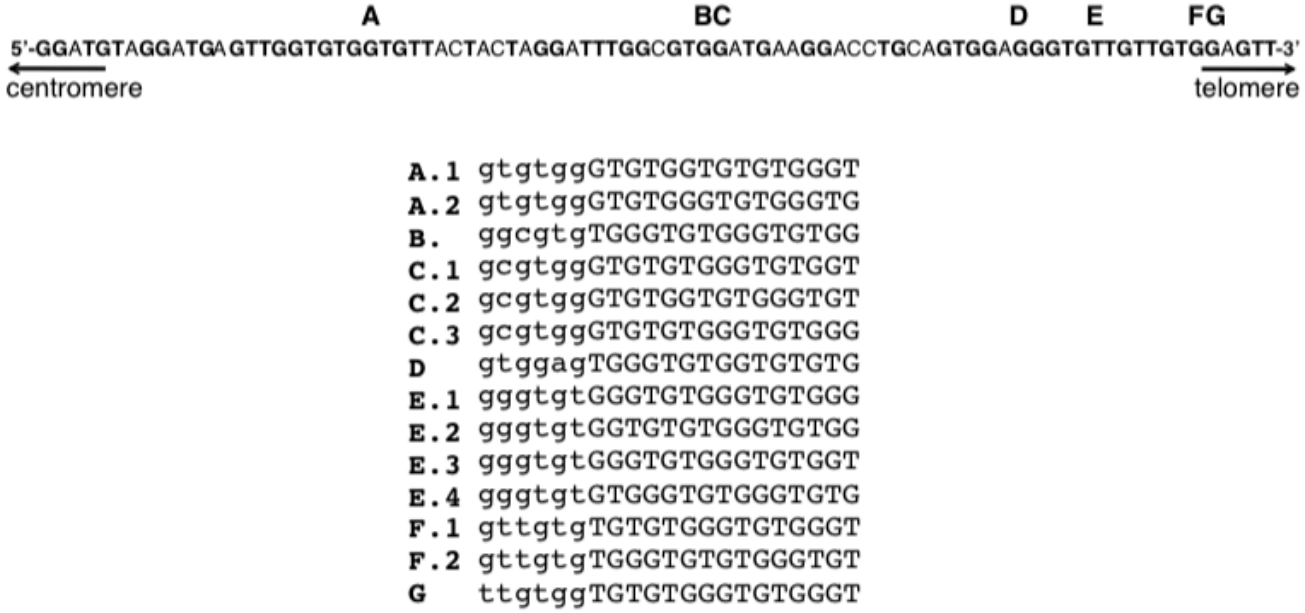

Figure 24. *De novo* telomere addition events within SiRTA 5L-35 are non-clonal.
Sequences of *de novo* telomere addition junctions in the WT strain, corresponding to the 14 events shown in Figure 23A. Lowercase letters represent the last 6 nucleotides of the sequenced *de novo* telomere that match the chromosomal sequence. Uppercase sequences represent a portion of the newly added telomere sequence.
Contributing authors: JS.

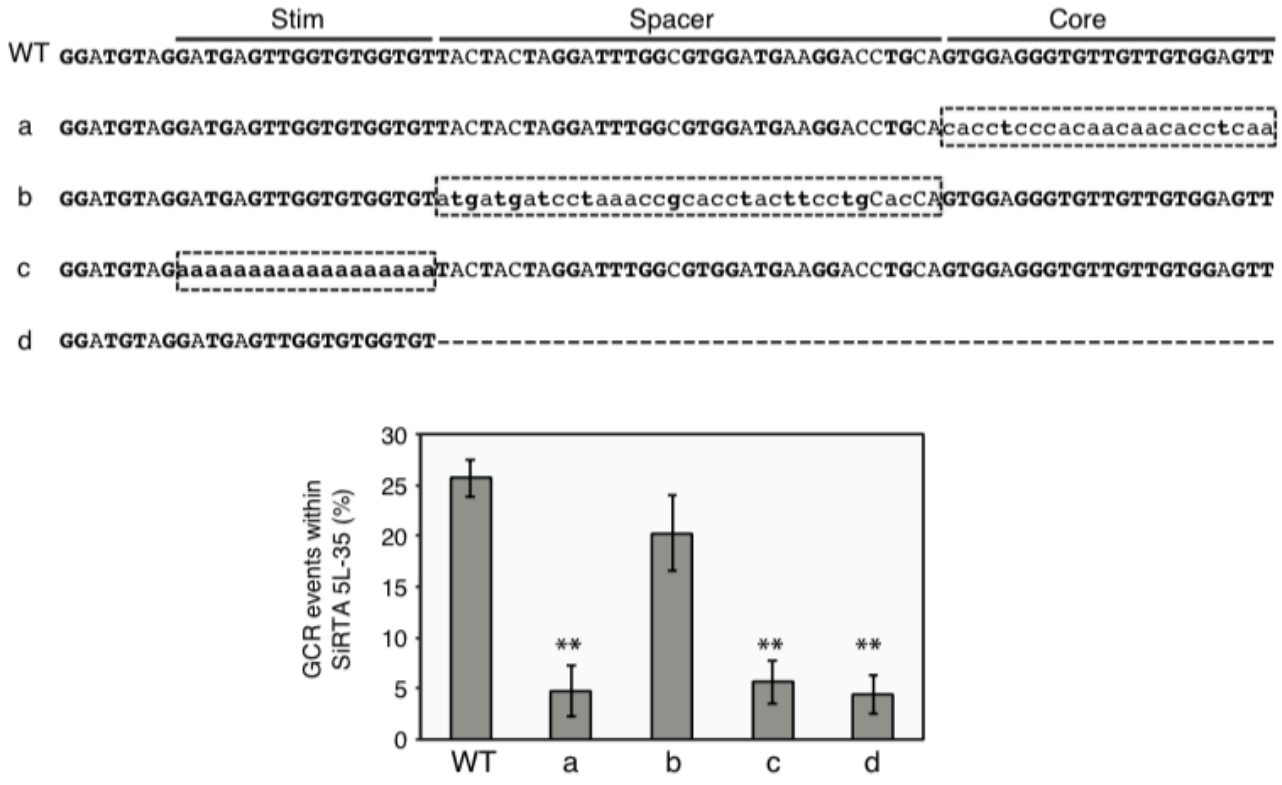

Figure 25. Mutations of the Core and Stim sequences affect the fraction of total GCR events that occur within SiRTA 5L-35.

Top: Mutations created in SiRTA 5L-35 (identical to those described in Figure 23). Bottom: Fraction of GCR events (%) that occur in SiRTA 5L-35 as determined by multiplex PCR in the indicated strains. *The indicated mutants are significantly different from WT ($p<0.01$) by ANOVA with post-hoc Tukey HSD.

Contributing authors: KLF, UCO, JS, NAD.

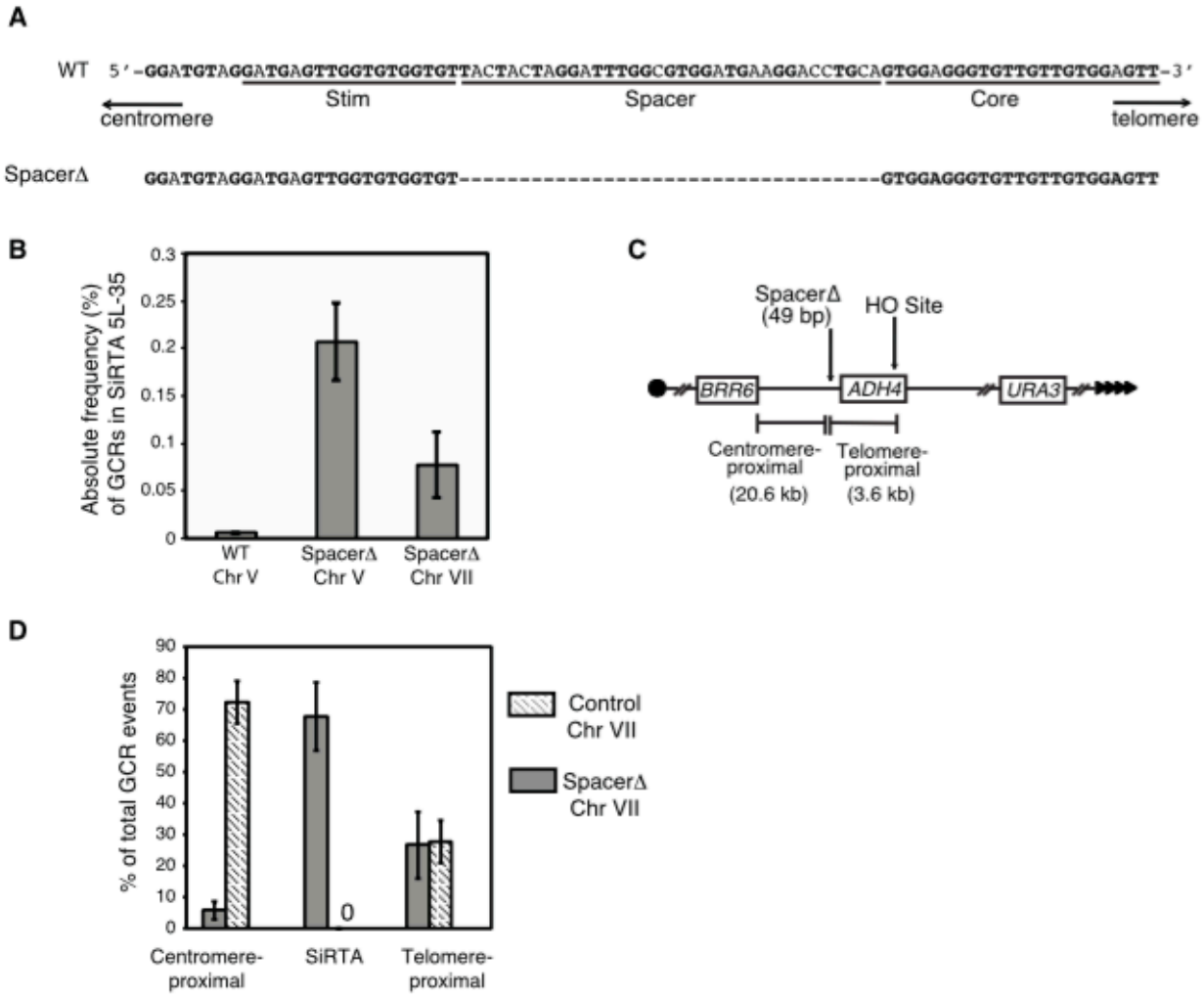

Figure 26. The SiRTA Stim and Core sequences are sufficient to stimulate *de novo* telomere addition at an ectopic location.

A. Top schematic: Sequence of SiRTA 5L-35 as in Figure 23A. Bottom schematic: SpacerΔ mutation created in SiRTA 5L-35. Dashed line indicates deleted nucleotides.

B. The absolute frequency (% total cells) of GCR formation at SiRTA 5L-35 is shown for the SpacerΔ variant at its endogenous location on chromosome V and at an ectopic site on chromosome VII. Data for WT SiRTA 5L-35 are shown for comparison (same as Figure 23B). Values are the average of three independent experiments with standard deviation.

C. Schematic of the modified left arm of chromosome VII. Sizes of the regions between the integrated Spacer sequence and either the HO cleavage site (telomere-proximal) or the most distal essential gene (*BRR6*; centromere-proximal) are indicated.

D. The percentage of GCR events occurring in each indicated region on chromosome VII is shown for the experimental strain (SiRTA 5L-35 SpacerΔ and a control strain (no integration). In the control strain, no GCR events were observed in the 219 bp region that is replaced by the SpacerΔ variant in the experimental strain. Values are averages of three independent experiments with standard deviation.

Contributing authors: EAE, JS, NAD.

4.2.3 The Core and Stim sequences of SiRTA 5L-35 are sufficient to stimulate high levels of *de novo* telomere addition at an ectopic site

Given that the spacer between the SiRTA 5L-35 Core and Stim sequences could be mutated with little effect on telomere addition, we tested the effect of deleting this sequence (Figure 26A). Strikingly, the overall rate of GCR formation within SiRTA 5L-35 following HO cleavage increased 36-fold compared to the wild-type SiRTA 5L-35 (spacerΔ; Figure 26B) and 74.2±15.6% of total GCR events occurred within SiRTA 5L-35. Analysis by Southern blot of 35 GCR events from one representative assay showed that all 28 events within SiRTA 5L-35 spacerΔ involved *de novo* telomere addition (data not shown). In addition, 5 of the remaining 7 events, originally classified as telomere-proximal by PCR, actually involved telomere addition within 100 bp of the spacerΔ variant of SiRTA 5L-35. No events of this type were observed among 69 GCR events characterized in the WT strain.

We took advantage of this remarkably high level of *de novo* telomere addition to ask whether the SiRTA 5L-35 Core and Stim sequences are sufficient to confer this property to an ectopic site. A 49-bp sequence containing the SiRTA 5L-35 Core and Stim sequences (SiRTA-spacerΔ) was integrated within nonessential sequences on chromosome VII-L, ~20 kb from the first essential gene (*BRR6*). The galactose-inducible HO cleavage cassette was placed 3 kb telomere-proximal to the ectopic SiRTA sequence and *URA3* was integrated to monitor the rate of terminal deletion (Figure 26C). A strain containing only the HO cleavage site and *URA3* marker served as a control.

In the control strain, no GCR events were observed within a 542-bp sequence corresponding to the insertion site and 72.2±6.9% of the GCR events occurred centromere-proximal to this location (Figure 26D). In striking contrast, 67.6±10.8% of total GCR events in the experimental strain occurred within SiRTA-spacerΔ and only 5.7±2.8% mapped to the centromere-proximal region (Figure 26D). Southern analysis was conducted on 35 events from a single experiment. Of 22 events mapped by PCR

to the SiRTA-spacerΔ sequence, 20 (91%) involved telomere addition. Furthermore, of 12 events that mapped telomere-proximal to the SiRTA-spacerΔ sequence, all but one involved telomere addition within 100 bp of SiRTA-spacerΔ. Therefore, in this subset of 35 GCR events, 91.4% involved *de novo* telomere addition within or immediately adjacent to the SiRTA-spacerΔ insert. The overall rate of GCR formation within SiRTA-spacerΔ was modestly (2.7 fold) lower on chromosome VII than at the endogenous location on chromosome V, but still much higher than observed for the endogenous SiRTA 5L-35 (Figure 26B).

Taken together, these results indicate that the SiRTA 5L-35 Core and Stim sequences are sufficient to support *de novo* telomere addition following a distal chromosome break. Reducing the spacing between the stimulatory and core sequences dramatically increases the rate of *de novo* telomere addition. Interestingly, sequences located within approximately 100 bp of the SiRTA nucleate telomere addition when the spacer sequence is deleted, most likely because the stimulatory sequence is now closer to these sites.

4.2.4 Sequences that bind Rap1 and Cdc13 stimulate *de novo* telomere addition at SiRTA 5L-35

We reasoned that the enhancing properties of SiRTA Stim may arise from one or more proteins bound at that site. Given the TG-rich nature of this sequence, we investigated the ability of Rap1 and Cdc13 to bind the SiRTA Stim sequence *in vitro*. Rap1 is a double-stranded DNA binding protein that binds at high frequency within the endogenous telomeric repeat (195), but binds additional internal chromosomal sites as a transcription factor (189). Cdc13 binds the single-stranded overhang at the yeast telomere (285-289) and could bind at SiRTA Stim following resection of a DSB at a distal site.

Electrophoretic mobility shift assays (EMSAs) were performed using recombinant Rap1 and the DNA binding domain of Cdc13 (Cdc13-DBD; amino acids 497 to 694) to monitor binding to

double-stranded or single-stranded target DNAs, respectively. The DNA binding domain of Cdc13 alone closely mimics the binding specificity of the full-length protein (290). Indeed, the endogenous SiRTA Stim sequence is bound by both Rap1 (Figure 27A and B, probe I) and by Cdc13-DBD (Figure 27A and C, probe III). As predicted, the polyA mutation that disrupts SiRTA Stim function (Figure 23) reduces binding by Rap1 and Cdc13-DBD (Figure 27A-C, probes II, IV, and V), consistent with one or both of these proteins playing a role in the stimulation of *de novo* telomere addition.

To address whether binding by Rap1 and/or Cdc13 is sufficient to stimulate *de novo* telomere addition, we designed a sequence predicted to contain two tandem Rap1 binding sites and to have the ability to bind Cdc13. By EMSA, this sequence (Stim-Subst; Figure 27D) binds Rap1 with higher affinity than the endogenous SiRTA Stim sequence (compare binding to probes I and VI, Figure 27B and E) and also binds Cdc13-DBD (Figure 27F, probes VIa and VIb). The Stim-Subst sequence was integrated in place of the SiRTA Stim sequence on chromosome V and the frequency of GCR events at SiRTA 5L-35 was measured. Consistent with either Rap1 and/or Cdc13 playing a role in the stimulation of telomere addition, this artificial sequence stimulated GCR events at SiRTA 5L-35 at a rate equivalent to the endogenous sequence and increased the fraction of GCR events occurring within SiRTA 5L-35 (Figure 27G).

To verify that the Stim-Subst sequence is not the direct target of telomere addition, we designed a reverse primer within the SiRTA spacer sequence that generates a PCR product only if a *de novo* telomere is added within or near the SiRTA Core sequence (Figure 28). Consistent with our sequencing results in the WT strain in which 12 of 14 telomere addition events were located distal to SiRTA Stim (85.7%; Figure 23A), 17 of 20 previously uncharacterized events generated a PCR product in this assay

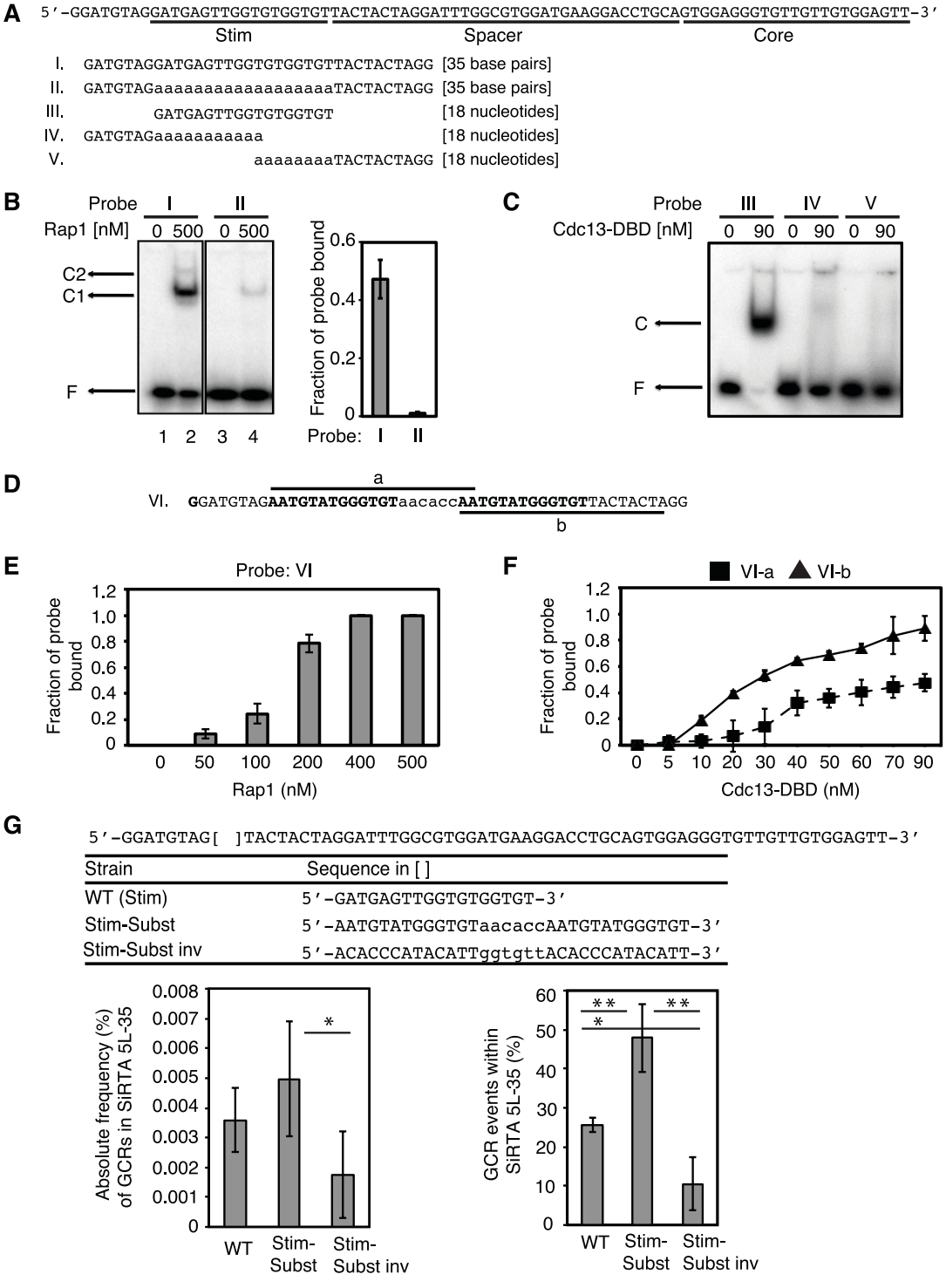
A
5′-GGATGTAGGATGAGTTGGTGTGGTGTTACTACTAGGATTTGGCGTGGATGAAGGACCTGCAGTGGAGGGTGTTGTTGTGGAGTT-3′
Stim
Spacer
Core
I. GATGTAGGATGAGTTGGTGTGGTGTTACTACTAGG [35 base pairs]
II. GATGTAGaaaaaaaaaaaaaaaaaaTACTACTAGG [35 base pairs]
III. GATGAGTTGGTGTGGTGT [18 nucleotides]
IV. GATGTAGaaaaaaaaaaa [18 nucleotides]
V. aaaaaaaaTACTACTAGG [18 nucleotides]
B
Probe I II
Rap1 [nM] 0 500 0 500
C2
C1
F
1 2 3 4
Fraction of probe bound
Probe: I II
C
Probe III IV V
Cdc13-DBD [nM] 0 90 0 90 0 90
C
F
D
a
VI. GGATGTAGAATGTATGGGTGTaacaccAATGTATGGGTGTTACTACTAGG
b
E
Probe: VI
Fraction of probe bound
Rap1 (nM)
F
VI-a VI-b
Fraction of probe bound
Cdc13-DBD (nM)
G
5′-GGATGTAG[ ]TACTACTAGGATTTGGCGTGGATGAAGGACCTGCAGTGGAGGGTGTTGTTGTGGAGTT-3′
Strain Sequence in [ ]
WT (Stim) 5′-GATGAGTTGGTGTGGTGT-3′
Stim-Subst 5′-AATGTATGGGTGTaacaccAATGTATGGGTGT-3′
Stim-Subst inv 5′-ACACCCATACATTggtgttACACCCATACATT-3′
Absolute frequency (%) of GCRs in SiRTA 5L-35
WT
Stim-Subst
Stim-Subst inv
GCR events within SiRTA 5L-35 (%)
WT
Stim-Subst
Stim-Subst inv

Figure 27. The Stim sequence of SiRTA 5L-35 binds Cdc13 and Rap1 *in vitro* and can be functionally replaced with a sequence that binds both proteins.
(A) Top schematic: Sequence of SiRTA 5L-35 as in Figure 23A. Bottom schematic: Sequences of probes utilized for Cdc13-DBD and Rap1 binding assays. Mutated bases are shown in lower case. Probes are identified with Roman numerals and this numbering is maintained throughout the manuscript. Probes I and II are double-stranded; probes III-V are single-stranded.
(B) Binding of recombinant Rap1 to probe I (WT SiRTA 5L-35) and probe II (Stim polyA mutation, Figure 23A). The mobility of free probe (F) and two bound complexes (C1 and C2) is indicated. The fraction of probe bound when utilizing 500 nM Rap1 is quantified on the right from three independent experiments. Error bars represent standard deviation.
(C) Binding of recombinant Cdc13-DBD to probes III, IV, and V, as indicated. Probe III contains the WT SiRTA 5L-35 sequence. Probes IV and V contain the Stim polyA mutation from Figure 23A. This sequence was tested in two pieces to avoid the formation of secondary structure. The mobility of free probe (F) and bound complex (C) is indicated.
(D) The sequence shown was designed to contain two predicted Rap1 binding sites (bold) separated by a linker sequence (lower case). Probe VI is double-stranded and is utilized in (E). Probes VI-a and VI-b are single-stranded sequences as indicated and are utilized in (F).
(E) Binding of the indicated concentration of recombinant Rap1 to probe VI.
(F) Binding of the indicated concentration of recombinant Cdc13-DBD to probes VI-a or VI-b. For (E) and (F) the average fraction of probe bound was determined from three independent experiments. Error bars represent standard deviation.
(G) The SiRTA 5L-35 Stim sequence (indicated by brackets) was replaced at the endogenous locus on chromosome V with the three sequences depicted here. Stim-Subst is identical to the sequence of Probe VI. Stim-Subst inv is the reverse complement of the Stim-Subst sequence. Average results and standard deviation of three HO-cleavage assays are shown as the absolute frequency (%) of GCR formation within SiRTA 5L-35 (left graph) or the percent of total GCR events that occur within SiRTA 5L-35 (right graph). Samples with statistically different values by ANOVA with post-hoc Tukey HSD are indicated (* $p<0.05$; ** $p<0.01$).
Contributing authors: UCO, EAE.

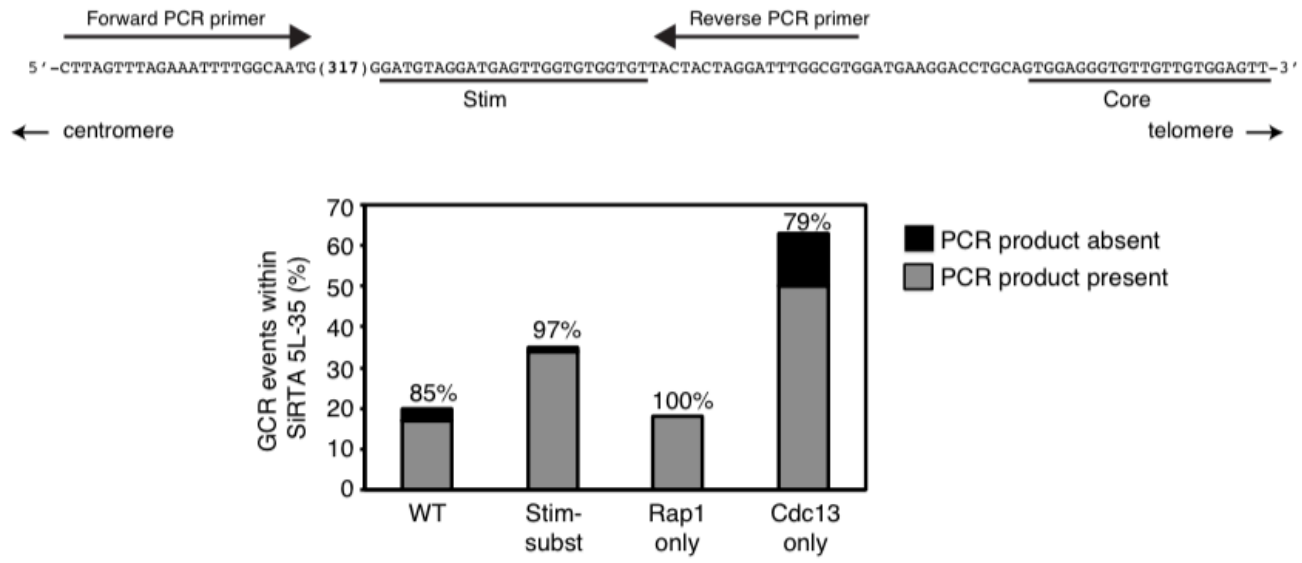

Figure 28. Most *de novo* telomere addition events occur telomere-proximal to the Stim sequence.
Top: The sequence of SiRTA 5L-35 is shown along with the locations of the Core and Stim sequences. Forward and reverse primers shown were used to amplify genomic DNA isolated from strains in which a GCR event occurred within SiRTA 5L-35. If a PCR product is generated, chromosome truncation (*i.e.* telomere addition) must have occurred telomere-proximal to the location of the reverse primer.
Bottom: For the indicated strains, the percentage of total GCR events that occurred in SiRTA 5L-35 is graphed. Of those events, the percent that generated a PCR product using the primers described above is indicated.
Contributing authors: UCO.

(85.0%; Figure 28). Importantly, PCR product was obtained in 34 of 35 (97.1%) SiRTA GCR events in the Stim-Subst strain (Figure 28), indicating that Stim-Subst enhances the probability of telomere addition within the SiRTA Core.

To test whether stimulation is orientation-dependent, we inverted the Stim-Subst sequence. Inversion reduced the rate of GCR formation at SiRTA 5L-35 by 2.8 fold and reduced the fraction of GCR events within SiRTA 5L-35 from 47.8±7.1% to 10.4±6.8% (Figure 27G). Rap1 is expected to retain binding to the Stim-Subst sequence regardless of orientation. In contrast, the ability of Cdc13 to bind requires orientation-dependent exposure of its single-stranded TG-rich binding site during

resection from a distal double-strand break, suggesting that Cdc13 may be the functionally relevant protein in this context.

4.2.5 Binding of Cdc13 within SiRTA Stim is sufficient to drive *de novo* telomere addition at the neighboring Core sequence

To distinguish effects by Rap1 and Cdc13, we designed sequences to support differential binding. To create a sequence that binds Rap1, but not Cdc13, we began with the Stim-Subst sequence containing two sites predicted to bind Rap1 separated by an AC-rich spacer sequence (Figures 27D and 29A, probe VI). Since the 5' portion of this sequence binds weakly to Cdc13-DBD (Figure 27F, probe VIa), we mutated only the most 3' residue in this repeat, a change predicted to retain Rap1 association but disrupt Cdc13 binding. At the second Rap1 site, we mutated both that same 3' nucleotide and several nucleotides that lie adjacent to the defined Stim sequence (Figure 29A, probe VII). As shown in Figure 29B, the engineered "Rap1 only" sequence binds Rap1 with higher affinity than either the original SiRTA-Subst sequence or the endogenous SiRTA Stim. Mutations in the second Rap1 binding site essentially eliminate Cdc13-DBD binding to this sequence (compare Figure 27F, probe VIb, with Figure 29C, probe VIII).

We took a similar approach to create a sequence capable of binding Cdc13 and not Rap1. Here, the starting sequence was 11 bases shown to support strong association with Cdc13 (287) (Figure 29A, probe IX). The second base of this sequence [known to have little or no effect on Cdc13 binding (291)] was mutated to reduce similarity with the Rap1 binding consensus and two of these sites were placed in tandem. As shown in Figure 29B, this "Cdc13 only" sequence shows no detectable binding to Rap1 (probe X). Binding of this sequence to Cdc13 was measured using two probes that monitor binding to the 5' (probe XI) or 3' (probe XII) repeat. The 3' repeat shows similar affinity for Cdc13-DBD as the

A

Purpose	Probes used in EMSA
WT	I - GATGTAGGATGAGTTGGTGTGGTGTTACTACTAGG (Rap1 EMSA) III - GATGAGTTGGTGTGGTGT (Cdc13 EMSA)
Stim-subst*	VI - GGATGTAG**AATGTATGGGTGT**aacacc**AATGTATGGGTGT**TACTACTAGG (Rap1 EMSA)
Rap1 only	VII - GGATGTAG**AATGTATGGGTGC**aacacc**AATGTATGGGTGC**AACACCTAGG (Rap1 EMSA) VIII - **AATGTATGGGTGC**AACACCTA (Cdc13 EMSA)
Cdc13 consensus**	IX - **GTGTGGGTGTG** (Cdc13 EMSA)
Cdc13 only	X - GGATGTAG**GAGTGTGTGTG**aacacc**GAGTGTGTGTG**TACTACTAGG (Rap1 EMSA) XI - **GAGTGTGTGTG**aacacc**GA** (Cdc13 EMSA) XII - **GAGTGTGTGTG**TACTACTA (Cdc13 EMSA)

* This sequence contains two predicted Rap1 binding sites (bold) and was used as the base for creating the "Rap1 only" sequence; identical to the Stim-Subst sequence utilized in Figure 4.

** This sequence conforms to a canonical Cdc13 binding site; used as the base for creating the "Cdc13 only" sequence.

B

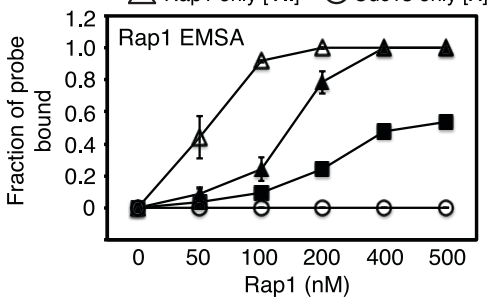

C

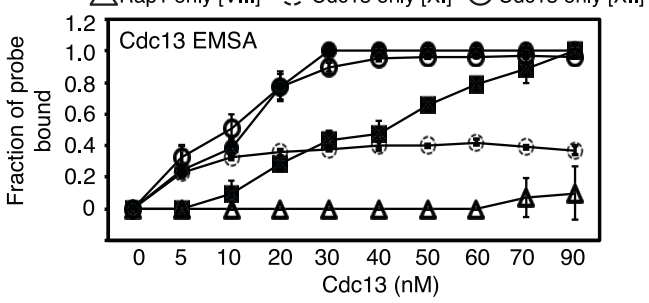

D

5′-GGATGTAG[ ]TACTACTAGGATTTGGCGTGGATGAAGGACCTGCAGTGGAGGGTGTTGTTGTGGAGTT-3′

Strain	Sequence within brackets
Rap1 only	[AATGTATGGGTGCaacaccAATGTATGGGTGC]AACAC#
Cdc13 only	GAGTGTGTGTGaacaccGAGTGTGTGTG

#Additional mutations were made beyond the bracketed sequence to prevent Cdc13 binding.

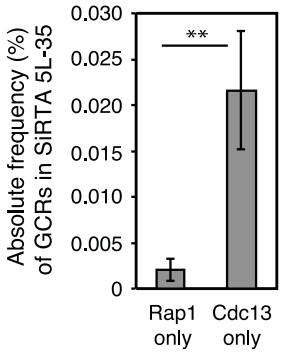

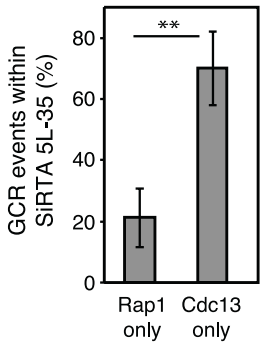

Figure 29. The rate of *de novo* telomere addition at SiRTA 5L-35 correlates with the ability of the SiRTA Stim sequence to bind Cdc13.
(A) Probes utilized for Cdc13-DBD and Rap1 binding assays. Probes I, III, and VI are identical to those used in Figure 27. Probes followed by "Rap1 EMSA" are double-stranded. Those indicated with "Cdc13 EMSA" are single-stranded.
(B) Binding of the indicated concentration of recombinant Rap1 to double-stranded probes shown in (A).
(C) Binding of the indicated concentration of recombinant Cdc13-DBD to single-stranded probes shown in (A). In (B) and (C), the average fraction of probe bound was determined from three independent experiments. Error bars represent standard deviation.
(D) The SiRTA 5L-35 Stim sequence (indicated by brackets) was replaced at the endogenous locus on chromosome V with the sequences depicted here. Average results and standard deviation of three HO-cleavage assays are shown as absolute frequency (%) of GCR formation within SiRTA 5L-35 (left graph) or percent of total GCR events within SiRTA 5L-35 (right graph). Averages indicated (**) are significantly different ($p<0.01$) by unpaired Student's T test.
Contributing authors: UCO, KLF.

11 base consensus sequence (Figure 29C, compare probes IX and XII), and both of these probes are bound more strongly than is the endogenous SiRTA Stim (Figure 29C, probe III). The 5' repeat is also bound by Cdc13-DBD, although more weakly than the 3' repeat (Figure 29C, probe XI). In conclusion, these *in vitro* binding analyses demonstrate that binding by Rap1 and Cdc13 can be separated, allowing us to test the specific effects of these proteins on SiRTA 5L-35 function.

The sequences defined above were integrated in place of the endogenous SiRTA Stim sequence on chromosome V (Figure 29D). Integration of the "Rap1 only" sequence reduced the overall frequency of GCR formation at SiRTA 5L-35 to about half that of the Stim-Subst sequence upon which it is based, a rate similar to that observed for the Stim-Subst inverted sequence (compare Figure 29D with Figure 27G). In contrast, the sequence containing only binding sites for Cdc13 resulted in a GCR rate eight fold higher than that of the endogenous sequence, 70.0±9.8% of all GCR events occurred within SiRTA 5L-35 (Figure 29D), and all of those events were the result of *de novo* telomere addition (data not shown). We again used a PCR-based strategy to determine where telomere addition occurred

within SiRTA 5L-35. Despite the telomere-like nature of the "Cdc13 only" sequence, 50 of 63 (79.4%) *de novo* telomeres were added at least 20 bp distal to that site (Figure 28).

To confirm the ability of Cdc13 to stimulate *de novo* telomere addition, we replaced the SiRTA Stim sequence with two copies of the Gal4 upstream activating sequence (stim::2XUAS), which is recognized by the Gal4 DNA binding domain (292) (GBD; Figure 30A). Into this strain, we introduced either an empty vector or a plasmid expressing a fusion of GBD with full-length Cdc13 or Rap1. As expected, the strain containing stim::2XUAS and empty vector supported a rate of GCR formation at SiRTA 5L-35 indistinguishable from a strain containing the stim::polyA mutation (Figure 30B; comparable to mutation c in Figure 23). Expression of the GBD-Rap1 fusion protein in the stim::2XUAS strain failed to increase the rate of GCR formation at SiRTA 5L-35 (Figure 30B), suggesting that Rap1 plays either no role or a minor role in stimulating telomere addition following a DSB.

In contrast, expression of the GBD-Cdc13 fusion protein in the stim::2XUAS strain increased the rate of GCR formation at SiRTA 5L-35 nearly 15-fold relative to the strain containing vector only (Figure 30B). This increase is largely attributable to the recruitment of GBD-Cdc13 to the 2XUAS sequences on chromosome V since expression of the fusion protein in the stim::polyA strain had no significant effect on GCR formation at SiRTA 5L-35 compared to the same strain containing the empty vector (Figure 30B).

Taken together, these results are consistent with a model in which resection of the 5' strand following a DSB exposes one or more sites at which Cdc13 is able to associate with the SiRTA Stim sequence. Such binding is required to increase the rate at which the more telomere-proximal Core sequence is capable of nucleating *de novo* telomere addition and explains why the telomere-like SiRTA 5L-35 Core sequence alone is insufficient to maintain a high rate of GCR formation at that site.

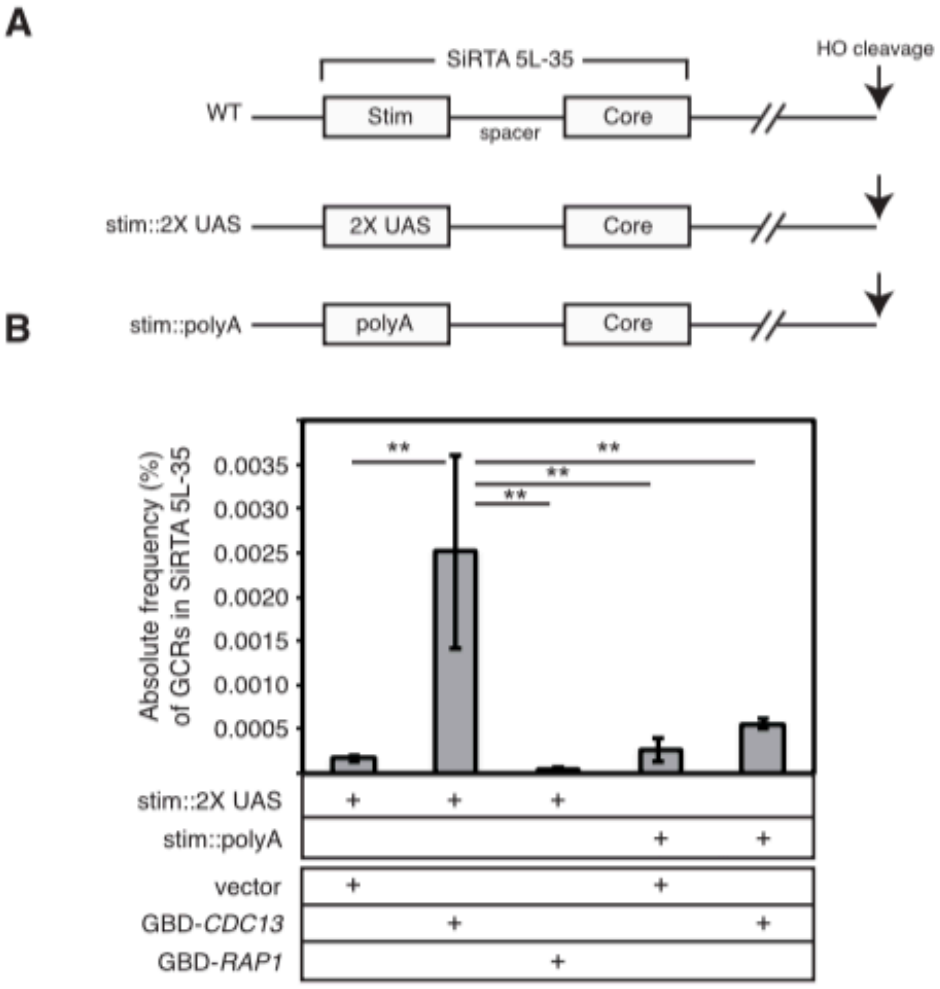

Figure 30. Artificial recruitment of Cdc13 to the SiRTA 5L-35 stimulatory site increases the rate of GCR formation.

(A) The SiRTA 5L-35 Stim sequence was replaced with two tandem copies of the Gal4 Upstream Activating Sequence (2X UAS) or with a string of adenines (polyA; identical sequence to that of mutation d in Figure 23A).

(B) The rate of GCR formation within SiRTA 5L-35 is shown for strains containing either the 2X UAS or polyA sequences integrated in place of SiRTA 5L-35 Stim. Cells are transformed with pRS314 (empty vector) or with pRS414 expressing either *CDC13* or *RAP1* as N-terminal fusions with the Gal4 DNA binding domain (GBD). Values for the three right-most columns are maximum estimates (see Materials and Methods). Error bars indicate standard deviation of three independent experiments. Averages indicated (**) are significantly different ($p<0.01$) by ANOVA with post-hoc Tukey HSD.

Contributing authors: UCO, EAE, KLF.

4.2.6 A second SiRTA on chromosome IX also has a bipartite structure

In searching for additional sequences with the hallmarks of a SiRTA, we identified a TG-rich sequence within the *BNR1* gene. This site is located ~16 kb distal to the first essential gene, *MCM10*, on chromosome IX-L. We integrated the HO recognition site ~3 kb distal to this sequence (Figure 31A) in a strain that expresses the HO endonuclease under galactose regulation and placed *URA3* on the distal arm, allowing us to select GCR events as described above for SiRTA 5L-35. Our PCR strategy was designed to capture GCR events occurring in the most prominent TG-rich sequence ("Core 1," Figure 31B). However, Southern blotting revealed a second cluster of *de novo* telomere addition events ~130 bp distal to the original sequence ("Core 2," Figure 31B; Figure 32). These two sequences result in a combined frequency of GCR formation of 0.015±0.006%, approximately three times higher than the rate observed at SiRTA 5L-35 (Figure 31C). We subsequently refer to this site as SiRTA 9L-44 (SiRTA, 44 kb from the left telomere of chromosome IX). Similar to SiRTA 5L-35, 33.0±1.4% of the GCR events obtained on chromosome IX occurred within SiRTA 9L-44 (including both Core sequences; Figure 31D). Interestingly, although Core 1 lies centromere-proximal to Core 2 (and therefore will be rendered single-stranded after Core 2 in response to a distal DSB), 28.2± 5.2% of all GCR events occurred within Core 1, while 4.8±4.4% occurred in Core 2 (data not shown), suggesting that Core 1 is more efficiently targeted. No GCR events occurred within the ~16 kb region between SiRTA 9L-44 and the first essential gene (Figure 31D).

Given that we identified a stimulatory sequence within SiRTA 5L-35 capable of binding to Cdc13 (Figures 23 and 27), we sought to identify similar sequence(s) that may contribute to telomere addition at SiRTA 9L-44. Using EMSA, we identified two sites that bind Cdc13-DBD *in vitro* (Cdc13 BS1 and Cdc13 BS2; Figure 31B and E). Mutation of Cdc13 BS1 to poly-adenine had no effect on the

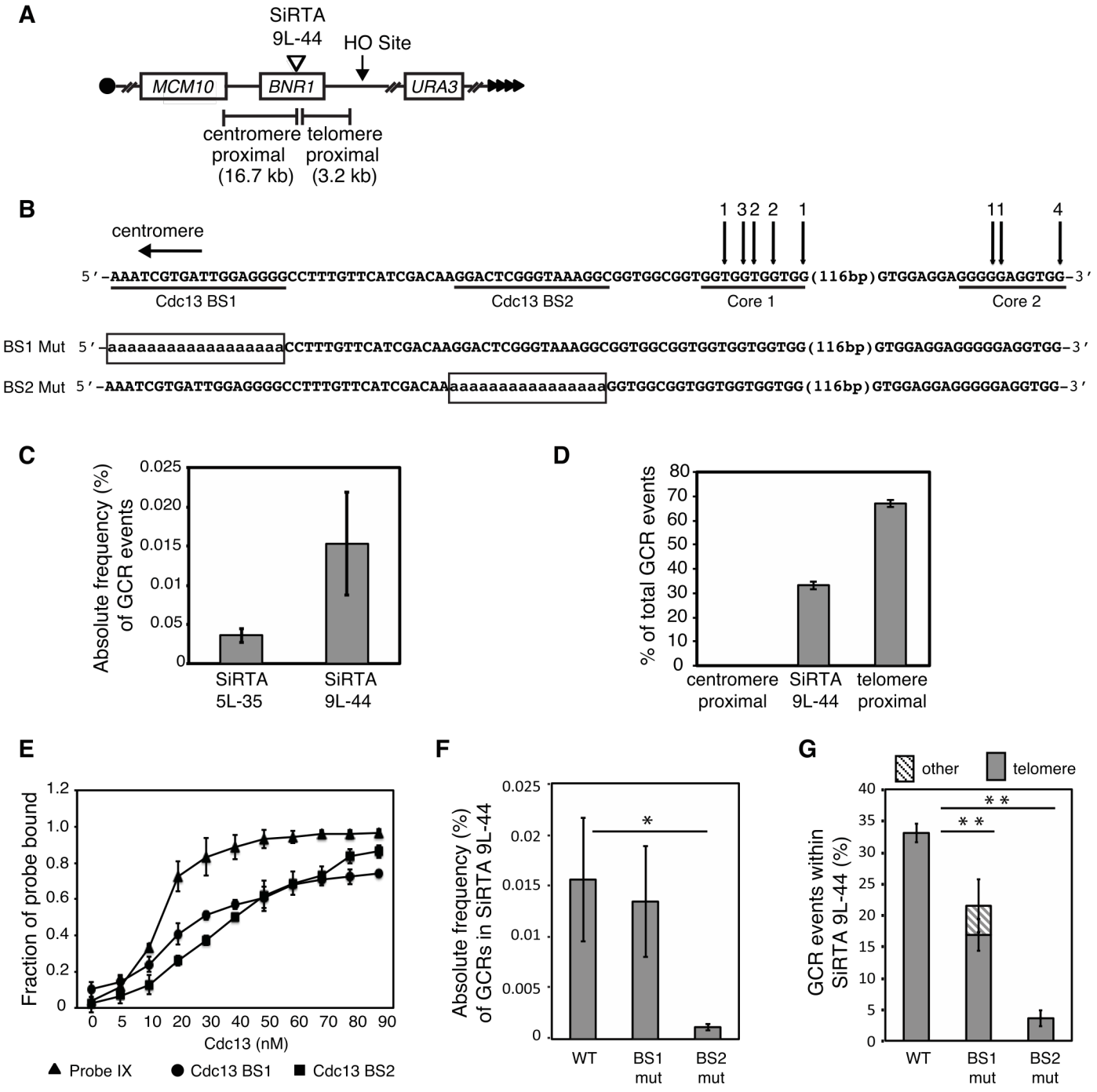
A
SiRTA
9L-44
HO Site
MCM10
BNR1
URA3
centromere
proximal
(16.7 kb)
telomere
proximal
(3.2 kb)
B
centromere
1 3 2 2 1
11 4
5′-AAATCGTGATTGGAGGGGCCTTTGTTCATCGACAAGGACTCGGGTAAAGGCGGTGGCGGTGGTGGTGGTGG(116bp)GTGGAGGAGGGGGAGGTGG-3′
Cdc13 BS1
Cdc13 BS2
Core 1
Core 2
BS1 Mut 5′-aaaaaaaaaaaaaaaaaaCCTTTGTTCATCGACAAGGACTCGGGTAAAGGCGGTGGCGGTGGTGGTGGTGG(116bp)GTGGAGGAGGGGGAGGTGG-3′
BS2 Mut 5′-AAATCGTGATTGGAGGGGCCTTTGTTCATCGACAAaaaaaaaaaaaaaaaaGGTGGCGGTGGTGGTGGTGG(116bp)GTGGAGGAGGGGGAGGTGG-3′
C
Absolute frequency (%) of GCR events
0.025
0.020
0.015
0.01
0.05
0
SiRTA 5L-35
SiRTA 9L-44
D
% of total GCR events
80
70
60
50
40
30
20
10
0
centromere proximal
SiRTA 9L-44
telomere proximal
E
Fraction of probe bound
1.2
1.0
0.8
0.6
0.4
0.2
0
0 5 10 20 30 40 50 60 70 80 90
Cdc13 (nM)
Probe IX
Cdc13 BS1
Cdc13 BS2
F
Absolute frequency (%) of GCRs in SiRTA 9L-44
0.025
0.02
0.015
0.01
0.005
0
*
WT
BS1 mut
BS2 mut
G
other
telomere
GCR events within SiRTA 9L-44 (%)
40
35
30
25
20
15
10
5
0
* *
* *
WT
BS1 mut
BS2 mut

Figure 31. A site at which *de novo* telomere addition occurs at high frequency on chromosome IX (SiRTA 9L-44) has a similar organization to SiRTA 5L-35.
(A) Schematic of the left arm of chromosome IX. Sizes of the regions between SiRTA 9L-44 and either the HO cleavage site (telomere-proximal) or the most distal essential gene (*MCM10*; centromere-proximal) are indicated.
(B) Top schematic: Sequence of SiRTA 9L-44 with vertical arrows indicating sites of *de novo* telomere addition. The sequence is oriented with the telomere to the right so that the DNA strand depicted is the direct 3' primer upon which telomerase acts. In each case, the most 3' chromosomal nucleotide with identity to the cloned *de novo* telomere is indicated. Numbers above arrows indicate the number of independent telomere addition events mapped to each site. Sequences predicted to bind Cdc13 are underlined (Cdc13 BS1 and Cdc13 BS2). Bottom schematic: Mutations created in SiRTA 9L-44. Uppercase letters represent unchanged nucleotides, lowercase letters enclosed in box represent mutated nucleotides.
(C) The absolute frequency (%) of GCR events within SiRTA 5L-35 or SiRTA 9L-44 is shown.
(D) The percentage of GCR events occurring in each indicated region on chromosome IX is shown. No GCR events were observed in the region centromere-proximal to SiRTA 9L-44. Values in (C) and (D) are averages of three independent experiments with standard deviation.
(E) Binding of the indicated concentration of recombinant Cdc13-DBD to single-stranded probe IX (see Figure 29A) or single-stranded probes corresponding to the underlined sequences in (B). The average fraction of probe bound was determined from three independent experiments. Error bars represent standard deviation.
(F) The BS1 mut and BS2 mut sequences shown in (B) were inserted at the endogenous SiRTA 9L-44 locus on chromosome IX and the absolute frequency (%) of *de novo* formation within SiRTA 9L-44 was determined.
(G) The percent of total GCR events that occur within SiRTA 9L-44 for WT and the indicated mutant strains is shown. GCR events involving *de novo* telomere addition were identified by Southern blot; any event that does not involve telomere addition is classified as "other." Results in (F) and (G) are the average and standard deviation of three independent experiments. Samples with statistically different values by ANOVA with post-hoc Tukey HSD are indicated (* $p<0.05$; ** $p<0.01$).
Contributing authors: EAE, UCO.

overall frequency of GCR events at SiRTA 9L-44 relative to WT (Figure 31F), although the fraction of GCR events that occurred within SiRTA 9L-44 was significantly reduced (from 33.0±1.4% to 21.4±6.2%; Figure 31G). This reduction occurred specifically at Core 1, since the fraction of events at Core 2 remained similar to WT (4.8±4.4% in WT versus 7.5±1.5% in BS1). 4.6±4.2% of the GCR events that occurred at SiRTA 9L-44 when Cdc13 BS1 was mutated were not *de novo* telomere addition events, a phenomenon never observed in WT cells (Figure 31G). Together, these results suggest a minor contribution by Cdc13 BS1 to the high rate of *de novo* telomere addition at SiRTA 9L-44.

In contrast, mutation of Cdc13 BS2 to poly-adenine strongly reduced the overall rate of GCR formation at SiRTA 9L-44 (~18-fold; Figure 31F). Only 3.5±1.3% of GCR events occurred within SiRTA 9L-44 (Figure 31G) and none were within Core 2. Cdc13-DBD binds similarly to BS1 and BS2 *in vitro*, suggesting that the efficacy of these sequences in stimulating telomere addition correlates poorly with the strength of binding by Cdc13 (compare Figure 31E to 31F and G). The functional difference between these sequences may be explained, at least in part, by their differing proximity to the sites of *de novo* telomere addition at Core 1 and Core 2.

In conclusion, we identified a SiRTA on chromosome IX that bears striking similarities to the SiRTA on chromosome V. Both SiRTAs contain TG-rich tracts within which telomere addition occurs and the high rate of *de novo* telomere addition at these SiRTAs relative to neighboring sequences can be attributed to stimulatory sequences that lie centromere-proximal to the major sites of telomere addition. Finally, EMSA analysis shows that Cdc13 binds these stimulatory sequences *in vitro*. Thus, increased telomerase activity at SiRTAs is likely achieved, at least in part, by the association of Cdc13 with one or more stimulatory sequences upstream of the sites of actual *de novo* telomere addition.

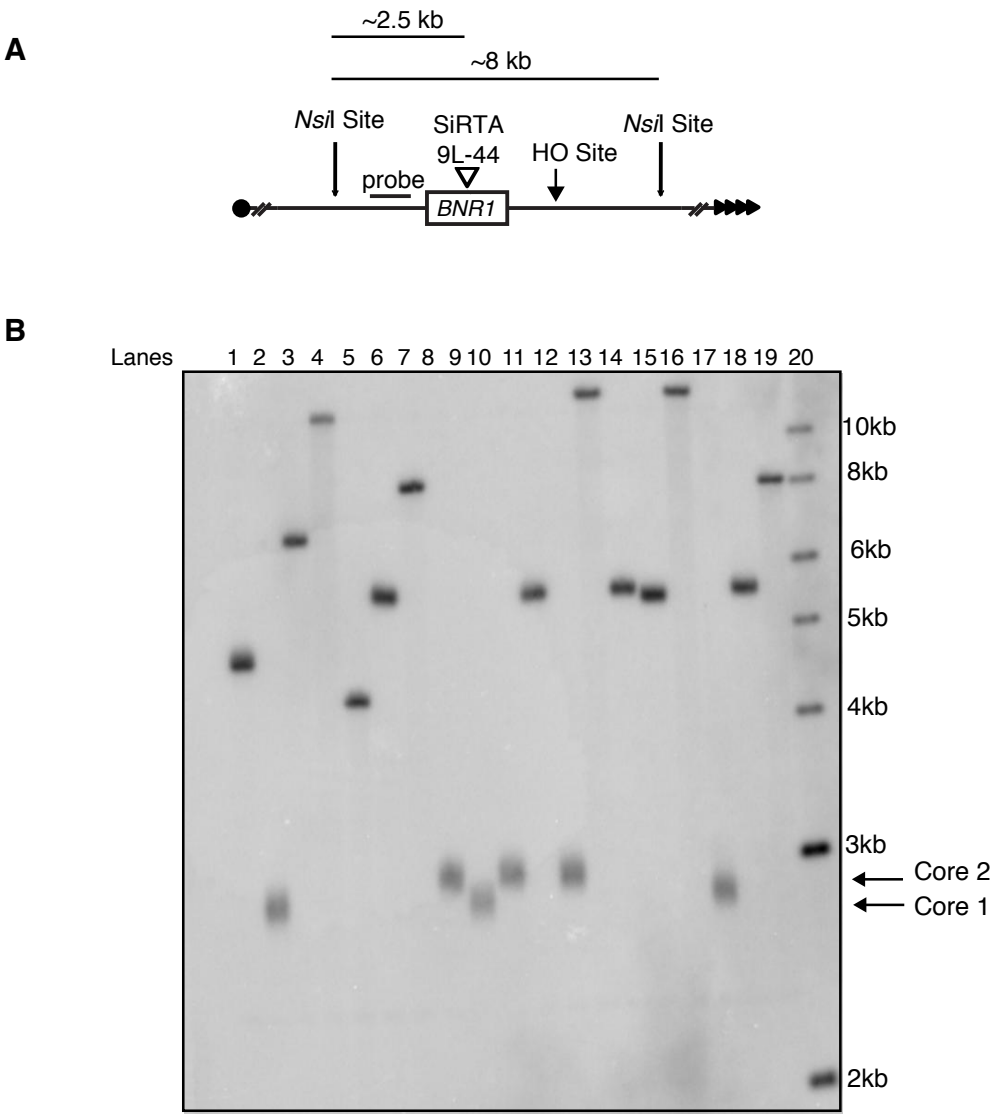

Figure 32: Southern blot analysis of GCR events in or near SiRTA 9L-44.
(A) Map of region containing SiRTA 9L-44. Genomic DNA was cleaved with *Nsi*I; the location of the probe is shown.
(B) Southern blot analysis of 18 independent GCR events on chromosome IX. Arrows indicate bands indicative of *de novo* telomere addition at either Core1 (lanes 2, 9 and 17) or Core 2 (lanes 8, 10, 12). Lane 19 contains the DNA isolated from the parent strain prior to selection for GCR events. Note detection of the expected band of ~8 kb. Lane 20 contains molecular weight marker as indicated.
Contributing authors: EAE.

4.3 Discussion

Endogenous sites of *de novo* telomere addition can affect genome stability, and have been associated with cancer (293) and congenital disorders (294-296). While *S. cerevisiae* provides a useful model system to study mechanisms of *de novo* telomere addition, most studies utilize artificial sequences to stimulate telomere formation. The goal of this study was to examine naturally occurring sites at which *de novo* telomere addition is greatly favored and to identify *cis*- and *trans*-acting factors contributing to this property. We characterized two genomic sites (SiRTAs) at which *de novo* telomere addition occurs at a remarkably (at least 200 fold) increased rate compared to neighboring sequences. Zakian and colleagues reported a third hotspot of *de novo* telomere addition on chromosome VII at a location 50 kb internal to an HO cleavage site (268). Unlike the two sequences studied here, the chromosome VII site lies internal to the last essential gene on the chromosome arm (a disomic strain lacking *RAD52* was used to maintain viability and limit homologous recombination). Given the ease with which these sites have been found, it seems likely that additional SiRTAs remain to be identified.

While many assays of *de novo* telomere addition utilize short telomeric tracts placed immediately adjacent (within 20-30 nt) to the HO cleavage site [*e.g.* (271, 272, 297, 298)], the natural SiRTAs described here are located several kilobases internal to the induced break, requiring extensive resection prior to telomere addition. In our assays, we also observe telomere addition at or very close to the HO cut site (Figure 21). This propensity is at least partially a consequence of the TGTT-3' overhang produced by HO endonuclease cleavage. When the recognition site is inverted to generate the complementary ACAA-3' overhang, *de novo* telomere addition at the HO site is reduced and the fraction of events at SiRTA 5L-35 is increased (data not shown). Given these observations, studies of telomere addition at endogenous sites located at a distance from an induced break may more faithfully

capture the mechanism of repair of a random chromosomal break than models in which a telomeric seed sequence is intentionally placed adjacent to the HO cleavage site.

We observe that both SiRTA 5L-35 and 9L-44 contain sequences that enhance telomerase action, but act rarely, if ever, as the direct target of telomerase action (SiRTA Stim sequences). Because the telomere-binding proteins Cdc13 and Rap1 stimulate *de novo* telomere addition at artificial sequences in *S. cerevisiae* (271, 276, 277, 282, 298), we hypothesized that one or both of these proteins could be responsible for the enhancing activity of the Stim sequence. Although Cdc13 and Rap1 bind similar sequences, we were able to design artificial sequences that bind with great preference to one protein as measured *in vitro*. Using this approach, we found that a sequence designed to facilitate Cdc13 binding is much more effective in the stimulation of *de novo* telomere addition than one binding primarily Rap1 (Figure 29D). Importantly, artificial recruitment of GBD-Cdc13 to SiRTA 5L-35 (Figure 30) led to high frequencies of telomere addition, suggesting that Cdc13 binding, and not the TG-rich sequences *per se*, stimulates *de novo* telomere addition. Replacement of Stim with the "Rap1 only" sequence did not reduce telomere addition as dramatically as the replacement of Stim with a poly A sequence or with the Gal4 UAS (compare Figure 29D with Figures 23B and 30B), so binding by Rap1 may also contribute to the stimulation of *de novo* telomere addition. Consistent with the proposal that binding by Cdc13 is important for the stimulatory effect of the Stim sequence, we find that high levels of telomere addition at SiRTA 9L-44 require a sequence capable of binding Cdc13 (BS2, Figure 31B) and that this sequence stimulates telomere addition over a distance of more than 100 bp. Rap1 does not bind to the BS2 sequence *in vitro* (data not shown), suggesting that Cdc13 is sufficient to stimulate *de novo* telomere addition at this SiRTA.

The stimulation of *de novo* telomere addition by telomere-like sequences located internal to the site of telomerase action has been previously observed in both artificial and natural contexts. For

example, *de novo* telomeres generated following DNA cleavage by HO endonuclease near a TG-rich seed sequence are frequently added at the 3' overhang of the HO endonuclease target site rather than within the telomeric seed itself (270). At the SiRTA on chromosome VII reported by Mangahas *et al*. (268), telomere addition occurs at several closely spaced sequences located 37-49 bp distal to a 35 bp GT dinucleotide repeat. This sequence matches the $GxGT(T/G)_7$ consensus for Cdc13 binding (291), consistent with the GT dinucleotide repeat acting as a Stim sequence in the manner we report here for SiRTAs 5L-35 and 9L-44. However, as is the case at SiRTA 5L-35, the TG dinucleotide tract on chromosome VII may also bind Rap1 (192), so a contribution of Rap1 to Stim function cannot be ruled out.

Kramer and Haber reported that *de novo* telomere addition occurs ~15-100 bp distal to an ectopic tract of 13 T_2G_4 repeats (*Tetrahymena thermophila* telomeric sequence) and a similar phenomenon was reported on plasmid substrates (269, 299). The *Tetrahymena* telomeric sequence contains the $GxGT(T/G)_7$ consensus sequence for Cdc13 binding (291), although a $(T_2G_4)_3$ oligonucleotide was shown to compete poorly with the yeast telomeric sequence for Cdc13 binding *in vitro* (285). This short sequence is predicted to contain only a single Cdc13 binding site, while the tract of 13 repeats utilized by Kramer and Haber has multiple potential binding sites (269). Combined with our observation that the Stim sequences in both SiRTA 5L-35 and 9L-44 bind Cdc13 with lower affinity than an optimized sequence from the yeast telomere (Figures 29C and 31E), it is reasonable to suggest that the stimulatory effect observed by Kramer and Haber is due to Cdc13 binding to the ectopic T_2G_4 tract.

How might the bipartite structure of SiRTA 5L-35 facilitate *de novo* telomere addition? Genetic and biochemical analysis suggest that Cdc13 protects telomeres from extensive 5' strand degradation (213, 300-302). One possibility is that Cdc13 bound to the Stim sequence inhibits resection past SiRTA,

thereby providing a grace period to allow for the formation of a stable telomere at the Core sequence. However, inhibition of resection alone does not account for the increased efficacy of the Stim when it is brought in close proximity to the Core (Figure 26B). Another possibility is that Cdc13 must be bound to both the Stim and Core sequences to stably recruit telomerase to the SiRTA. This proposal is congruent with the results of Hirano and Sugimoto that show greatly increased stimulation of telomerase recruitment and *de novo* telomere addition when two tandem Cdc13 binding sites are placed adjacent to an HO-induced break, compared to the effect of a single site (298).

In addition to its C-terminal oligonucleotide/oligosaccharide binding (OB) fold domain (also known as its DNA-binding domain), Cdc13 contains an N-terminal OB fold that is involved in Cdc13 dimerization (303). The minimal binding site for both full-length Cdc13 and its isolated DBD is an 11-mer $TG_{1\text{-}3}$ sequence. However, as demonstrated by EMSA, the Cdc13 N-terminal OB fold, which exists as a stable dimer in solution, does not bind to this 11-mer, but binds with stronger affinity to ssDNA sequences at least 37 nucleotides long (303). These observations support a model in which each Cdc13 monomer binds to a separate site on a single molecule of ssDNA, with optimal binding depending on the distance between the two sites. Finally, mutations that disrupt Cdc13 dimerization *in vitro* cause telomere shortening when introduced *in vivo* (303). We propose that dimerization between Cdc13 monomers bound to the Stim and Core sequences is required to stably recruit telomerase to the SiRTA. This model additionally accounts for the increased efficacy of the Stim when it is juxtaposed with the Core, since in that context, the distance between the two monomers may be more optimally suited to stable telomerase recruitment.

4.4 Materials and Methods

4.4.1 Yeast strains and plasmids

Table 1 contains a complete list of strains used in this study. Unless otherwise noted, strains were grown in yeast extract/peptone/dextrose (YEPD) at 30˚C. In strains utilized for HO cleavage assays (YKF1310 and YKF1308), the *HMRa* sequence on chromosome III was replaced with *nat*, which confers resistance to nourseothricin. All gene deletions were generated by one-step gene replacement with a selectable marker and were confirmed by PCR. *hxt13*::*URA3* disruptions were created by using a plasmid in which the *Kpn*I-*Sph*I restriction fragment from *HXT13* was replaced with *URA3* or by amplifying the *hxt13::URA3* locus from an existing strain using primers hxt13::URA3 F and hxt13::URA3 R (Table 2). The HO cleavage site was integrated on chromosomes VII and IX by one-step gene replacement using plasmid pJH2017 (*HOcs::HPH*; gift of J. Haber) as template with selection for hygromycin B resistance. *URA3* was integrated on chromosome VII by one-step gene replacement at the *PAU11* locus and on chromosome IX by one-step gene replacement at the *SOA1* locus. Primers utilized for PCR are listed in Table 2.

Strain YKF1409 (*rad52*::*LEU2*) was generated by transformation with BamHI-digested plasmid pSM20, which contains the *rad52*::*LEU2* disruption allele (304).

Mutations in SiRTA 5L-35 described in Figures 23, 26, and 27 were introduced by two-step gene replacement (305). DNA fragments containing each mutation were generated by PCR using Gene Splicing by Overlap Extension (Gene SOEing; (306)). Met-NPR2 For primer was used with a reverse primer containing the desired mutation to generate fragment I and NPR2 mid-Rev primer was used with a forward primer containing the same mutation to generate fragment II (Table 2). Fragments I and II were extended by mutually primed synthesis using the Met *NPR2* For and Mid *NPR2* Rev primers

to generate a final PCR product that was cleaved with *Hin*dIII and *Xba*I for ligation into pRS306. The integration plasmid was linearized with *BamH*I or *Bcl*I prior to transformation and selection for Ura+ integrants. To facilitate the identification of strains containing the desired mutations following selection on media containing 5-FOA, two-step integration was first used to create strain YKF1366 in which SiRTA 5L-35 is deleted. Subsequent strains were created by reintroducing mutated versions of SiRTA 5L-35 into strain YKF1366 by two-step integration. Resulting 5-FOA^R isolates were screened by PCR and candidates were sequenced to confirm the presence of the desired mutations.

For mutations described in Figures 29 and 30, a portion of SiRTA 5L-35 including the Stim sequence was replaced with *URA3* in strain YKF1323 by one-step gene replacement to generate strain YKF1585. Sequences to be integrated were generated by PCR using the HS forward and HS reverse primers and transformed into strain YKF1585. After allowing cells to recover for 24 - 48 hours on rich media, cells were replica plated to media containing 5-FOA. Mutations were confirmed by sequencing.

SiRTA 5L-35 spacerΔ was integrated on chromosome VII and mutations were introduced at SiRTA 9L-44 by two-step gene replacement essentially as described above. Table 2 contains the sequences of primers used for strain construction.

Plasmid pAB180 (pRS414-ADHpromoter-GBD-*CDC13*) was a gift from A. Bianchi. pAB180-Rap1 was created by replacing the *CDC13* open reading frame in pAB180 with the full-length *RAP1* open reading frame at the *Nco*I and *Aat*II sites. All amplified regions were confirmed by sequencing.

4.4.2 GCR assays

For spontaneous GCR assays, cells cultured overnight in synthetic drop-out medium lacking uracil (SD-Ura) were used to inoculate YEPD cultures (approximately 30 per strain). YEPD cultures were grown overnight to saturation (approximately 24 hours) and plated to medium containing 5-FOA

and canavanine to isolate GCRs (5-FOA^R Can^R colonies). Only one colony was analyzed from each plate to ensure independence. The approximate location and nature of GCR events was determined by multiplex PCR ((307) and Figure 20) and Southern blot (see below).

For HO-cleavage GCR assays, cells were grown in SD-Ura media (with 2% raffinose) to OD_{600} of ~ 0.3 – 1. Cells were plated on yeast extract/peptone medium with 2% galactose (YEPG) and a dilution was plated on YEPD to determine total cell number. After three days, colonies were counted and galactose-resistant colonies were transferred to SD medium containing 5-FOA to isolate GCR events. At least 100 gal^R colonies were individually plated on media containing 5-FOA to determine the rate of *URA3* loss. If necessary, additional colonies were obtained by replica plating. The approximate location and nature of GCR events was determined by multiplex PCR ((307) and Figure 21) and Southern blot (see below).

The absolute frequency at which GCR events occur within a SiRTA is calculated by multiplying the rate of survival on galactose (colonies on galactose/colonies on glucose, corrected for dilution factor) by the fraction of gal^R colonies capable of growth on media containing 5-FOA and the fraction of gal^R 5-FOA^R colonies in which the GCR event occurred within the SiRTA as measured by PCR. Approximately 30 gal^R 5-FOA^R colonies were analyzed for each experiment and averages and standard deviations presented are derived from a minimum of three independent experiments. In a few cases, rates shown are upper estimates because no 5-FOA resistant colonies were detected among 100 colonies analyzed or no events were obtained within the SiRTA sequence among ~30 gal^R 5-FOA^R colonies. These cases are indicated in the figure legend where applicable.

4.4.3 Southern blotting

For the characterization of GCR events, approximate locations determined by multiplex PCR

were used to design restriction enzyme digests and probes for Southern blot analysis. Information about the restriction enzymes and primers utilized are available upon request. Digested fragments were separated on a 0.7% agarose gel, transferred to nylon membrane (Hybond N+), and probed with [32P] dCTP-labelled telomeric DNA. Radioactive membranes were exposed to Phosphor screens (Molecular Dynamics) and screens were scanned with Typhoon TRIO Variable Mode Imager (GE Healthcare). Telomere addition was determined by visualization of the characteristic smear generated by the heterogeneous telomere sequence at a size consistent with the PCR result.

4.4.4 Protein purification

Plasmid pET21a-Cdc13-DBD-His_6 (290) was a gift from Deborah Wuttke [University of Colorado, Boulder, CO]. BL21 (DE3) *Escherichia coli* transformed with pET21a-Cdc13-DBD-His_6 were grown at 37°C in LB media with ampicillin (50 mg/L) to an OD_{600} of ~0.6. Cdc13-DBD-His_6 expression was induced with IPTG (isopropyl-β-d-thiogalactopyranoside) at a final concentration of 1 mM at 22°C for approximately 6 hours, after which cells were harvested by centrifugation. Cells were resuspended in buffer A [25 mM HEPES-NaOH, 10% glycerol, 300 mM NaCl, 0.01% NP-40, 20 mM imidazole, 1 mM benzamidine, 0.2 mM phenylmethylsulfonyl fluoride] and cell lysis was achieved by incubation with lysozyme solution [1 mg/mL lysozyme, 1 mM Tris-HCl pH 8.0, 0.1 mM EDTA, 10 mM NaCl, 0.5% Triton-X-100], followed by sonication for 60 sec (two 30-sec cycles) using a Branson 450 Sonifier (power setting 3, 70% duty cycle). Supernatant was separated from cellular debris by centrifugation, and Cdc13-DBD-His_6 was purified from supernatant with Ni-NTA (Ni-nitrilotriacetic acid) agarose beads. Beads were washed in buffer A and protein was eluted from beads in buffer B [25 mM HEPES-NaOH, 10% glycerol, 300 mM NaCl, 0.01% NP-40, 200 mM imidazole, 1 mM benzamidine, 0.2 mM phenylmethylsulfonyl fluoride]. Eluted protein was dialyzed overnight in buffer

C [25 mM HEPES-NaOH, 10% glycerol, 300 mM NaCl]. Protein concentration was estimated by polyacrylamide gel electrophoresis, using bovine serum albumin as standard. Purification of Rap1 has been previously described (308).

4.4.5 Electrophoretic mobility shift assays (EMSA)

To generate EMSA probes, oligonucleotide pairs were mixed in equimolar ratios, boiled in 1X annealing buffer (10 mM Tris-HCl pH 7.5, 100 mM NaCl, 1 mM EDTA), and slowly cooled to room temperature. Probes were radiolabelled with T4 polynucleotide kinase or by fill-in synthesis with Klenow polymerase. For Rap1 EMSAs, each 20 µl EMSA reaction contained binding buffer (20 mM Tris-HCl pH 7.5, 1 mM DTT, 70 mM KCl, 1 mM EDTA, 5% glycerol, 2.5 ng/µl BSA), 1.5 µg herring sperm DNA (Sigma-Aldrich), labeled probe (30 - 50 nM), and the indicated amounts of Rap1. Reactions were separated by 5% native polyacrylamide gel electrophoresis (PAGE) in 0.5X TBE at 100V for 45 min. Gels were fixed in 10% acetic acid/20% methanol and then exposed to Phosphor Screens. Screens were scanned using the Typhoon TRIO Variable Mode Imager and results were analyzed with ImageQuant TL 7.0 software (GE Heathcare). For Cdc13 EMSAs, each 20µl EMSA reaction contained binding buffer (50 mM Tris-HCl pH 7.5, 1 mM DTT, 75 mM KCl, 75 mM NaCl, 0.1 mM EDTA, 15% glycerol, 1 mg/ml BSA), labeled probe (62.5 nM), and the indicated amount of Cdc13-DBD protein. Reactions were separated on 6% native polyacrylamide gels (containing 5% glycerol) in 1X TBE buffer at 200V for 30 min. Subsequent steps were as described for Rap1 above.

4.4.6 Cloning and sequencing of *de novo* telomeres

Cloning of telomeric DNA was performed as previously described (270) with minor modifications. Blunting of genomic DNA ends was done with T4 DNA polymerase (NEB) in the

presence of 0.1 mM dNTPs. Sequences for ds oligo 1 and ds oligo 2 (used to create the double-stranded oligonucleotide that was ligated to the blunted DNA ends) can be found in Table

2. Telomere PCR was performed with ds oligo 2 and a primer internal to the *de novo* telomere (Table 2). PCR products were separated in 2% agarose gels, purified, and ligated into pGEM-T Easy vector (Promega) or pDrive Vector (Qiagen). Sequencing of inserts was carried out by GenHunter (Nashville, TN) or Genewiz (South Plainfield, NJ) using the primer M13F (-20) (Table 2).

Table 1. List of strains

Strain	Genotype	Source
YKF201	*MAT**a** trp1 leu2 ura3 his7*	T. Formosa[1]
YKF870	YKF201 *hxt13*::*URA3* (Fig. 1A, B)	This study
YKF1310	CL11-7: *MAT**a**::ΔHOcs::hisG hml✓Δ::hisG HMRa-stk ura3Δ851 trp1Δ63 leu2Δ*::*KAN*^{R} *ade3*::*GAL10*::*HO*	J.E. Haber[2]
YKF1308	JRL017: *MAT**a**::ΔHOcs::hisG hml✓Δ::hisG HMRa-stk ura3Δ851 trp1Δ63 leu2Δ*::*KAN*^{R} *ade3*::*GAL10*::*HO can1,1-1446*::*HOcs*::*HPH*^{R}	J.E. Haber[2]
YKF1333	YKF1310 *hmra-stkΔ*::*NAT*^{R}	This study
YKF1323	YKF1308 *hmra-stkΔ*::*NAT*^{R}	This study
YKF1342	YKF1323 *hxt13*::*URA3* (Fig. 1C, D; Fig. 2, 3, 4, 5)	This study
YKF1366	YKF1323 SiRTA 5L-35Δ	This study
YKF1403	YKF1366* SiRTA 5L-35 core mut *hxt13::URA3* (Fig. 2, mutation a)	This study
YKF1401	YKF1366* SiRTA 5L-35 spacer mut *hxt13::URA3* (Fig. 2, mutation b)	This study
YKF1385	YKF1366* SiRTA 5L-35 stim::polyA *hxt13::URA3* (Figs. 2 and 6, mutation c)	This study
YKF1464	YKF1366* SiRTA 5L-35 spacer/coreΔ *hxt13::URA3* (Fig. 2, mutation d)	This study
YKF1477	YKF1366* SiRTA 5L-35 spacerΔ *hxt13::URA3* (Fig. 3)	This study
YKF1459	YKF1366* SiRTA 5L-35 stim subst *hxt13::URA3* (Fig. 4)	This study
YKF1517	YKF1366* SiRTA 5L-35 stim subst inv *hxt13::URA3* (Fig. 4)	This study
YKF1585	YKF1323 SiRTA 5L-35::*URA3*	This study

YKF1592	YKF1585** SiRTA 5L-35 Rap1 only *hxt13::URA3* (Fig. 5)	This study
YKF1630	YKF1585** SiRTA 5L-35 Cdc13 only *hxt13::URA3* (Fig. 5)	This study
YKF1588	YKF1585** SiRTA 5L-35 stim::2X UAS *hxt13::URA3* (Fig. 6)	This study
YKF1510	YKF1333 spacerΔ (chr. VII) *pau11::URA3* (Fig. 3)	This study
YKF1518	YKF1333 SiRTA 9L-44 *soa1*::*URA3* (Fig 7)	This study
YKF1610	YKF1333 SiRTA 9L-44 Cdc13 BS Mut1 *soa1*::*URA3* (Fig 7)	This study
YKF1652	YKF1333 SiRTA 9L-44 Cdc13 BS Mut2 *soa1*:: *URA3* (Fig 7)	This study

* Strain YKF1366 contains a deletion of the complete SiRTA 5L-35 sequence. This strain was used as the recipient strain for two-step integration of the indicated SiRTA 5L-35 mutations to facilitate the identification of correct strains following growth on media containing 5-FOA.

** Strain YKF1585 contains a *URA3* cassette replacing a portion of SiRTA 5L-35. This strain was used as the recipient for one-step gene replacement by the indicated SiRTA 5L-35 mutations, with selection for integration on media containing 5-FOA.

1 **Formosa T and Nittis T.** 1999. Dna2 mutants reveal interactions with DNA polymerase alpha and Ctf4, a Pol alpha accessory factor, and show that full Dna2 helicase activity is not essential for growth. Genetics **151**:1459– 1470.

2 **Lydeard JR, Lipkin-Moore Z, Jain S, Eapen VV, Haber JE.** 2010. Sgs1 and Exo1 redundantly inhibit break-induced replication and *de novo* telomere addition at broken chromosome ends. PLoS Genet **6:**e1000973.

Table 2. List of Primers

Name	Sequence	Reference and/or Use
hxt13::URA3 F	5'-CCCCTGGATATATGCGC-3'	Amplify *hxt13::URA3* allele from existing strain for one-step integration
hxt13::URA3 R	5'-CCCCATATCATTTCACTCC-3'	
hmra-stkΔ::NATR F	5'-ACAAATCTAGAAATTACCAGAGCTATCCATCTTGTTCAAGAAGGTAGGCGCGGATCCCCGGGTTAATTAA-3'	Replace sequences with homology to the HO cleavage site with nat gene
hmra-stkΔ::NATR R	5'-TTGAATAAACCTGGTCTCAAATAAAATTGGTAGAATGACCGAATTCGAGCTCGTTTAAAC-3'	
Met-NPR2 For	5'-CATGTCTAGAATGCTAAGCTATTTCCAAGGG-3'	Fragment I
NPR2-mid Rev	5'-GTACAAGCTTGTGGATCAGTCAAAAAATTCC-3'	Fragment II
stim::polyA fragment I	5'-GGATGTAG**AAAAAAAAAAAAAAAAAA**TACTACTAGGATTTGGCGTG-3'	Use with Met-NPR2 For and NPR2-mid Rev. Fig. 2, mutation c and Fig. 6.
stim::polyA fragment II	5'-GTA**TTTTTTTTTTTTTTTTTT**CTACATCCGAAAAGGATACAAAGG-3'	
core mut fragment I	5'-**CACCTCCCACAACAACACCTCAA**TTCCAACACCTTCAAATCGAAG-3'	Use with Met-NPR2 For and NPR2-mid Rev. Fig. 2, mutation a.
core mut fragment II	5'-**TTGAGGTGTTGTTGTGGGAGGTG**GCAGGTCCTTCATCCACGCC-3'	
spacer mut fragment I	5'-**ATGATGATCCTAAACCGCACCTACTTCCTGCACCA**GTGGAGGGTGTTGTTGTGG-3'	Use with Met-NPR2 For and NPR2-mid Rev. Fig. 2, mutation b.
spacer mut fragment II	5'-**GGTGCGGTTTAGGATCATCAT**ACACCACACCAACTCATCCTAC-3'	
spacer/coreD fragment I	5'-GGTGTGGTGTTTTCCAACACCTTCAAATCGAAG-3'	Use with Met-NPR2 For and NPR2-mid Rev. Fig. 2, mutation d.
spacer/coreD fragment II	5'-AGGTGTTGGAAAACACCACACCAACTCATCCTACATCCG-3'	

spacerD fragment I	5'-GTAGGATGAGTTGGTGTGGTGTGTGGAGGGTGTTGTTGTGGAGTTTTC-3'	Use with Met-NPR2 For and NPR2-mid Rev. Fig. 3 (chr. V).
spacerD fragment II	5'-ACACCACACCAACTCATCCTAC-3'	
stim subst fragment I	5'-GGATGTAG**AATGTATGGGTGT**AACACC**AATGTATGGGTGT**TACTACTAGGATTTGGCGTG-3'	Use with Met-NPR2 For and NPR2-mid Rev. Fig 4G.
stim subst fragment II	5'-GTA**ACACCCATACATT**GGTGTT**ACACCCATACATT**CTACATCCGAAAAGGATACAAAGG-3'	
stim subst inv fragment I	5'-GGATGTAG**ACACCCATACATT**GGTGTT**ACACCCATACATT**TACTACTAGGATTTGGCGTG-3'	Use with Met-NPR2 For and NPR2-mid Rev. Fig 4G.
stim subst inv fragment II	5'-GTA**AATGTATGGGTGT**AACACC**AATGTATGGGTGT**CTACATCCGAAAAGGATACAAAGG-3'	
stim::URA3 for	5'-CACTGTATCTGCTGCTTCTCATATCCTTTGTATCCTTTTCGTACTGAGAGTGCACCACGC-3'	Use to replace SiRTA 5L-35 stim with URA3 by one-step gene replacement.
stim::URA3 rev	5'-AACAACACCCTCCACTGCAGGTCCTTCATCCACGCCAAATCTCCTTACGCATCTGTGCGG'3'	
HS forward	5'-TACTGCATTTCCCTCATCAATTG-3'	fragment I
HS reverse	5'-GACGTCTCCCTACGAACCAG-3'	fragment II
Cdc13 only fragment I	5'-ATCCTAGTAGTA**CACACACACTC**GGTGTT**CACACACACTC**CTACATCCGAAAAGGATACAAAG-3'	Use with HS forward and HS reverse to replace URA3 in stim::URA3. Fig. 5D.
Cdc13 only fragment II	5'-**GAGTGTGTGTG**AACACC**GAGTGTGTGTG**TACTACTAGGATTTGGCGTGG-3'	
Rap1 only fragment I	5'-**CCAAATCCTAGGTGTTGCACCCATACATTGGTGTTGCACCCATACATT**CTACATCCGAAAAGGATACAAAG-3'	Use with HS forward and HS reverse to replace URA3 in stim::URA3. Fig. 5D.
Rap1 only fragment II	5'-**GGTGCAACAC**CTAGGATTTGGCGTGGATGAAG-3'	
stim::2X UAS fragment I	5'-CTAGTAGTA**GTGTCGGCGCAGAGATCTCCGAGTGTCGGCGCAGAGATCTCCGA**GAAAAGGATACAAAGGATATGAG-3'	Use with HS forward and HS reverse to replace URA3

stim::2X UAS fragment II	5'-**GCGCCGACAC**TACTACTAGGATTTGGCGTGG-3'	in stim::URA3. Fig. 6.
Rap1 for	5'-AGGCGCCATGGCTTCTAGTCCAGATGATTTTGAAAC-3'	Use to clone full-length *RAP1* into pAB180.
Rap1 rev	5'-TAGTGACGTCACTGCAATTTGGCACCGCCGCGTTGGGCTGCGCGGATCATGTCTCATAACAGGTCCTTCTCAAAAAATC-3'	
Adj HO for	CATGCTCGAGGAGCTCATGTCGCCGTAATC	Fragment I
Adj HO rev	GTACACTAGTGCGCAAATTGAAAAGTCGGG	Fragment II
SpacerΔ ChrVII fragment I	CAACACCCTCCACACACCACACCAACTCATCCTACATCCGGAAAACAAGCGGCACCAATCTTCAATTGG	Use with Adj HO for and Rev. Fig 3, spacerΔ ChrVII
SpacerΔ ChrVII fragment II	TTGGTGTGGTGTGTGGAGGGTGTTGTTGTGGAGTTGGAAACTGAATTAACTGCTGTGATACAGAAC	
ChrVII HO for	CAATTTCACCTAATCTCTTCTTGGCCTTTGGACATTGCATGTTGGCCTCTCCAGCTGAAGCTTCGTACGC	Use to integrate Hocs on chromosome VII, 3kb away from SIRTA SpacerΔ
ChrVII HO rev	CCGCCTCTAACCCAATCACCGATGCCTGTGCTTTGAAGGGTATTGATTTGCGCATAGGCCACTAGTGGATCTG	
PAU11:URA3 for	CAAATTAACTTCAATCGAAGCTGGTGTCGCTGCCATCGCTGCTACTGCTTCCGCGTACTGAGAGTGCACCACGC	Use to replace *PAU11* with URA3 by one-step gene replacement on ChrVII
PAU11:URA3 rev	GATGAAAATGCTGTCCACGGTGAATTATATTTTAACACATATGGGGGGTTGCTCCTTACGCATCTGTGCGG	
BNR1 for	GTACAAGCTTGGACAATGTCGTTATCACAGTTC	Fragment I
BNR1 rev	CATGTCTAGACTCTGCCCAAGCGTTCAACTAG	Fragment II
Cdc13 BS Mut1 fragment I	CT**AAAAAAAAAAAAAAAAA**CCTTTGTTCATCGACAAGGACTCGGG	Use with BNR1 for and Rev. Fig. 7, mutation Cdc13 BS Mut1
Cdc13 BS Mut1 fragment II	CAAAGG**TTTTTTTTTTTTTTTTT**AGTTACTCCTCCAGCTCCACC	
Cdc13 BS Mut2 fragment I	GGAGGGGCCTTTGTTCATCGAC**AAAAAAAAAAAAAAAAA**GGTGGCGGTGGTGGTGGTGGAACGGCGCCCAAGTTTTAG	Use with BNR1 for and Rev. Fig. 7, mutation Cdc13 BS Mut1
Cdc13 BS Mut2 fragment II	CTAAAACTTGTGGCGCCGTTCCACCACCACCACCGCCACC**TTTTTTTTTTTTTTTTT**GTCGATGAACAAAGGCCCCTCC	

SOA1:URA3 for	CCTCGAGCAAATAGGCTACATTTGCTGCTGCACCCCTTTACAGCACAAAGTCGGTACTGAGAGTGCACCACGC	Use to replace *SOA1* with *URA3* by one-step gene replacement on ChrIX.
SOA1:URA3 rev	GCGTAGGTCCTCTACGCATTAAATAAAAGGATGCCACGCCAACAGAAAGGACCTCCTTACGCATCTGTGCGG	
ChrIX HO for	AATTTCGAGCGGTTTTTAAGATACACCATGTTTCAAGTAACCACCTTTCGCGCATAGGCCACTAGTGGATCTG	Use to integrate Hocs on chromosome IX, 3kb away from SIRTA 9L-44
ChrIX HO rev	TATGTAGTGTTATATTCACTCTGTACTCAGAGCCACAAGAAATAACCATTCGCATAGGCCACTAGTGGATCTG	
ds oligo 1	5'-GGGTTCGAATGACCGGCAGCAGCAAAATG-3'	Telomere cloning
ds oligo 2	5'-CATTTTGCTGCTGCCGGTCATTCGAACCC-3'	Telomere PCR/cloning
9L-44 mapping for	5'GTCTGGTTATTGATAGACACTGAGG-3'	Telomere PCR/cloning chr. IX
ChrV telomere-internal	5'-CTGATAATGTAACACACTTATAG-3'	Telomere PCR/cloning chr. V
M13F (-20)	5'-GTAAAACGACGGCCAG-3'	Telomere sequencing
HS TELO rev1	5'-CACGCCAAATCCTAGTAGTA-3'	Used to determine the proportion of telomere addition events in the SiRTA Stim vs. SiRTA Core. Fig. E6
Internal NPR2 rev2	5'-CTTAGTTTAGAAATTTTGGCAATG-3'	

CHAPTER V

CONCLUSIONS AND FUTURE DIRECTIONS[3]

Telomeres, nucleoprotein structures at the ends of eukaryotic chromosomes, protect chromosome ends from nucleolytic degradation and serve to distinguish natural chromosome ends from ends generated by DSBs (186). Telomeres shorten following each cell division because of incomplete replication by the DNA replication machinery, and therefore require an additional, compensatory mechanism to replenish the lost sequences. In most eukaryotic cells, the enzyme telomerase fulfills this function. Telomerase action, is however, not limited to natural chromosome ends. Very rarely, telomerase can add new (*de novo*) telomeres to ends generated by DSBs, a process that results in terminal chromosomal deletions, i.e. deletions that extend all the way to the end of the chromosome.

How this process of *de novo* telomere addition is regulated is a burgeoning field of study because terminal chromosomal deletions are associated with diseases such as cancer (293) and congenital disorders (294-296). Much of our current knowledge of how *de novo* telomere addition is regulated has been derived from studies of telomere addition at DSBs induced immediately adjacent to a short (81 bp) telomeric seed sequence (271, 276, 277, 282, 298). However, endogenous sites of *de novo* telomere addition, by their very nature, should not always be expected to be located in close proximity to DSB sites or to be homogeneous in length. It has been reported that long-range resection inhibits *de novo* telomere addition, likely because the long ssDNA generated by resection is a more

[3] This chapter relates only to the published work presented in Chapter IV. Conclusions and future directions for the Rif1 project are included within the Discussion section of Chapter II.

optimal substrate for homologous recombination. Also, as I discussed in Chapter III, the length of the telomeric seed sequence is a contributing factor to the efficiency of *de novo* telomere addition.

The goal of our study was to address the *cis*- and *trans*-acting requirements for *de novo* telomere addition at endogenous sites of *de novo* telomere addition, which we call SiRTAs (**S**ites of **R**epair-associated **T**elomere **A**ddition). We show that *de novo* telomere addition at two SiRTAs in *S. cerevisiae* requires a bipartite structure, in which Cdc13 binding to a stimulatory (Stim) sequence promotes telomere addition at a separate target (Core) sequence. At the SiRTA on chromosome V (SiRTA 5L-35), both Rap1 and Cdc13 bind to the Stim sequence. To tease apart which of these proteins stimulate telomere addition at SiRTA 5L-35, we designed "Rap1 only" sites and "Cdc13 only" sites and substituted them for the Stim sequence. These experiments revealed that Cdc13 primarily provides the stimulatory function at SiRTA 5L-35, with Rap1 playing a minor role. We did not observe Rap1 binding to the SiRTA on chromosome IX (SiRTA 9L-44) *in vitro* (Epum E; unpublished data), indicating that Rap1 is unlikely to play a stimulatory role at SiRTA 9L-44.

Because we observed a minor contribution from Rap1 to telomere addition at SiRTA 5L-35 when the Stim was replaced with two copies of the "Rap1 only" sequence, it may be prudent to explore whether the effect by Rap1 would be magnified when more Rap1 molecules are targeted to SiRTA 5L-35. In the same vein, although we did not observe Rap1 binding to SiRTA 9L-44 *in vitro*, Rap1 could, in principle, still stimulate telomere addition if targeted there in multiple copies and this possibility should be addressed in the future. As more SiRTAs are identified, the same questions (whether or not Rap1 actually stimulates telomere addition at the SiRTA, and if not, whether targeting Rap1 to the SiRTA in multiple copies stimulates telomere addition at the SiRTA) should be addressed. If the discovery is made that the effect of Rap1 at these SiRTAs increases proportionately to the number of Rap1 molecules targeted there, this finding could have evolutionary implications. Rap1 is a much more

abundant protein (~4,000 copies per haploid cell) than Cdc13 (~300 copies per cell) (309). Moreover, most or all of Cdc13 is probably telomere-bound, whereas only 10-15% of Rap1 is telomere-bound (188). Furthermore, telomere-bound Rap1 relocalizes to sites of DNA damage (211). Therefore, given Rap1's abundance and its propensity to relocalize to DNA damage sites, it would be advantageous to keep SiRTA length to a minimum to prevent *de novo* telomere addition from occurring much more frequently.

In our study, we did not address whether or not *de novo* telomere addition at SiRTA 5L-35 and SiRTA 9L-44 also requires Cdc13 binding to the Core sequences and/or sequences adjacent to the Core. We have found that Cdc13 binds to the Core sequences in SiRTA 9L-44 (Epum E; unpublished data), although we have not yet addressed whether this is also the case for the Core sequence in SiRTA 5L-35. This question can be addressed by EMSA experiments to determine whether Cdc13 binds to the SiRTA 5L-35 Core sequence *in vitro*. Future experiments should address whether or not Cdc13 binding to the Core sequences (at SiRTA 9L-44 and/or SiRTA 5L-35) is functionally relevant for *de novo* telomere addition *in vivo*. Such analysis could be impeded by the fact that TG sequences in the Core are themselves targeted for telomere addition, but may nevertheless be possible if variants of the Core sequences are designed that have similar TG contents as the WT Core sequences, but are defective in Cdc13 binding. Should the Core sequences also be able to bind Cdc13, another question that could be addressed is whether the Core and Stim sequences are functionally interchangeable. We assume that the Core serves as the target site for *de novo* telomere addition because it is encountered first as resection proceeds inwards from the break site. But if the Core sequences do indeed bind Cdc13, then theoretically, Core sequences should acquire the Stim function when substituted for the original Stim sequences. Conversely, the Stim sequences, because they contain TG sequences, should acquire the Core function when substituted for the original Core sequences.

An interesting observation that we reported in our study is that the SpacerΔ variant of SiRTA 5L-35, in which the spacer sequence separating the Stim and Core is deleted, exhibited an approximately 36-fold increase in *de novo* telomere addition compared to wild-type SiRTA 5L-35. One explanation that could account for this result is that simultaneous binding by Cdc13 to both the Stim and Core sequences is required for optimal recruitment of telomerase to the SiRTA. The N-terminal oligonucleotide/oligosaccharide binding (OB) fold of Cdc13 is involved in Cdc13 dimerization and exists as a stable dimer in solution (303). *In vitro*, the Cdc13 N-terminal OB fold does not bind to the minimal 11-mer Cdc13 consensus sequence, but binds to longer ssDNA sequences of at least 37 nucleotides (303). Based on these findings, we propose a model in which Cdc13 monomers bind to the Stim and Core sequences, with optimal Cdc13 binding (and therefore, telomerase recruitment) depending on the distance between the Core and Stim. This hypothesis opens up more interesting avenues for study. One question to address is the effect of varying the length of the spacer sequences, to determine the optimal distance between the Stim and Core sequences that supports *de novo* telomere addition. Another question to address is whether Cdc13 dimerization is required for telomere addition at both SiRTA 5L-35 and SiRTA 9L-44. Residues L84, I87, and L91 in the Cdc13 N-terminal OB fold are involved in Cdc13 dimerization; $Cdc13^{L91A}$ and $Cdc13^{L84A/I87A}$ mutations significantly disrupt Cdc13 dimerization *in vitro* and cause decreased telomere lengths *in vivo* (303). Hence, these mutants may be employed to determine whether Cdc13 dimerization promotes *de novo* telomere addition at SiRTA 5L-35 and SiRTA 9L-44. Finally, Cdc13 recruitment to the SiRTAs *in vivo* should also be analyzed by ChIP to address: whether the presence of Stim and/or Core sequences near DSBs increases Cdc13 recruitment to the break (Oza *et al.* observed Cdc13 recruitment to a DSB even in the absence of telomere-like sequences near the break (310)), the effect of varying the length of the spacer sequence

on Cdc13 recruitment, and whether the Cdc13 dimerization mutants decrease Cdc13 recruitment to the SiRTAs.

In an effort to determine whether the Stim and Core sequences at SiRTA 5L-35 were sufficient for telomere addition at an ectopic site in the genome, we moved the SpacerΔ variant of SiRTA 5L-35 (see paragraph above) to chromosome VII. Although SiRTA 5L-35 SpacerΔ was sufficient for telomere addition at its ectopic location on chromosome VII, the overall rate of GCR formation at the site on chromosome VII was lower than for the SpacerΔ at its endogenous location on chromosome V. As the spacer sequence is itself not required for telomere addition, it remains possible that additional sequences near SiRTA 5L-35 may also be involved in stimulating telomere addition at SiRTA 5L-35. On a similar note, further experiments should be aimed at elucidating whether the spacer sequences in SiRTA 9L-44 make any contributions to *de novo* telomere addition at that site.

Techniques are being developed in our lab that are aimed at identifying additional SiRTAs in *S. cerevisiae*. These techniques include bioinformatic tools to scan the yeast genome for potential SiRTAs, as well as biochemical approaches. While a bioinformatics approach is useful and should not be discounted, a potential disadvantage is that because it involves searching the yeast genome using pre-determined criteria for what constitutes a SiRTA, actual SiRTAs that do not meet the criteria may go unidentified. A biochemical approach circumvents this problem because it makes no assumptions about the properties of the SiRTAs. The lab is currently developing a CRISPR-based approach (see Chapter II) for this purpose. An advantage of using the CRISPR system is that many guide RNAs can be designed, easily integrated into a plasmid, and transformed into a single strain. This approach could allow for unprecedented coverage of the genome, as DSBs can be generated at hundreds, and potentially thousands, of locations in the genome. Following DSB cleavage, surviving colonies would

be pooled for genomic DNA extraction and whole-genome sequencing to identify sites at which *de novo* telomere addition has occurred.

The identification of more SiRTAs would allow for a more comprehensive analysis of their properties. Important questions to address would be whether most or all SiRTAs have similar bipartite structures as SiRTA 5L-35 and SiRTA 9L-44, and whether Rap1 and/or Cdc13 also stimulate telomere addition at those sites. Another potential point of interest should be whether SiRTAs show a bias in their locations within the genome. Both SiRTA 5L-35 and SiRTA 9L-44 are, of note, located within open reading frames. DNA transcription has been reported to promote homologous recombination in yeast and mouse cells (311, 312). It is tempting to speculate that the location of these SiRTAs in open reading frames may be a mechanism to limit their usage perhaps by tipping the balance toward repair by homologous recombination. I performed a preliminary experiment to test this hypothesis at SiRTA 5L-35 by placing the *NPR2* gene, in which SiRTA 5L-35 is located, under control of the inducible promoter from the *MET25* gene. I observed no change in the frequency of GCR formation at SiRTA 5L-35 when *NPR2* was placed under the control of the *MET25* promoter and cells were grown under inducible conditions (Obodo, U; unpublished results). However, this experiment may require several modifications before a conclusion can be reached on the effect of transcription on *de novo* telomere addition at the SiRTA 5L-35. Studies in yeast show that stimulation of homologous recombination by transcription requires both the donor and template regions to be transcribed (312). However, the haploid strains utilized in our assays essentially lack donor sequences with significant homology to promote homologous recombination. To address this problem, a second copy of the *NPR2* gene could be integrated on a different chromosome or introduced on a plasmid to serve as a donor for homologous recombination. The transcriptional status of both the endogenous copy of *NPR2* (located ~ 3 kb centromere-proximal to an HO cleavage site) and the ectopic copy of *NPR2* may be modified by placing

them under control of promoters of different strengths, as well as by deleting the promoters. Transcription under these different conditions may be monitored by Northern blotting, RT-PCR, or by ChIP to measure RNA polymerase II occupancy at *NPR2*. Comparisons of the frequency of *de novo* telomere addition at SiRTA 5L-35 among these strains and the WT strain (containing only the endogenous copy of *NPR2*) should reveal whether transcription inhibits *de novo* telomere addition at the SiRTA and whether the strength of transcription correlates with the frequency of *de novo* telomere addition.

The role of the DNA damage checkpoint in regulating *de novo* telomere addition has been studied using assays in which DSBs are immediately preceded by short TG sequences. Using such assays, Zhang and Durocher elucidated the role of the checkpoint kinase Mec1 in the regulation of *de novo* telomere addition at DSBs. At DSBs immediately preceded by 0 or 5 nucleotides of TG sequence, deletion of *MEC1* increases the frequency of *de novo* telomere addition, indicating that Mec1 inhibits *de novo* telomere addition in these contexts (272). However, when preceded by an 11-nt TG sequence, corresponding to the minimal sequence length for stable Cdc13 binding, a DSB becomes refractory to Mec1 inhibition; in other words, deletion of *MEC1* does not change the frequency of telomere addition in this context (272). Additionally, tethering Cdc13 adjacent to a DSB renders the break refractory to inhibition by Mec1, suggesting a role for Mec1 in regulating Cdc13 access to DSBs. Indeed, the authors found that Mec1 phosphorylates Cdc13, inhibiting its accumulation at DSBs (272). For reasons noted earlier, in the second paragraph of this chapter, the mechanism of repair of DSBs immediately preceded by TG sequences may not be faithfully representative of the mechanism of repair of a random chromosomal break. Therefore, it would be prudent to determine if SiRTAs 5L-35 and 9L-44 which may more faithfully capture repair of a random chromosomal DSB, due to their location ~ 3 kb from the DSB, are subject to the same mechanism of regulation by Mec1, as determined by Zhang and

Durocher. Our finding that the Cdc13 consensus sequence, which binds to Cdc13 more strongly than the endogenous Stim sequence in SiRTA 5L-35, increases *de novo* telomere addition by ~ 8-fold when substituted for the Stim suggests that increased occupancy by Cdc13 stimulates telomere addition more strongly in a manner completely independent of Mec1, and that endogenous SiRTA 5L-35 may be subject to regulation by Mec1. Analysis of *de novo* telomere addition frequencies at SiRTAs 5L-35 and 9L-44 in a *mec1Δ* strain should reveal whether these SiRTAs are subject to Mec1 regulation.

A more detailed understanding of the mechanisms regulating *de novo* telomere addition at endogenous SiRTAs requires the identification of unknown factors that regulate telomere addition. To this end, our laboratory is developing a transposon-based insertional mutagenesis screen to identify mutants with altered frequencies of *de novo* telomere addition at SiRTAs 5L-35 and 9L-44. Of particular interest is the identification of a nuclease required for *de novo* telomere addition (Figure 33). Telomerase uses an RNA, TLC1, as template for the synthesis of new TG telomere sequences. Alignment of the RNA template to a free 3' end generates a 5' overhang that is then used as a template for telomere synthesis by telomerase using the 3' end as a primer. (Figure 33A). Therefore, the long 3' strand generated following resection of a DSB must be cleaved, whether before or after template binding, to reveal the free 3' end to prime synthesis (Figure 33B). It remains to be determined what factor(s) regulate this process, and such factor(s) could be identified by development of a high-throughput screen, as described above, to identify mutants in which *de novo* telomere addition is affected. Given that the 3' strand is stable for up to 6 hours following a DSB (313), the nuclease involved in this process is more likely to be an endonuclease whose recruitment to SiRTAs may be coordinated with the arrival of telomerase. Alternatively, cleavage of the 3' strand may be accomplished by a highly processive exonuclease.

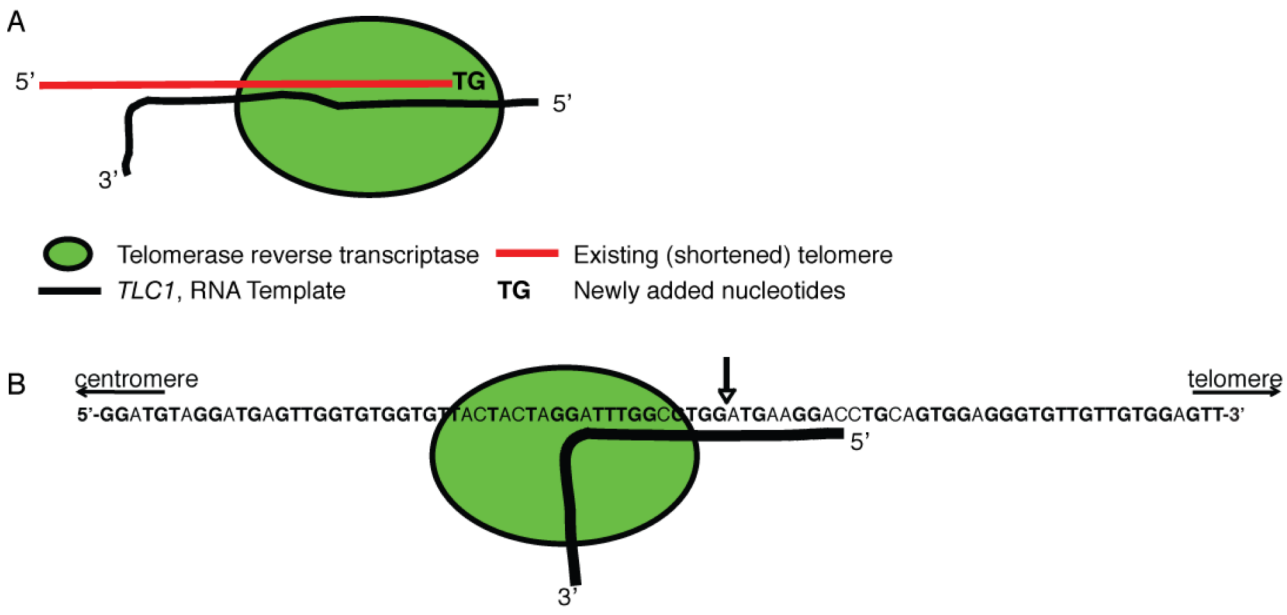

Figure 33: *De novo* telomere addition at internal sites in the genome requires cleavage to reveal the free 3' end for priming telomere synthesis.
(A) New telomere synthesis can only be initiated at an RNA template 5' overhang.
(B) Hypothetical telomere addition scenario at SiRTA 5L-35. In this scenario, 5' strand resection has occurred, generating a 3' overhang. However, before a telomere can be added at the position on the 3' strand indicated by an arrow, the sequences telomere-proximal to that site must be removed to reveal the free 3' end to prime synthesis.

SiRTAs present with some interesting questions from an evolutionary perspective. One question is: how did SiRTAs or internal telomere-like sequences, in general, arise? Perhaps, they arose by telomere fusions between chromosome pairs? In this case, breakage on either side of the fused telomeres, followed by *de novo* telomere addition, would result in one of the chromosomes internalizing the fused telomere sequences. In this model, the internalized telomere sequences would have to be whittled down in size over time. Another interesting evolutionary question is: what purpose do internal telomere-like sequences serve? In *Caenorhabditis elegans*, telomerase-negative survivors utilize internal telomere-like sequences for **A**lternative **L**engthening of **T**elomeres (ALT)-mediated telomere maintenance (314). While the phenomenon of ALT itself is not novel (telomerase-negative *S.*

cerevisiae also utilize ALT for telomere maintenance) and the genes involved in ALT have been characterized, this report is novel in that it identified two specific internal genomic regions, containing telomere-like sequences, that are utilized as templates for ALT. Although it cannot be said with certainty that internal telomere-like regions arose and were conserved for this purpose (i.e. to serve as reservoir of sorts for telomere maintenance when telomerase is inactivated), it is still an intriguing possibility to consider. Related to this "reservoir" hypothesis, another attractive possibility (though one that will be challenging to address) for why internal telomere-like sequences, like the two SiRTAs we describe here, arise and persist in the genome is that *de novo* telomere addition at these sites is a backup mechanism to ensure cell survival when other repair pathways fail. An important function such as this might be expected to be evolutionarily conserved. Therefore, one way to test this idea is to look for the conservation of SiRTAs across yeast species evolutionarily related to *S. cerevisiae*. Conservation, in other *Saccharomyces sensu stricto* species, of the SiRTAs identified in *S. cerevisiae* would be one piece of evidence that these SiRTAs serve a very important function that warrants their preservation despite their deleterious nature.

In conclusion, we have shown that endogenous **Si**tes of **R**epair-associated **T**elomere **A**ddition (SiRTAs) in *S. cerevisiae* possess a bipartite structure, wherein binding by Cdc13 at a Stim sequence stimulates *de novo* telomere addition at nearby Core sequences. In humans, *de novo* telomere additions are associated with cancer, congenital disorders, and mental retardation (265, 293-296, 315). In some of these patients, a GGGGG motif has been found near the telomere addition sites (reviewed in (265)), lending credence to the idea that the bipartite SiRTA structure that we have described may also exist in humans.

REFERENCES

1. **Iyer BV, Kenward M, Arya G.** 2011. Hierarchies in eukaryotic genome organization: Insights from polymer theory and simulations. BMC Biophys **4:**8.
2. **Benbow RM.** 1992. Chromosome structures. Sci Prog **76:**425-450.
3. **Gilbert N, Gilchrist S, Bickmore WA.** 2005. Chromatin organization in the mammalian nucleus. Int Rev Cytol **242:**283-336.
4. **Ehrenhofer-Murray AE.** 2004. Chromatin dynamics at DNA replication, transcription and repair. Eur J Biochem **271:**2335-2349.
5. **Helleday T, Eshtad S, Nik-Zainal S.** 2014. Mechanisms underlying mutational signatures in human cancers. Nat Rev Genet **15:**585-598.
6. **Caldecott KW.** 2004. Detection and repair of DNA single strand breaks, p 49-63. *In* Caldecott KW (ed), Eukaryotic DNA damage surveillance and repair. Springer Science and Business Media, NY.
7. **Caldecott KW.** 2008. Single-strand break repair and genetic disease. Nat Rev Genet **9:**619-631.
8. **Wu J, Liu LF.** 1997. Processing of topoisomerase I cleavable complexes into DNA damage by transcription. Nucleic Acids Res **25:**4181-4186.
9. **Georgakilas AG.** 2008. Processing of DNA damage clusters in human cells: current status of knowledge. Mol Biosyst **4:**30-35.
10. **Dudley DD, Chaudhuri J, Bassing CH, Alt FW.** 2005. Mechanism and control of V(D)J recombination versus class switch recombination: similarities and differences. Adv Immunol **86:**43-112.
11. **Haber JE.** 2012. Mating-type genes and MAT switching in *Saccharomyces cerevisiae*. Genetics **191:**33-64.
12. **Fleck O, Nielsen O.** 2004. DNA repair. J Cell Sci **117:**515-517.
13. **Nickoloff JA.** 2014. DNA Repair Dysregulation in Cancer: From Molecular Mechanisms to Synthetic Lethal Opportunities, p 7-28. *In* Wondrak GT (ed), Stress Response Pathways in Cancer. Springer Netherlands
14. **Wu D, Topper LM, Wilson TE.** 2008. Recruitment and dissociation of nonhomologous end joining proteins at a DNA double-strand break in *Saccharomyces cerevisiae*. Genetics **178:**1237-1249.
15. **Zhang Y, Hefferin ML, Chen L, Shim EY, Tseng HM, Kwon Y, Sung P, Lee SE, Tomkinson AE.** 2007. Role of Dnl4-Lif1 in nonhomologous end-joining repair complex assembly and suppression of homologous recombination. Nat Struct Mol Biol **14:**639-646.
16. **Rupnik A, Lowndes NF, Grenon M.** 2010. MRN and the race to the break. Chromosoma **119:**115-135.
17. **Morrow DM, Tagle DA, Shiloh Y, Collins FS, Hieter P.** 1995. TEL1, an *S. cerevisiae* homolog of the human gene mutated in ataxia telangiectasia, is functionally related to the yeast checkpoint gene MEC1. Cell **82:**831-840.
18. **Nakada D, Matsumoto K, Sugimoto K.** 2003. ATM-related Tel1 associates with double-strand breaks through an Xrs2-dependent mechanism. Genes Dev **17:**1957-1962.
19. **Kondo T, Wakayama T, Naiki T, Matsumoto K, Sugimoto K.** 2001. Recruitment of Mec1 and Ddc1 checkpoint proteins to double-strand breaks through distinct mechanisms. Science **294:**867-870.

20. **Melo JA, Cohen J, Toczyski DP.** 2001. Two checkpoint complexes are independently recruited to sites of DNA damage in vivo. Genes Dev **15:**2809-2821.
21. **Navadgi-Patil VM, Burgers PM.** 2009. The unstructured C-terminal tail of the 9-1-1 clamp subunit Ddc1 activates Mec1/ATR via two distinct mechanisms. Mol Cell **36:**743-753.
22. **Downs JA, Lowndes NF, Jackson SP.** 2000. A role for *Saccharomyces cerevisiae* histone H2A in DNA repair. Nature **408:**1001-1004.
23. **Lacoste N, Utley RT, Hunter JM, Poirier GG, Cote J.** 2002. Disruptor of telomeric silencing-1 is a chromatin-specific histone H3 methyltransferase. J Biol Chem **277:**30421-30424.
24. **Hammet A, Magill C, Heierhorst J, Jackson SP.** 2007. Rad9 BRCT domain interaction with phosphorylated H2AX regulates the G1 checkpoint in budding yeast. EMBO Rep **8:**851-857.
25. **Grenon M, Costelloe T, Jimeno S, O'Shaughnessy A, Fitzgerald J, Zgheib O, Degerth L, Lowndes NF.** 2007. Docking onto chromatin via the *Saccharomyces cerevisiae* Rad9 Tudor domain. Yeast **24:**105-119.
26. **Paciotti V, Lucchini G, Plevani P, Longhese MP.** 1998. Mec1p is essential for phosphorylation of the yeast DNA damage checkpoint protein Ddc1p, which physically interacts with Mec3p. Embo j **17:**4199-4209.
27. **Puddu F, Granata M, Di Nola L, Balestrini A, Piergiovanni G, Lazzaro F, Giannattasio M, Plevani P, Muzi-Falconi M.** 2008. Phosphorylation of the budding yeast 9-1-1 complex is required for Dpb11 function in the full activation of the UV-induced DNA damage checkpoint. Mol Cell Biol **28:**4782-4793.
28. **Wang H, Elledge SJ.** 2002. Genetic and physical interactions between DPB11 and DDC1 in the yeast DNA damage response pathway. Genetics **160:**1295-1304.
29. **Wang G, Tong X, Weng S, Zhou H.** 2012. Multiple phosphorylation of Rad9 by CDK is required for DNA damage checkpoint activation. Cell Cycle **11:**3792-3800.
30. **Schwartz MF, Duong JK, Sun Z, Morrow JS, Pradhan D, Stern DF.** 2002. Rad9 phosphorylation sites couple Rad53 to the *Saccharomyces cerevisiae* DNA damage checkpoint. Mol Cell **9:**1055-1065.
31. **Sun Z, Hsiao J, Fay DS, Stern DF.** 1998. Rad53 FHA domain associated with phosphorylated Rad9 in the DNA damage checkpoint. Science **281:**272-274.
32. **Gilbert CS, Green CM, Lowndes NF.** 2001. Budding yeast Rad9 is an ATP-dependent Rad53 activating machine. Mol Cell **8:**129-136.
33. **Abreu CM, Kumar R, Hamilton D, Dawdy AW, Creavin K, Eivers S, Finn K, Balsbaugh JL, O'Connor R, Kiely PA, Shabanowitz J, Hunt DF, Grenon M, Lowndes NF.** 2013. Site-specific phosphorylation of the DNA damage response mediator rad9 by cyclin-dependent kinases regulates activation of checkpoint kinase 1. PLoS Genet **9:**e1003310.
34. **Chen Y, Caldwell JM, Pereira E, Baker RW, Sanchez Y.** 2009. ATRMec1 phosphorylation-independent activation of Chk1 in vivo. J Biol Chem **284:**182-190.
35. **Yamamoto A, Guacci V, Koshland D.** 1996. Pds1p, an inhibitor of anaphase in budding yeast, plays a critical role in the APC and checkpoint pathway(s). J Cell Biol **133:**99-110.
36. **Agarwal R, Tang Z, Yu H, Cohen-Fix O.** 2003. Two distinct pathways for inhibiting pds1 ubiquitination in response to DNA damage. J Biol Chem **278:**45027-45033.
37. **Finn K, Lowndes NF, Grenon M.** 2012. Eukaryotic DNA damage checkpoint activation in response to double-strand breaks. Cell Mol Life Sci **69:**1447-1473.

38. **Mehta A, Haber JE.** 2014. Sources of DNA double-strand breaks and models of recombinational DNA repair. Cold Spring Harb Perspect Biol **6:**a016428.
39. **McVey M, Lee SE.** 2008. MMEJ repair of double-strand breaks (director's cut): deleted sequences and alternative endings. Trends Genet **24:**529-538.
40. **Stafa A, Donnianni RA, Timashev LA, Lam AF, Symington LS.** 2014. Template switching during break-induced replication is promoted by the Mph1 helicase in *Saccharomyces cerevisiae*. Genetics **196:**1017-1028.
41. **Sugawara N, Ira G, Haber JE.** 2000. DNA length dependence of the single-strand annealing pathway and the role of *Saccharomyces cerevisiae* RAD59 in double-strand break repair. Mol Cell Biol **20:**5300-5309.
42. **Ozenberger BA, Roeder GS.** 1991. A unique pathway of double-strand break repair operates in tandemly repeated genes. Mol Cell Biol **11:**1222-1231.
43. **Colaiacovo MP, Paques F, Haber JE.** 1999. Removal of one nonhomologous DNA end during gene conversion by a RAD1- and MSH2-independent pathway. Genetics **151:**1409-1423.
44. **Fishman-Lobell J, Haber JE.** 1992. Removal of nonhomologous DNA ends in double-strand break recombination: the role of the yeast ultraviolet repair gene RAD1. Science **258:**480-484.
45. **Sugawara N, Paques F, Colaiacovo M, Haber JE.** 1997. Role of *Saccharomyces cerevisiae* Msh2 and Msh3 repair proteins in double-strand break-induced recombination. Proc Natl Acad Sci U S A **94:**9214-9219.
46. **Li F, Dong J, Pan X, Oum JH, Boeke JD, Lee SE.** 2008. Microarray-based genetic screen defines SAW1, a gene required for Rad1/Rad10-dependent processing of recombination intermediates. Mol Cell **30:**325-335.
47. **Surtees JA, Alani E.** 2006. Mismatch repair factor MSH2-MSH3 binds and alters the conformation of branched DNA structures predicted to form during genetic recombination. J Mol Biol **360:**523-536.
48. **Flott S, Alabert C, Toh GW, Toth R, Sugawara N, Campbell DG, Haber JE, Pasero P, Rouse J.** 2007. Phosphorylation of Slx4 by Mec1 and Tel1 regulates the single-strand annealing mode of DNA repair in budding yeast. Mol Cell Biol **27:**6433-6445.
49. **Toh GW, Sugawara N, Dong J, Toth R, Lee SE, Haber JE, Rouse J.** 2010. Mec1/Tel1-dependent phosphorylation of Slx4 stimulates Rad1-Rad10-dependent cleavage of non-homologous DNA tails. DNA Repair (Amst) **9:**718-726.
50. **Fricke WM, Brill SJ.** 2003. Slx1-Slx4 is a second structure-specific endonuclease functionally redundant with Sgs1-Top3. Genes Dev **17:**1768-1778.
51. **Bi B, Rybalchenko N, Golub EI, Radding CM.** 2004. Human and yeast Rad52 proteins promote DNA strand exchange. Proc Natl Acad Sci U S A **101:**9568-9572.
52. **Kagawa W, Kurumizaka H, Ikawa S, Yokoyama S, Shibata T.** 2001. Homologous pairing promoted by the human Rad52 protein. J Biol Chem **276:**35201-35208.
53. **Sung P.** 1997. Yeast Rad55 and Rad57 proteins form a heterodimer that functions with replication protein A to promote DNA strand exchange by Rad51 recombinase. Genes Dev **11:**1111-1121.
54. **Ogawa T, Yu X, Shinohara A, Egelman EH.** 1993. Similarity of the yeast RAD51 filament to the bacterial RecA filament. Science **259:**1896-1899.
55. **Sung P.** 1994. Catalysis of ATP-dependent homologous DNA pairing and strand exchange by yeast RAD51 protein. Science **265:**1241-1243.

56. **Li X, Heyer WD.** 2009. RAD54 controls access to the invading 3'-OH end after RAD51-mediated DNA strand invasion in homologous recombination in *Saccharomyces cerevisiae*. Nucleic Acids Res **37:**638-646.
57. **Li X, Zhang XP, Solinger JA, Kiianitsa K, Yu X, Egelman EH, Heyer WD.** 2007. Rad51 and Rad54 ATPase activities are both required to modulate Rad51-dsDNA filament dynamics. Nucleic Acids Res **35:**4124-4140.
58. **Fawcett JA, Innan H.** 2011. Neutral and non-neutral evolution of duplicated genes with gene conversion. Genes (Basel) **2:**191-209.
59. **Kadyk LC, Hartwell LH.** 1992. Sister chromatids are preferred over homologs as substrates for recombinational repair in *Saccharomyces cerevisiae*. Genetics **132:**387-402.
60. **Cortes-Ledesma F, Aguilera A.** 2006. Double-strand breaks arising by replication through a nick are repaired by cohesin-dependent sister-chromatid exchange. EMBO Rep **7:**919-926.
61. **Munoz-Galvan S, Jimeno S, Rothstein R, Aguilera A.** 2013. Histone H3K56 acetylation, Rad52, and non-DNA repair factors control double-strand break repair choice with the sister chromatid. PLoS Genet **9:**e1003237.
62. **Cejka P, Plank JL, Bachrati CZ, Hickson ID, Kowalczykowski SC.** 2010. Rmi1 stimulates decatenation of double Holliday junctions during dissolution by Sgs1-Top3. Nat Struct Mol Biol **17:**1377-1382.
63. **Ashton TM, Mankouri HW, Heidenblut A, McHugh PJ, Hickson ID.** 2011. Pathways for Holliday junction processing during homologous recombination in *Saccharomyces cerevisiae*. Mol Cell Biol **31:**1921-1933.
64. **Matos J, West SC.** 2014. Holliday junction resolution: regulation in space and time. DNA Repair (Amst) **19:**176-181.
65. **Ira G, Malkova A, Liberi G, Foiani M, Haber JE.** 2003. Srs2 and Sgs1-Top3 suppress crossovers during double-strand break repair in yeast. Cell **115:**401-411.
66. **Esposito MS.** 1978. Evidence that spontaneous mitotic recombination occurs at the two-strand stage. Proc Natl Acad Sci U S A **75:**4436-4440.
67. **Stark JM, Jasin M.** 2003. Extensive loss of heterozygosity is suppressed during homologous repair of chromosomal breaks. Mol Cell Biol **23:**733-743.
68. **Virgin JB, Bailey JP, Hasteh F, Neville J, Cole A, Tromp G.** 2001. Crossing over is rarely associated with mitotic intragenic recombination in *Schizosaccharomyces pombe*. Genetics **157:**63-77.
69. **Lydeard JR, Lipkin-Moore Z, Sheu YJ, Stillman B, Burgers PM, Haber JE.** 2010. Break-induced replication requires all essential DNA replication factors except those specific for pre-RC assembly. Genes Dev **24:**1133-1144.
70. **Donnianni RA, Symington LS.** 2013. Break-induced replication occurs by conservative DNA synthesis. Proc Natl Acad Sci U S A **110:**13475-13480.
71. **Saini N, Ramakrishnan S, Elango R, Ayyar S, Zhang Y, Deem A, Ira G, Haber JE, Lobachev KS, Malkova A.** 2013. Migrating bubble during break-induced replication drives conservative DNA synthesis. Nature **502:**389-392.
72. **Boulton SJ, Jackson SP.** 1996. Identification of a *Saccharomyces cerevisiae* Ku80 homologue: roles in DNA double strand break rejoining and in telomeric maintenance. Nucleic Acids Res **24:**4639-4648.
73. **Milne GT, Jin S, Shannon KB, Weaver DT.** 1996. Mutations in two Ku homologs define a DNA end-joining repair pathway in *Saccharomyces cerevisiae*. Mol Cell Biol **16:**4189-4198.

74. **Porter SE, Greenwell PW, Ritchie KB, Petes TD.** 1996. The DNA-binding protein Hdf1p (a putative Ku homologue) is required for maintaining normal telomere length in *Saccharomyces cerevisiae*. Nucleic Acids Res **24:**582-585.
75. **Boulton SJ, Jackson SP.** 1998. Components of the Ku-dependent non-homologous end-joining pathway are involved in telomeric length maintenance and telomeric silencing. Embo j **17:**1819-1828.
76. **Feldmann H, Winnacker EL.** 1993. A putative homologue of the human autoantigen Ku from *Saccharomyces cerevisiae*. J Biol Chem **268:**12895-12900.
77. **Taccioli GE, Gottlieb TM, Blunt T, Priestley A, Demengeot J, Mizuta R, Lehmann AR, Alt FW, Jackson SP, Jeggo PA.** 1994. Ku80: product of the XRCC5 gene and its role in DNA repair and V(D)J recombination. Science **265:**1442-1445.
78. **Smider V, Rathmell WK, Lieber MR, Chu G.** 1994. Restoration of X-ray resistance and V(D)J recombination in mutant cells by Ku cDNA. Science **266:**288-291.
79. **Siede W, Friedl AA, Dianova I, Eckardt-Schupp F, Friedberg EC.** 1996. The *Saccharomyces cerevisiae* Ku autoantigen homologue affects radiosensitivity only in the absence of homologous recombination. Genetics **142:**91-102.
80. **Clerici M, Mantiero D, Guerini I, Lucchini G, Longhese MP.** 2008. The Yku70-Yku80 complex contributes to regulate double-strand break processing and checkpoint activation during the cell cycle. EMBO Rep **9:**810-818.
81. **Palmbos PL, Wu D, Daley JM, Wilson TE.** 2008. Recruitment of *Saccharomyces cerevisiae* Dnl4-Lif1 complex to a double-strand break requires interactions with Yku80 and the Xrs2 FHA domain. Genetics **180:**1809-1819.
82. **Chen L, Trujillo K, Ramos W, Sung P, Tomkinson AE.** 2001. Promotion of Dnl4-catalyzed DNA end-joining by the Rad50/Mre11/Xrs2 and Hdf1/Hdf2 complexes. Mol Cell **8:**1105-1115.
83. **Roy R, Meier B, McAinsh AD, Feldmann HM, Jackson SP.** 2004. Separation-of-function mutants of yeast Ku80 reveal a Yku80p-Sir4p interaction involved in telomeric silencing. J Biol Chem **279:**86-94.
84. **Stellwagen AE, Haimberger ZW, Veatch JR, Gottschling DE.** 2003. Ku interacts with telomerase RNA to promote telomere addition at native and broken chromosome ends. Genes Dev **17:**2384-2395.
85. **Ribes-Zamora A, Mihalek I, Lichtarge O, Bertuch AA.** 2007. Distinct faces of the Ku heterodimer mediate DNA repair and telomeric functions. Nat Struct Mol Biol **14:**301-307.
86. **Moore JK, Haber JE.** 1996. Cell cycle and genetic requirements of two pathways of nonhomologous end-joining repair of double-strand breaks in *Saccharomyces cerevisiae*. Mol Cell Biol **16:**2164-2173.
87. **Furuse M, Nagase Y, Tsubouchi H, Murakami-Murofushi K, Shibata T, Ohta K.** 1998. Distinct roles of two separable in vitro activities of yeast Mre11 in mitotic and meiotic recombination. Embo j **17:**6412-6425.
88. **Moreau S, Ferguson JR, Symington LS.** 1999. The nuclease activity of Mre11 is required for meiosis but not for mating type switching, end joining, or telomere maintenance. Mol Cell Biol **19:**556-566.
89. **Lewis LK, Storici F, Van Komen S, Calero S, Sung P, Resnick MA.** 2004. Role of the nuclease activity of *Saccharomyces cerevisiae* Mre11 in repair of DNA double-strand breaks in mitotic cells. Genetics **166:**1701-1713.

90. **Dudasova Z, Dudas A, Chovanec M.** 2004. Non-homologous end-joining factors of *Saccharomyces cerevisiae*. FEMS Microbiol Rev **28:**581-601.
91. **Hopfner KP, Craig L, Moncalian G, Zinkel RA, Usui T, Owen BA, Karcher A, Henderson B, Bodmer JL, McMurray CT, Carney JP, Petrini JH, Tainer JA.** 2002. The Rad50 zinc-hook is a structure joining Mre11 complexes in DNA recombination and repair. Nature **418:**562-566.
92. **Bressan DA, Baxter BK, Petrini JH.** 1999. The Mre11-Rad50-Xrs2 protein complex facilitates homologous recombination-based double-strand break repair in *Saccharomyces cerevisiae*. Mol Cell Biol **19:**7681-7687.
93. **Palmbos PL, Daley JM, Wilson TE.** 2005. Mutations of the Yku80 C terminus and Xrs2 FHA domain specifically block yeast nonhomologous end joining. Mol Cell Biol **25:**10782-10790.
94. **Yang H, Matsumoto Y, Trujillo KM, Lees-Miller SP, Osley MA, Tomkinson AE.** 2015. Role of the yeast DNA repair protein Nej1 in end processing during the repair of DNA double strand breaks by non-homologous end joining. DNA Repair (Amst) **31:**1-10.
95. **Daley JM, Laan RL, Suresh A, Wilson TE.** 2005. DNA joint dependence of pol X family polymerase action in nonhomologous end joining. J Biol Chem **280:**29030-29037.
96. **Wilson TE, Lieber MR.** 1999. Efficient processing of DNA ends during yeast nonhomologous end joining. Evidence for a DNA polymerase beta (Pol4)-dependent pathway. J Biol Chem **274:**23599-23609.
97. **Wu X, Wilson TE, Lieber MR.** 1999. A role for FEN-1 in nonhomologous DNA end joining: the order of strand annealing and nucleolytic processing events. Proc Natl Acad Sci U S A **96:**1303-1308.
98. **Tseng SF, Gabriel A, Teng SC.** 2008. Proofreading activity of DNA polymerase Pol2 mediates 3'-end processing during nonhomologous end joining in yeast. PLoS Genet **4:**e1000060.
99. **Frank-Vaillant M, Marcand S.** 2001. NHEJ regulation by mating type is exercised through a novel protein, Lif2p, essential to the ligase IV pathway. Genes Dev **15:**3005-3012.
100. **Kegel A, Sjostrand JO, Astrom SU.** 2001. Nej1p, a cell type-specific regulator of nonhomologous end joining in yeast. Curr Biol **11:**1611-1617.
101. **Chen X, Tomkinson AE.** 2011. Yeast Nej1 is a key participant in the initial end binding and final ligation steps of nonhomologous end joining. J Biol Chem **286:**4931-4940.
102. **Ma JL, Kim EM, Haber JE, Lee SE.** 2003. Yeast Mre11 and Rad1 proteins define a Ku-independent mechanism to repair double-strand breaks lacking overlapping end sequences. Mol Cell Biol **23:**8820-8828.
103. **Lee K, Lee SE.** 2007. *Saccharomyces cerevisiae* Sae2- and Tel1-dependent single-strand DNA formation at DNA break promotes microhomology-mediated end joining. Genetics **176:**2003-2014.
104. **Villarreal DD, Lee K, Deem A, Shim EY, Malkova A, Lee SE.** 2012. Microhomology directs diverse DNA break repair pathways and chromosomal translocations. PLoS Genet **8:**e1003026.
105. **Simsek D, Brunet E, Wong SY, Katyal S, Gao Y, McKinnon PJ, Lou J, Zhang L, Li J, Rebar EJ, Gregory PD, Holmes MC, Jasin M.** 2011. DNA ligase III promotes alternative nonhomologous end-joining during chromosomal translocation formation. PLoS Genet **7:**e1002080.

106. **Truong LN, Li Y, Shi LZ, Hwang PY, He J, Wang H, Razavian N, Berns MW, Wu X.** 2013. Microhomology-mediated End Joining and Homologous Recombination share the initial end resection step to repair DNA double-strand breaks in mammalian cells. Proc Natl Acad Sci U S A **110:**7720-7725.
107. **de Koning AP, Gu W, Castoe TA, Batzer MA, Pollock DD.** 2011. Repetitive elements may comprise over two-thirds of the human genome. PLoS Genet **7:**e1002384.
108. **Kuhn RM, Karolchik D, Zweig AS, Trumbower H, Thomas DJ, Thakkapallayil A, Sugnet CW, Stanke M, Smith KE, Siepel A, Rosenbloom KR, Rhead B, Raney BJ, Pohl A, Pedersen JS, Hsu F, Hinrichs AS, Harte RA, Diekhans M, Clawson H, Bejerano G, Barber GP, Baertsch R, Haussler D, Kent WJ.** 2007. The UCSC genome browser database: update 2007. Nucleic Acids Res **35:**D668-673.
109. **Bishop AJ, Schiestl RH.** 2000. Homologous recombination as a mechanism for genome rearrangements: environmental and genetic effects. Hum Mol Genet **9:**2427-2334.
110. **Cox MM.** 2011. Molecular Biology: Principles and Practice. Palgrave Macmillan, United Kingdom.
111. **Takashima Y, Sakuraba M, Koizumi T, Sakamoto H, Hayashi M, Honma M.** 2009. Dependence of DNA double strand break repair pathways on cell cycle phase in human lymphoblastoid cells. Environ Mol Mutagen **50:**815-822.
112. **Liao S, Tammaro M, Yan H.** 2016. The structure of ends determines the pathway choice and Mre11 nuclease dependency of DNA double-strand break repair. Nucleic Acids Res doi:10.1093/nar/gkw274.
113. **Aylon Y, Liefshitz B, Kupiec M.** 2004. The CDK regulates repair of double-strand breaks by homologous recombination during the cell cycle. Embo j **23:**4868-4875.
114. **Ira G, Pellicioli A, Balijja A, Wang X, Fiorani S, Carotenuto W, Liberi G, Bressan D, Wan L, Hollingsworth NM, Haber JE, Foiani M.** 2004. DNA end resection, homologous recombination and DNA damage checkpoint activation require CDK1. Nature **431:**1011-1017.
115. **Cannavo E, Cejka P.** 2014. Sae2 promotes dsDNA endonuclease activity within Mre11-Rad50-Xrs2 to resect DNA breaks. Nature **514:**122-125.
116. **Garcia V, Phelps SE, Gray S, Neale MJ.** 2011. Bidirectional resection of DNA double-strand breaks by Mre11 and Exo1. Nature **479:**241-244.
117. **Mimitou EP, Symington LS.** 2008. Sae2, Exo1 and Sgs1 collaborate in DNA double-strand break processing. Nature **455:**770-774.
118. **Zhu Z, Chung WH, Shim EY, Lee SE, Ira G.** 2008. Sgs1 helicase and two nucleases Dna2 and Exo1 resect DNA double-strand break ends. Cell **134:**981-994.
119. **Fu Q, Chow J, Bernstein KA, Makharashvili N, Arora S, Lee CF, Person MD, Rothstein R, Paull TT.** 2014. Phosphorylation-regulated transitions in an oligomeric state control the activity of the Sae2 DNA repair enzyme. Mol Cell Biol **34:**778-793.
120. **Huertas P, Cortes-Ledesma F, Sartori AA, Aguilera A, Jackson SP.** 2008. CDK targets Sae2 to control DNA-end resection and homologous recombination. Nature **455:**689-692.
121. **Bonetti D, Clerici M, Anbalagan S, Martina M, Lucchini G, Longhese MP.** 2010. Shelterin-like proteins and Yku inhibit nucleolytic processing of *Saccharomyces cerevisiae* telomeres. PLoS Genet **6:**e1000966.
122. **Shim EY, Chung WH, Nicolette ML, Zhang Y, Davis M, Zhu Z, Paull TT, Ira G, Lee SE.** 2010. *Saccharomyces cerevisiae* Mre11/Rad50/Xrs2 and Ku proteins regulate association of Exo1 and Dna2 with DNA breaks. Embo j **29:**3370-3380.

123. **Mimitou EP, Symington LS.** 2010. Ku prevents Exo1 and Sgs1-dependent resection of DNA ends in the absence of a functional MRX complex or Sae2. Embo j **29:**3358-3369.
124. **Llorente B, Symington LS.** 2004. The Mre11 nuclease is not required for 5' to 3' resection at multiple HO-induced double-strand breaks. Mol Cell Biol **24:**9682-9694.
125. **Ferrari M, Dibitetto D, De Gregorio G, Eapen VV, Rawal CC, Lazzaro F, Tsabar M, Marini F, Haber JE, Pellicioli A.** 2015. Functional interplay between the 53BP1-ortholog Rad9 and the Mre11 complex regulates resection, end-tethering and repair of a double-strand break. PLoS Genet **11:**e1004928.
126. **Lazzaro F, Sapountzi V, Granata M, Pellicioli A, Vaze M, Haber JE, Plevani P, Lydall D, Muzi-Falconi M.** 2008. Histone methyltransferase Dot1 and Rad9 inhibit single-stranded DNA accumulation at DSBs and uncapped telomeres. Embo j **27:**1502-1512.
127. **Hardy CF, Sussel L, Shore D.** 1992. A RAP1-interacting protein involved in transcriptional silencing and telomere length regulation. Genes Dev **6:**801-814.
128. **Silverman J, Takai H, Buonomo SB, Eisenhaber F, de Lange T.** 2004. Human Rif1, ortholog of a yeast telomeric protein, is regulated by ATM and 53BP1 and functions in the S-phase checkpoint. Genes Dev **18:**2108-2119.
129. **Dimitrova N, Chen YC, Spector DL, de Lange T.** 2008. 53BP1 promotes non-homologous end joining of telomeres by increasing chromatin mobility. Nature **456:**524-528.
130. **Moynahan ME, Cui TY, Jasin M.** 2001. Homology-directed dna repair, mitomycin-c resistance, and chromosome stability is restored with correction of a Brca1 mutation. Cancer Res **61:**4842-4850.
131. **Ward IM, Reina-San-Martin B, Olaru A, Minn K, Tamada K, Lau JS, Cascalho M, Chen L, Nussenzweig A, Livak F, Nussenzweig MC, Chen J.** 2004. 53BP1 is required for class switch recombination. J Cell Biol **165:**459-464.
132. **Zhang J, Willers H, Feng Z, Ghosh JC, Kim S, Weaver DT, Chung JH, Powell SN, Xia F.** 2004. Chk2 phosphorylation of BRCA1 regulates DNA double-strand break repair. Mol Cell Biol **24:**708-718.
133. **Chapman JR, Sossick AJ, Boulton SJ, Jackson SP.** 2012. BRCA1-associated exclusion of 53BP1 from DNA damage sites underlies temporal control of DNA repair. J Cell Sci **125:**3529-3534.
134. **Bunting SF, Callen E, Wong N, Chen HT, Polato F, Gunn A, Bothmer A, Feldhahn N, Fernandez-Capetillo O, Cao L, Xu X, Deng CX, Finkel T, Nussenzweig M, Stark JM, Nussenzweig A.** 2010. 53BP1 inhibits homologous recombination in Brca1-deficient cells by blocking resection of DNA breaks. Cell **141:**243-254.
135. **Bouwman P, Aly A, Escandell JM, Pieterse M, Bartkova J, van der Gulden H, Hiddingh S, Thanasoula M, Kulkarni A, Yang Q, Haffty BG, Tommiska J, Blomqvist C, Drapkin R, Adams DJ, Nevanlinna H, Bartek J, Tarsounas M, Ganesan S, Jonkers J.** 2010. 53BP1 loss rescues BRCA1 deficiency and is associated with triple-negative and BRCA-mutated breast cancers. Nat Struct Mol Biol **17:**688-695.
136. **Bothmer A, Robbiani DF, Di Virgilio M, Bunting SF, Klein IA, Feldhahn N, Barlow J, Chen HT, Bosque D, Callen E, Nussenzweig A, Nussenzweig MC.** 2011. Regulation of DNA end joining, resection, and immunoglobulin class switch recombination by 53BP1. Mol Cell **42:**319-329.
137. **Chapman JR, Barral P, Vannier JB, Borel V, Steger M, Tomas-Loba A, Sartori AA, Adams IR, Batista FD, Boulton SJ.** 2013. RIF1 is essential for 53BP1-dependent

nonhomologous end joining and suppression of DNA double-strand break resection. Mol Cell **49:**858-871.
138. **Di Virgilio M, Callen E, Yamane A, Zhang W, Jankovic M, Gitlin AD, Feldhahn N, Resch W, Oliveira TY, Chait BT, Nussenzweig A, Casellas R, Robbiani DF, Nussenzweig MC.** 2013. Rif1 prevents resection of DNA breaks and promotes immunoglobulin class switching. Science **339:**711-715.
139. **Escribano-Diaz C, Orthwein A, Fradet-Turcotte A, Xing M, Young JT, Tkac J, Cook MA, Rosebrock AP, Munro M, Canny MD, Xu D, Durocher D.** 2013. A cell cycle-dependent regulatory circuit composed of 53BP1-RIF1 and BRCA1-CtIP controls DNA repair pathway choice. Mol Cell **49:**872-883.
140. **Feng L, Fong KW, Wang J, Wang W, Chen J.** 2013. RIF1 counteracts BRCA1-mediated end resection during DNA repair. J Biol Chem **288:**11135-11143.
141. **Zimmermann M, Lottersberger F, Buonomo SB, Sfeir A, de Lange T.** 2013. 53BP1 regulates DSB repair using Rif1 to control 5' end resection. Science **339:**700-704.
142. **Martina M, Bonetti D, Villa M, Lucchini G, Longhese MP.** 2014. *Saccharomyces cerevisiae* Rif1 cooperates with MRX-Sae2 in promoting DNA-end resection. EMBO Rep **15:**695-704.
143. **Cornacchia D, Dileep V, Quivy JP, Foti R, Tili F, Santarella-Mellwig R, Antony C, Almouzni G, Gilbert DM, Buonomo SB.** 2012. Mouse Rif1 is a key regulator of the replication-timing programme in mammalian cells. Embo j **31:**3678-3690.
144. **Peace JM, Ter-Zakarian A, Aparicio OM.** 2014. Rif1 regulates initiation timing of late replication origins throughout the *S. cerevisiae* genome. PLoS One **9:**e98501.
145. **Yamazaki S, Ishii A, Kanoh Y, Oda M, Nishito Y, Masai H.** 2012. Rif1 regulates the replication timing domains on the human genome. Embo j **31:**3667-3677.
146. **Dave A, Cooley C, Garg M, Bianchi A.** 2014. Protein phosphatase 1 recruitment by Rif1 regulates DNA replication origin firing by counteracting DDK activity. Cell Rep **7:**53-61.
147. **Hiraga S, Alvino GM, Chang F, Lian HY, Sridhar A, Kubota T, Brewer BJ, Weinreich M, Raghuraman MK, Donaldson AD.** 2014. Rif1 controls DNA replication by directing Protein Phosphatase 1 to reverse Cdc7-mediated phosphorylation of the MCM complex. Genes Dev **28:**372-383.
148. **Mattarocci S, Shyian M, Lemmens L, Damay P, Altintas DM, Shi T, Bartholomew CR, Thoma NH, Hardy CF, Shore D.** 2014. Rif1 controls DNA replication timing in yeast through the PP1 phosphatase Glc7. Cell Rep **7:**62-69.
149. **Mattarocci S, Hafner L, Lezaja A, Shyian M, Shore D.** 2016. Rif1: A Conserved Regulator of DNA Replication and Repair Hijacked by Telomeres in Yeasts. Front Genet **7:**45.
150. **Bennett CB, Lewis AL, Baldwin KK, Resnick MA.** 1993. Lethality induced by a single site-specific double-strand break in a dispensable yeast plasmid. Proc Natl Acad Sci U S A **90:**5613-5617.
151. **Chen JM, Cooper DN, Ferec C, Kehrer-Sawatzki H, Patrinos GP.** 2010. Genomic rearrangements in inherited disease and cancer. Semin Cancer Biol **20:**222-233.
152. **Betermier M, Bertrand P, Lopez BS.** 2014. Is non-homologous end-joining really an inherently error-prone process? PLoS Genet **10:**e1004086.
153. **Bahmed K, Nitiss KC, Nitiss JL.** 2010. Yeast Tdp1 regulates the fidelity of nonhomologous end joining. Proc Natl Acad Sci U S A **107:**4057-4062.
154. **Bahmed K, Seth A, Nitiss KC, Nitiss JL.** 2011. End-processing during non-homologous end-joining: a role for exonuclease 1. Nucleic Acids Res **39:**970-978.

155. **Liang Z, Sunder S, Nallasivam S, Wilson TE.** 2016. Overhang polarity of chromosomal double-strand breaks impacts kinetics and fidelity of yeast non-homologous end joining. Nucleic Acids Res **44:**2769-2781.
156. **Granata M, Panigada D, Galati E, Lazzaro F, Pellicioli A, Plevani P, Muzi-Falconi M.** 2013. To trim or not to trim: progression and control of DSB end resection. Cell Cycle **12:**1848-1860.
157. **Hayano M, Kanoh Y, Matsumoto S, Renard-Guillet C, Shirahige K, Masai H.** 2012. Rif1 is a global regulator of timing of replication origin firing in fission yeast. Genes Dev **26:**137-150.
158. **Park S, Patterson EE, Cobb J, Audhya A, Gartenberg MR, Fox CA.** 2011. Palmitoylation controls the dynamics of budding-yeast heterochromatin via the telomere-binding protein Rif1. Proc Natl Acad Sci U S A **108:**14572-14577.
159. **Foti R, Gnan S, Cornacchia D, Dileep V, Bulut-Karslioglu A, Diehl S, Buness A, Klein FA, Huber W, Johnstone E, Loos R, Bertone P, Gilbert DM, Manke T, Jenuwein T, Buonomo SC.** 2016. Nuclear Architecture Organized by Rif1 Underpins the Replication-Timing Program. Mol Cell **61:**260-273.
160. **DiCarlo JE, Norville JE, Mali P, Rios X, Aach J, Church GM.** 2013. Genome engineering in *Saccharomyces cerevisiae* using CRISPR-Cas systems. Nucleic Acids Res **41:**4336-4343.
161. **Decottignies A.** 2007. Microhomology-mediated end joining in fission yeast is repressed by pku70 and relies on genes involved in homologous recombination. Genetics **176:**1403-1415.
162. **Paques F, Haber JE.** 1997. Two pathways for removal of nonhomologous DNA ends during double-strand break repair in *Saccharomyces cerevisiae*. Mol Cell Biol **17:**6765-6771.
163. **Carter SD, Vigasova D, Chen J, Chovanec M, Astrom SU.** 2009. Nej1 recruits the Srs2 helicase to DNA double-strand breaks and supports repair by a single-strand annealing-like mechanism. Proc Natl Acad Sci U S A **106:**12037-12042.
164. **Wotton D, Shore D.** 1997. A novel Rap1p-interacting factor, Rif2p, cooperates with Rif1p to regulate telomere length in *Saccharomyces cerevisiae*. Genes Dev **11:**748-760.
165. **Shi T, Bunker RD, Mattarocci S, Ribeyre C, Faty M, Gut H, Scrima A, Rass U, Rubin SM, Shore D, Thoma NH.** 2013. Rif1 and Rif2 shape telomere function and architecture through multivalent Rap1 interactions. Cell **153:**1340-1353.
166. **Pannunzio NR, Li S, Watanabe G, Lieber MR.** 2014. Non-homologous end joining often uses microhomology: implications for alternative end joining. DNA Repair (Amst) **17:**74-80.
167. **Boulton SJ, Jackson SP.** 1996. *Saccharomyces cerevisiae* Ku70 potentiates illegitimate DNA double-strand break repair and serves as a barrier to error-prone DNA repair pathways. Embo j **15:**5093-5103.
168. **Ruiz JF, Pardo B, Sastre-Moreno G, Aguilera A, Blanco L.** 2013. Yeast pol4 promotes tel1-regulated chromosomal translocations. PLoS Genet **9:**e1003656.
169. **Muller HJ.** 1938. The remaking of chromosomes. Collecting Net **13:**181-198.
170. **McClintock B.** 1931. Cytological observations of deficiencies involving known genes, translocations and an inversion in Zea mays. Missouri Agricultural Experiment Research Station Research Bulletin **163:**4-30.
171. **McClintock B.** 1932. A Correlation of Ring-Shaped Chromosomes with Variegation in Zea Mays. Proc Natl Acad Sci U S A **18:**677-681.
172. **McClintock B.** 1939. The behavior in successive nuclear divisions of a chromosome broken at meiosis. Genetics **25:**405-416.

173. **Olovnikov AM.** 1971. [Principle of marginotomy in template synthesis of polynucleotides]. Dokl Akad Nauk SSSR **201:**1496-1499.
174. **Watson JD.** 1972. Origin of concatemeric T7 DNA. Nat New Biol **239:**197-201.
175. **Soudet J, Jolivet P, Teixeira MT.** 2014. Elucidation of the DNA end-replication problem in *Saccharomyces cerevisiae*. Mol Cell **53:**954-964.
176. **Osterhage JL, Friedman KL.** 2009. Chromosome end maintenance by telomerase. J Biol Chem **284:**16061-16065.
177. **Wellinger RJ.** 2014. In the end, what's the problem? Mol Cell **53:**855-856.
178. **Blackburn EH, Gall JG.** 1978. A tandemly repeated sequence at the termini of the extrachromosomal ribosomal RNA genes in Tetrahymena. J Mol Biol **120:**33-53.
179. **Orias E.** 1998. Mapping the germ-line and somatic genomes of a ciliated protozoan, Tetrahymena thermophila. Genome Res **8:**91-99.
180. **Blackburn E.** Appendix: A personal Account of the Discovery of Telomerase, Telomeres, 2 ed. Cold Spring Harbor Laboratories., Cold Spring Harbor, NY.
181. **Greider CW, Blackburn EH.** 1985. Identification of a specific telomere terminal transferase activity in Tetrahymena extracts. Cell **43:**405-413.
182. **Shampay J, Szostak JW, Blackburn EH.** 1984. DNA sequences of telomeres maintained in yeast. Nature **310:**154-157.
183. **Greider CW, Blackburn EH.** 1987. The telomere terminal transferase of Tetrahymena is a ribonucleoprotein enzyme with two kinds of primer specificity. Cell **51:**887-898.
184. **Greider CW, Blackburn EH.** 1989. A telomeric sequence in the RNA of Tetrahymena telomerase required for telomere repeat synthesis. Nature **337:**331-337.
185. **Yu GL, Bradley JD, Attardi LD, Blackburn EH.** 1990. In vivo alteration of telomere sequences and senescence caused by mutated Tetrahymena telomerase RNAs. Nature **344:**126-132.
186. **Blackburn EH.** 1991. Structure and function of telomeres. Nature **350:**569-573.
187. **Gottschling DE, Aparicio OM, Billington BL, Zakian VA.** 1990. Position effect at *S. cerevisiae* telomeres: reversible repression of Pol II transcription. Cell **63:**751-762.
188. **Wellinger RJ, Zakian VA.** 2012. Everything you ever wanted to know about *Saccharomyces cerevisiae* telomeres: beginning to end. Genetics **191:**1073-1105.
189. **Shore D, Nasmyth K.** 1987. Purification and cloning of a DNA binding protein from yeast that binds to both silencer and activator elements. Cell **51:**721-732.
190. **Berman J, Tachibana CY, Tye BK.** 1986. Identification of a telomere-binding activity from yeast. Proc Natl Acad Sci U S A **83:**3713-3717.
191. **Lieb JD, Liu X, Botstein D, Brown PO.** 2001. Promoter-specific binding of Rap1 revealed by genome-wide maps of protein-DNA association. Nat Genet **28:**327-334.
192. **Rhee HS, Pugh BF.** 2011. Comprehensive genome-wide protein-DNA interactions detected at single-nucleotide resolution. Cell **147:**1408-1419.
193. **Gotta M, Laroche T, Formenton A, Maillet L, Scherthan H, Gasser SM.** 1996. The clustering of telomeres and colocalization with Rap1, Sir3, and Sir4 proteins in wild-type *Saccharomyces cerevisiae*. J Cell Biol **134:**1349-1363.
194. **Klein F, Laroche T, Cardenas ME, Hofmann JF, Schweizer D, Gasser SM.** 1992. Localization of RAP1 and topoisomerase II in nuclei and meiotic chromosomes of yeast. J Cell Biol **117:**935-948.

195. **Conrad MN, Wright JH, Wolf AJ, Zakian VA.** 1990. RAP1 protein interacts with yeast telomeres in vivo: overproduction alters telomere structure and decreases chromosome stability. Cell **63:**739-750.
196. **Vignais ML, Huet J, Buhler JM, Sentenac A.** 1990. Contacts between the factor TUF and RPG sequences. J Biol Chem **265:**14669-14674.
197. **Buchman AR, Lue NF, Kornberg RD.** 1988. Connections between transcriptional activators, silencers, and telomeres as revealed by functional analysis of a yeast DNA-binding protein. Mol Cell Biol **8:**5086-5099.
198. **Del Vescovo V, De Sanctis V, Bianchi A, Shore D, Di Mauro E, Negri R.** 2004. Distinct DNA elements contribute to Rap1p affinity for its binding sites. J Mol Biol **338:**877-893.
199. **Graham IR, Haw RA, Spink KG, Halden KA, Chambers A.** 1999. In vivo analysis of functional regions within yeast Rap1p. Mol Cell Biol **19:**7481-7490.
200. **Moretti P, Freeman K, Coodly L, Shore D.** 1994. Evidence that a complex of SIR proteins interacts with the silencer and telomere-binding protein RAP1. Genes Dev **8:**2257-2269.
201. **Luo K, Vega-Palas MA, Grunstein M.** 2002. Rap1-Sir4 binding independent of other Sir, yKu, or histone interactions initiates the assembly of telomeric heterochromatin in yeast. Genes Dev **16:**1528-1539.
202. **Marcand S, Pardo B, Gratias A, Cahun S, Callebaut I.** 2008. Multiple pathways inhibit NHEJ at telomeres. Genes Dev **22:**1153-1158.
203. **Pardo B, Marcand S.** 2005. Rap1 prevents telomere fusions by nonhomologous end joining. Embo j **24:**3117-3127.
204. **Anbalagan S, Bonetti D, Lucchini G, Longhese MP.** 2011. Rif1 supports the function of the CST complex in yeast telomere capping. PLoS Genet **7:**e1002024.
205. **Levy DL, Blackburn EH.** 2004. Counting of Rif1p and Rif2p on *Saccharomyces cerevisiae* telomeres regulates telomere length. Mol Cell Biol **24:**10857-10867.
206. **Marcand S, Gilson E, Shore D.** 1997. A protein-counting mechanism for telomere length regulation in yeast. Science **275:**986-990.
207. **Hass EP, Zappulla DC.** 2015. The Ku subunit of telomerase binds Sir4 to recruit telomerase to lengthen telomeres in *S. cerevisiae*. Elife **4**.
208. **Hirano Y, Fukunaga K, Sugimoto K.** 2009. Rif1 and rif2 inhibit localization of tel1 to DNA ends. Mol Cell **33:**312-322.
209. **Ritchie KB, Petes TD.** 2000. The Mre11p/Rad50p/Xrs2p complex and the Tel1p function in a single pathway for telomere maintenance in yeast. Genetics **155:**475-479.
210. **Goudsouzian LK, Tuzon CT, Zakian VA.** 2006. *S. cerevisiae* Tel1p and Mre11p are required for normal levels of Est1p and Est2p telomere association. Mol Cell **24:**603-610.
211. **Martin SG, Laroche T, Suka N, Grunstein M, Gasser SM.** 1999. Relocalization of telomeric Ku and SIR proteins in response to DNA strand breaks in yeast. Cell **97:**621-633.
212. **Mishra K, Shore D.** 1999. Yeast Ku protein plays a direct role in telomeric silencing and counteracts inhibition by rif proteins. Curr Biol **9:**1123-1126.
213. **Garvik B, Carson M, Hartwell L.** 1995. Single-stranded DNA arising at telomeres in cdc13 mutants may constitute a specific signal for the RAD9 checkpoint. Mol Cell Biol **15:**6128-6138.
214. **Grandin N, Damon C, Charbonneau M.** 2001. Ten1 functions in telomere end protection and length regulation in association with Stn1 and Cdc13. Embo j **20:**1173-1183.
215. **Puglisi A, Bianchi A, Lemmens L, Damay P, Shore D.** 2008. Distinct roles for yeast Stn1 in telomere capping and telomerase inhibition. Embo j **27:**2328-2339.

216. **Lundblad V, Szostak JW.** 1989. A mutant with a defect in telomere elongation leads to senescence in yeast. Cell **57:**633-643.
217. **Singer MS, Gottschling DE.** 1994. TLC1: template RNA component of *Saccharomyces cerevisiae* telomerase. Science **266:**404-409.
218. **Lendvay TS, Morris DK, Sah J, Balasubramanian B, Lundblad V.** 1996. Senescence mutants of *Saccharomyces cerevisiae* with a defect in telomere replication identify three additional EST genes. Genetics **144:**1399-1412.
219. **Lingner J, Hughes TR, Shevchenko A, Mann M, Lundblad V, Cech TR.** 1997. Reverse transcriptase motifs in the catalytic subunit of telomerase. Science **276:**561-567.
220. **Lingner J, Cech TR.** 1996. Purification of telomerase from *Euplotes aediculatus*: requirement of a primer 3' overhang. Proc Natl Acad Sci U S A **93:**10712-10717.
221. **Lingner J, Cech TR, Hughes TR, Lundblad V.** 1997. Three Ever Shorter Telomere (EST) genes are dispensable for in vitro yeast telomerase activity. Proc Natl Acad Sci U S A **94:**11190-11195.
222. **Evans SK, Lundblad V.** 1999. Est1 and Cdc13 as comediators of telomerase access. Science **286:**117-120.
223. **Pennock E, Buckley K, Lundblad V.** 2001. Cdc13 delivers separate complexes to the telomere for end protection and replication. Cell **104:**387-396.
224. **Wu Y, Zakian VA.** 2011. The telomeric Cdc13 protein interacts directly with the telomerase subunit Est1 to bring it to telomeric DNA ends in vitro. Proc Natl Acad Sci U S A **108:**20362-20369.
225. **Chan A, Boule JB, Zakian VA.** 2008. Two pathways recruit telomerase to *Saccharomyces cerevisiae* telomeres. PLoS Genet **4:**e1000236.
226. **Talley JM, DeZwaan DC, Maness LD, Freeman BC, Friedman KL.** 2011. Stimulation of yeast telomerase activity by the ever shorter telomere 3 (Est3) subunit is dependent on direct interaction with the catalytic protein Est2. J Biol Chem **286:**26431-26439.
227. **Diede SJ, Gottschling DE.** 1999. Telomerase-mediated telomere addition in vivo requires DNA primase and DNA polymerases alpha and delta. Cell **99:**723-733.
228. **Taggart AK, Teng SC, Zakian VA.** 2002. Est1p as a cell cycle-regulated activator of telomere-bound telomerase. Science **297:**1023-1026.
229. **Tuzon CT, Wu Y, Chan A, Zakian VA.** 2011. The *Saccharomyces cerevisiae* telomerase subunit Est3 binds telomeres in a cell cycle- and Est1-dependent manner and interacts directly with Est1 in vitro. PLoS Genet **7:**e1002060.
230. **Osterhage JL, Talley JM, Friedman KL.** 2006. Proteasome-dependent degradation of Est1p regulates the cell cycle-restricted assembly of telomerase in *Saccharomyces cerevisiae*. Nat Struct Mol Biol **13:**720-728.
231. **Lin KW, McDonald KR, Guise AJ, Chan A, Cristea IM, Zakian VA.** 2015. Proteomics of yeast telomerase identified Cdc48-Npl4-Ufd1 and Ufd4 as regulators of Est1 and telomere length. Nat Commun **6:**8290.
232. **Ferguson JL, Chao WC, Lee E, Friedman KL.** 2013. The anaphase promoting complex contributes to the degradation of the *S. cerevisiae* telomerase recruitment subunit Est1p. PLoS One **8:**e55055.
233. **Hector RE, Shtofman RL, Ray A, Chen BR, Nyun T, Berkner KL, Runge KW.** 2007. Tel1p preferentially associates with short telomeres to stimulate their elongation. Mol Cell **27:**851-858.

234. **McGee JS, Phillips JA, Chan A, Sabourin M, Paeschke K, Zakian VA.** 2010. Reduced Rif2 and lack of Mec1 target short telomeres for elongation rather than double-strand break repair. Nat Struct Mol Biol **17:**1438-1445.
235. **Phillips JA, Chan A, Paeschke K, Zakian VA.** 2015. The pif1 helicase, a negative regulator of telomerase, acts preferentially at long telomeres. PLoS Genet **11:**e1005186.
236. **Sabourin M, Tuzon CT, Zakian VA.** 2007. Telomerase and Tel1p preferentially associate with short telomeres in *S. cerevisiae*. Mol Cell **27:**550-561.
237. **Viscardi V, Bonetti D, Cartagena-Lirola H, Lucchini G, Longhese MP.** 2007. MRX-dependent DNA damage response to short telomeres. Mol Biol Cell **18:**3047-3058.
238. **Schulz VP, Zakian VA.** 1994. The *saccharomyces* PIF1 DNA helicase inhibits telomere elongation and de novo telomere formation. Cell **76:**145-155.
239. **Boule JB, Vega LR, Zakian VA.** 2005. The yeast Pif1p helicase removes telomerase from telomeric DNA. Nature **438:**57-61.
240. **Opresko PL, Shay JW.** 2016. Telomere-Associated Aging Disorders. Ageing Res Rev doi:10.1016/j.arr.2016.05.009.
241. **de Lange T.** 2005. Shelterin: the protein complex that shapes and safeguards human telomeres. Genes Dev **19:**2100-2110.
242. **Li B, Oestreich S, de Lange T.** 2000. Identification of human Rap1: implications for telomere evolution. Cell **101:**471-483.
243. **Kabir S, Hockemeyer D, de Lange T.** 2014. TALEN gene knockouts reveal no requirement for the conserved human shelterin protein Rap1 in telomere protection and length regulation. Cell Rep **9:**1273-1280.
244. **van Steensel B, de Lange T.** 1997. Control of telomere length by the human telomeric protein TRF1. Nature **385:**740-743.
245. **Smogorzewska A, van Steensel B, Bianchi A, Oelmann S, Schaefer MR, Schnapp G, de Lange T.** 2000. Control of human telomere length by TRF1 and TRF2. Mol Cell Biol **20:**1659-1668.
246. **van Steensel B, Smogorzewska A, de Lange T.** 1998. TRF2 protects human telomeres from end-to-end fusions. Cell **92:**401-413.
247. **Doksani Y, Wu JY, de Lange T, Zhuang X.** 2013. Super-resolution fluorescence imaging of telomeres reveals TRF2-dependent T-loop formation. Cell **155:**345-356.
248. **Sarek G, Marzec P, Margalef P, Boulton SJ.** 2015. Molecular basis of telomere dysfunction in human genetic diseases. Nat Struct Mol Biol **22:**867-874.
249. **Hockemeyer D, Sfeir AJ, Shay JW, Wright WE, de Lange T.** 2005. POT1 protects telomeres from a transient DNA damage response and determines how human chromosomes end. Embo j **24:**2667-2678.
250. **Xin H, Liu D, Wan M, Safari A, Kim H, Sun W, O'Connor MS, Songyang Z.** 2007. TPP1 is a homologue of ciliate TEBP-beta and interacts with POT1 to recruit telomerase. Nature **445:**559-562.
251. **Wang F, Podell ER, Zaug AJ, Yang Y, Baciu P, Cech TR, Lei M.** 2007. The POT1-TPP1 telomere complex is a telomerase processivity factor. Nature **445:**506-510.
252. **Lue NF.** 2004. Adding to the ends: what makes telomerase processive and how important is it? Bioessays **26:**955-962.
253. **Nandakumar J, Bell CF, Weidenfeld I, Zaug AJ, Leinwand LA, Cech TR.** 2012. The TEL patch of telomere protein TPP1 mediates telomerase recruitment and processivity. Nature **492:**285-289.

254. **Schmidt JC, Dalby AB, Cech TR.** 2014. Identification of human TERT elements necessary for telomerase recruitment to telomeres. Elife **3**.
255. **Hayflick L, Moorhead PS.** 1961. The serial cultivation of human diploid cell strains. Exp Cell Res **25:**585-621.
256. **Carrel A.** 1912. On the permanent life of tissues outside of the organism. J Exp Med **15:**516-528.
257. **Hayflick L.** 1965. The limited in vitro lifetime of human diploid cell strains. Exp Cell Res **37:**614-636.
258. **Newbold RF.** 2002. The significance of telomerase activation and cellular immortalization in human cancer. Mutagenesis **17:**539-550.
259. **Armanios M, Chen JL, Chang YP, Brodsky RA, Hawkins A, Griffin CA, Eshleman JR, Cohen AR, Chakravarti A, Hamosh A, Greider CW.** 2005. Haploinsufficiency of telomerase reverse transcriptase leads to anticipation in autosomal dominant dyskeratosis congenita. Proc Natl Acad Sci U S A **102:**15960-15964.
260. **Vulliamy T, Marrone A, Szydlo R, Walne A, Mason PJ, Dokal I.** 2004. Disease anticipation is associated with progressive telomere shortening in families with dyskeratosis congenita due to mutations in TERC. Nat Genet **36:**447-449.
261. **Xu Y, Goldkorn A.** 2016. Telomere and Telomerase Therapeutics in Cancer. Genes (Basel) **7**.
262. **Bar C, Blasco MA.** 2016. Telomeres and telomerase as therapeutic targets to prevent and treat age-related diseases. F1000Res **5**.
263. **Magnenat L, Tobler H, Muller F.** 1999. Developmentally regulated telomerase activity is correlated with chromosomal healing during chromatin diminution in Ascaris suum. Mol Cell Biol **19:**3457-3465.
264. **Chen C, Kolodner RD.** 1999. Gross chromosomal rearrangements in *Saccharomyces cerevisiae* replication and recombination defective mutants. Nat Genet **23:**81-85.
265. **Ribeyre C, Shore D.** 2013. Regulation of telomere addition at DNA double-strand breaks. Chromosoma **122:**159-173.
266. **Chattoo BB, Sherman F, Azubalis DA, Fjellstedt TA, Mehnert D, Ogur M.** 1979. Selection of lys2 Mutants of the Yeast *Saccharomyces cerevisiae* by the Utilization of alpha-aminoadipate. Genetics **93:**51-65.
267. **Putnam CD, Pennaneach V, Kolodner RD.** 2004. Chromosome healing through terminal deletions generated by de novo telomere additions in *Saccharomyces cerevisiae*. Proc Natl Acad Sci U S A **101:**13262-13267.
268. **Mangahas JL, Alexander MK, Sandell LL, Zakian VA.** 2001. Repair of chromosome ends after telomere loss in *Saccharomyces*. Mol Biol Cell **12:**4078-4089.
269. **Kramer KM, Haber JE.** 1993. New telomeres in yeast are initiated with a highly selected subset of TG1-3 repeats. Genes Dev **7:**2345-2356.
270. **Bairley RC, Guillaume G, Vega LR, Friedman KL.** 2011. A mutation in the catalytic subunit of yeast telomerase alters primer-template alignment while promoting processivity and protein-DNA binding. J Cell Sci **124:**4241-4252.
271. **Bianchi A, Negrini S, Shore D.** 2004. Delivery of yeast telomerase to a DNA break depends on the recruitment functions of Cdc13 and Est1. Mol Cell **16:**139-146.
272. **Zhang W, Durocher D.** 2010. De novo telomere formation is suppressed by the Mec1-dependent inhibition of Cdc13 accumulation at DNA breaks. Genes Dev **24:**502-515.

273. **Makovets S, Blackburn EH.** 2009. DNA damage signalling prevents deleterious telomere addition at DNA breaks. Nat Cell Biol **11:**1383-1386.
274. **Negrini S, Ribaud V, Bianchi A, Shore D.** 2007. DNA breaks are masked by multiple Rap1 binding in yeast: implications for telomere capping and telomerase regulation. Genes Dev **21:**292-302.
275. **Frank CJ, Hyde M, Greider CW.** 2006. Regulation of telomere elongation by the cyclin-dependent kinase CDK1. Mol Cell **24:**423-432.
276. **Lustig AJ, Kurtz S, Shore D.** 1990. Involvement of the silencer and UAS binding protein RAP1 in regulation of telomere length. Science **250:**549-553.
277. **Ray A, Runge KW.** 1998. The C terminus of the major yeast telomere binding protein Rap1p enhances telomere formation. Mol Cell Biol **18:**1284-1295.
278. **Hoeijmakers JH.** 2001. Genome maintenance mechanisms for preventing cancer. Nature **411:**366-374.
279. **Aylon Y, Kupiec M.** 2004. DSB repair: the yeast paradigm. DNA Repair (Amst) **3:**797-815.
280. **Kolodner RD, Putnam CD, Myung K.** 2002. Maintenance of genome stability in *Saccharomyces cerevisiae*. Science **297:**552-557.
281. **Pennaneach V, Putnam CD, Kolodner RD.** 2006. Chromosome healing by de novo telomere addition in *Saccharomyces cerevisiae*. Mol Microbiol **59:**1357-1368.
282. **Grossi S, Bianchi A, Damay P, Shore D.** 2001. Telomere formation by rap1p binding site arrays reveals end-specific length regulation requirements and active telomeric recombination. Mol Cell Biol **21:**8117-8128.
283. **Lydeard JR, Lipkin-Moore Z, Jain S, Eapen VV, Haber JE.** 2010. Sgs1 and exo1 redundantly inhibit break-induced replication and de novo telomere addition at broken chromosome ends. PLoS Genet **6:**e1000973.
284. **Lundblad V, Blackburn EH.** 1993. An alternative pathway for yeast telomere maintenance rescues est1- senescence. Cell **73:**347-360.
285. **Lin JJ, Zakian VA.** 1996. The *Saccharomyces* CDC13 protein is a single-strand TG1-3 telomeric DNA-binding protein in vitro that affects telomere behavior in vivo. Proc Natl Acad Sci U S A **93:**13760-13765.
286. **Nugent CI, Hughes TR, Lue NF, Lundblad V.** 1996. Cdc13p: a single-strand telomeric DNA-binding protein with a dual role in yeast telomere maintenance. Science **274:**249-252.
287. **Hughes TR, Weilbaecher RG, Walterscheid M, Lundblad V.** 2000. Identification of the single-strand telomeric DNA binding domain of the *Saccharomyces cerevisiae* Cdc13 protein. Proc Natl Acad Sci U S A **97:**6457-6462.
288. **Bourns BD, Alexander MK, Smith AM, Zakian VA.** 1998. Sir proteins, Rif proteins, and Cdc13p bind *Saccharomyces* telomeres in vivo. Mol Cell Biol **18:**5600-5608.
289. **Tsukamoto Y, Taggart AK, Zakian VA.** 2001. The role of the Mre11-Rad50-Xrs2 complex in telomerase- mediated lengthening of *Saccharomyces cerevisiae* telomeres. Curr Biol **11:**1328-1335.
290. **Anderson EM, Halsey WA, Wuttke DS.** 2002. Delineation of the high-affinity single-stranded telomeric DNA-binding domain of *Saccharomyces cerevisiae* Cdc13. Nucleic Acids Res **30:**4305-4313.
291. **Eldridge AM, Halsey WA, Wuttke DS.** 2006. Identification of the determinants for the specific recognition of single-strand telomeric DNA by Cdc13. Biochemistry **45:**871-879.
292. **Giniger E, Varnum SM, Ptashne M.** 1985. Specific DNA binding of GAL4, a positive regulatory protein of yeast. Cell **40:**767-774.

293. **Fouladi B, Sabatier L, Miller D, Pottier G, Murnane JP.** 2000. The relationship between spontaneous telomere loss and chromosome instability in a human tumor cell line. Neoplasia **2:**540-554.
294. **Kostiner DR, Nguyen H, Cox VA, Cotter PD.** 2002. Stabilization of a terminal inversion duplication of 8p by telomere capture from 18q. Cytogenet Genome Res **98:**9-12.
295. **Fortin F, Beaulieu Bergeron M, Fetni R, Lemieux N.** 2009. Frequency of chromosome healing and interstitial telomeres in 40 cases of constitutional abnormalities. Cytogenet Genome Res **125:**176-185.
296. **Bonaglia MC, Giorda R, Beri S, De Agostini C, Novara F, Fichera M, Grillo L, Galesi O, Vetro A, Ciccone R, Bonati MT, Giglio S, Guerrini R, Osimani S, Marelli S, Zucca C, Grasso R, Borgatti R, Mani E, Motta C, Molteni M, Romano C, Greco D, Reitano S, Baroncini A, Lapi E, Cecconi A, Arrigo G, Patricelli MG, Pantaleoni C, D'Arrigo S, Riva D, Sciacca F, Dalla Bernardina B, Zoccante L, Darra F, Termine C, Maserati E, Bigoni S, Priolo E, Bottani A, Gimelli S, Bena F, Brusco A, di Gregorio E, Bagnasco I, Giussani U, Nitsch L, Politi P, Martinez-Frias ML, et al.** 2011. Molecular mechanisms generating and stabilizing terminal 22q13 deletions in 44 subjects with Phelan/McDermid syndrome. PLoS Genet **7:**e1002173.
297. **Ribeyre C, Shore D.** 2012. Anticheckpoint pathways at telomeres in yeast. Nat Struct Mol Biol **19:**307-313.
298. **Hirano Y, Sugimoto K.** 2007. Cdc13 telomere capping decreases Mec1 association but does not affect Tel1 association with DNA ends. Mol Biol Cell **18:**2026-2036.
299. **Murray AW, Claus TE, Szostak JW.** 1988. Characterization of two telomeric DNA processing reactions in *Saccharomyces cerevisiae*. Mol Cell Biol **8:**4642-4650.
300. **Grandin N, Damon C, Charbonneau M.** 2001. Cdc13 prevents telomere uncapping and Rad50-dependent homologous recombination. Embo j **20:**6127-6139.
301. **Ngo HP, Lydall D.** 2010. Survival and growth of yeast without telomere capping by Cdc13 in the absence of Sgs1, Exo1, and Rad9. PLoS Genet **6:**e1001072.
302. **Greetham M, Skordalakes E, Lydall D, Connolly BA.** 2015. The Telomere Binding Protein Cdc13 and the Single-Stranded DNA Binding Protein RPA Protect Telomeric DNA from Resection by Exonucleases. J Mol Biol **427:**3023-3030.
303. **Mitchell MT, Smith JS, Mason M, Harper S, Speicher DW, Johnson FB, Skordalakes E.** 2010. Cdc13 N-terminal dimerization, DNA binding, and telomere length regulation. Mol Cell Biol **30:**5325-5334.
304. **Schild D, Calderon IL, Contopoulo R, Mortimer RK.** 1983. Cloning of yeast recombination repair genes and evidence that several are non-essential genes, p 417-427 *In* Friedberg EC, Bridges BA (ed), Cellular responses to DNA damage. Alan R Liss, New York, NY.
305. **Scherer S, David RW.** 1979. Replacement of chromosome segments with altered DNA sequences constructed *in vitro*. Proc Natl Acad Sci USA **76:**4951-4955.
306. **Horton RM, Cai ZL, Ho SN, Pease LR.** 1990. Gene splicing by overlap extension: tailor-made genes using the polymerase chain reaction. Biotechniques **8:**528-535.
307. **Paeschke K, Bochman ML, Garcia PD, Cejka P, Friedman KL, Kowalczykowski SC, Zakian VA.** 2013. Pif1 family helicases suppress genome instability at G-quadruplex motifs. Nature **497:**458-462.
308. **Ji H, Adkins CJ, Cartwright BR, Friedman KL.** 2008. Yeast Est2p affects telomere length by influencing association of Rap1p with telomeric chromatin. Mol Cell Biol **28:**2380-2390.

309. **Ghaemmaghami S, Huh WK, Bower K, Howson RW, Belle A, Dephoure N, O'Shea EK, Weissman JS.** 2003. Global analysis of protein expression in yeast. Nature **425:**737-741.
310. **Oza P, Jaspersen SL, Miele A, Dekker J, Peterson CL.** 2009. Mechanisms that regulate localization of a DNA double-strand break to the nuclear periphery. Genes Dev **23:**912-927.
311. **Nickoloff JA, Reynolds RJ.** 1990. Transcription stimulates homologous recombination in mammalian cells. Mol Cell Biol **10:**4837-4845.
312. **Voelkel-Meiman K, Keil RL, Roeder GS.** 1987. Recombination-stimulating sequences in yeast ribosomal DNA correspond to sequences regulating transcription by RNA polymerase I. Cell **48:**1071-1079.
313. **Vaze MB, Pellicioli A, Lee SE, Ira G, Liberi G, Arbel-Eden A, Foiani M, Haber JE.** 2002. Recovery from checkpoint-mediated arrest after repair of a double-strand break requires Srs2 helicase. Mol Cell **10:**373-385.
314. **Seo B, Kim C, Hills M, Sung S, Kim H, Kim E, Lim DS, Oh HS, Choi RM, Chun J, Shim J, Lee J.** 2015. Telomere maintenance through recruitment of internal genomic regions. Nat Commun **6:**8189.
315. **Lamb J, Wilkie AO, Harris PC, Buckle VJ, Lindenbaum RH, Barton NJ, Reeders ST, Weatherall DJ, Higgs DR.** 1989. Detection of breakpoints in submicroscopic chromosomal translocation, illustrating an important mechanism for genetic disease. Lancet **2:**819-824.